Standardized Drosophila ventral nerve cord morphology: Atlas generation and atlas applications

Dissertation zur Erlangung des akademischen Grades des Doktors der Naturwissenschaften (Dr. rer. nat)

eingereicht im Fachbereich Biologie, Chemie, Pharmazie der Freien Universität Berlin

vorgelegt von

Jana Börner
aus Sonneberg

Mai, 2009

Die vorliegende Arbeit wurde unter der Leitung von Prof. Dr. Carsten Duch im Institut für Neurobiologie angefertigt.

1. Gutachter: Prof. Dr. Carsten Duch
2. Gutachter: Prof. Dr. Hans-Joachim Pflüger

Disputation am: 17. Juni 2009

Contents

1 Introduction

Since the groundbreaking studies of neuroanatomists like Ramón y Cajal (1888; 1898) and Camillo Golgi (1906) it has become clear that brain structure reflects brain function. However, brains of the different individuals of the same species come in different sizes and different shapes. How do we decide whether two brains are similar, and whether differences in form might reflect abnormalities, such as those resulting from or occurring in neurological disorders? During recent years a statistically secured, quantitative and standardized description has been attempted by generating average shape atlases for multiple species and brain regions (Rein et al., 2002; Brandt et al., 2005; Diedrichsen, 2006; Lee et al., 2007; Kurylas et al., 2008; Oishi et al., 2008).

To display and communicate anatomical knowledge of the brain, collected data have conventionally been visualized in two-dimensional (2D) maps. Neuroanatomical descriptions are available as stereotaxic atlas for various vertebrate species (Talairach, 1988; Stokes et al., 1974; Nixdorf-Bergweiler and Bischof, 2007). In these 2D atlases the anatomical data are presented within a coordinate system to localize structures of the three-dimensional (3D) brain in relationship to each other.
However, the conventional 2D atlases do not allow for comparison and combining of data derived from different focal planes in a common reference space. A statistical measure of similarities or differences among samples within these atlases is not possible, nor the examination of 3D structures. Three-dimensional imaging techniques like magnetic resonance imaging (MRI) or confocal laser scanning microscopy make fast acquisition of digital images, such as virtual brain slices possible. Together with imaging analysis algorithms a generation of digital brain atlases can be achieved to handle the growing amount of diverse data. Digital brain atlases for human (Kikinis et al., 1996), mouse (Lee et al., 2007; Mackenzie-Graham et al., 2007), zebra finch (Poirier et al., 2008) and several insect species (Drosophila, (Rein et al., 2002); honey bee, (Brandt et al., 2005); locust, (Kurylas et al., 2008); cockroach, (Chiang et al., 2001)) were generated as spatial frameworks to relate data in a common coordinate system. The digital atlases reduce time in image interpretation and offer flexible ways of data presentation in 2D and 3D.
Most of these digitalized brain maps can be accessed via the world wide web, and thus, are available to the whole scientific community. Web based atlases offer an easy way to navigate, access, and visualize a wide range of neuroscientific data. Vice versa, web based atlases allow scientists from different labs worldwide to add their data to a common standardized neuroanatomical framework. Based on the anatomical frameworks the atlases are extendable with data derived from other samples

or scientists. This results in great power of web based atlases and generation of comprehensive databases where imaging, gene expression, and physiological data, virtually any information can be linked to the anatomical structures of the atlas.
For *Drosophila melanogaster* as one of the most useful genetic model organisms, information on the genetics and biology is maintained by several databases accessible over the web. *Flybase*, the *Interactive Fly*, *Flybrain*, and *FlyView* contain genetic, molecular, and developmental data on nervous system structure and function. Different genetic (Phelps and Brand, 1998; Lee and Luo, 1999; Pfeiffer et al., 2008) and classical neuroanatomical tools are available for the visualization of nervous system structures in Drosophila. With a common 3D neuroanatomical framework the increasing amount of image data could be collected and made easily accessible. The fly brain standard (Rein et al., 2002) offers such a common reference space for the adult Drosophila brain. However, no such standardized atlas exists for the thoracic ganglia, despite the fact that these contain the central pattern generators for motor behavior and most of the insect individually identified neurons. Therefore, the goals of this study are the generation of an average standard atlas for the adult Drosophila ventral nerve cord, testing the feasibility for integrating of various types of neuroanatomical data into this standard (from expression data to single neurons), and making the standard available for the scientific community via the world wide web.

Information content, complexity, resolution, and richness of details of an atlas depend on the research purpose. Some atlases are derived from an individual brain to display complex morphology exemplary. Not only the complexity of the brain can be described in an atlas but also its variability. In probability maps of the human cortex (Mazziotta et al., 2001) data from a population of subjects are contained and allow for visualization of the intersubject variability. For other applications it is more useful to compensate for individual differences and to display only the most probable appearance of a wide range of individuals. Since brains can differ in size and shape a most representative brain can be achieved by an average of many individuals registered to the same common reference space (Brandt et al., 2005). Only brain structures from several individuals with a high probability of overlap are assigned as reference structure to the standard atlas.
Such average digital brain atlases are based in general on stainings of neuroanatomical structures like white matter, axonal fiber tracts (Oishi et al., 2008) or neuropil (Brandt et al., 2005). For some brains and staining techniques it is still unavoidable to perform histological slices for image generation (MacKenzie-Graham et al., 2004). Hence, digital images of these slices have to be aligned automatically to

result in virtual image stacks. Based on virtual image stacks structures of interest are graphical reconstructed manually by the user or automatically through registration algorithms. The transformed digital images can be visualized as 3D virtual structures. Integration of multiple landmarks into a standard makes a precise localization and description of data within the atlas possible. Structures like tracts or subregions of the brain usually serve as such landmarks.
For all experimental data that is registered into the atlas reference space landmark structures have to be counterstained and graphically reconstructed in each sample. Mapping data onto an atlas is generally accomplished by deforming an individual brain to match the shape of the target atlas. Experimental data are carried passively along with the deformation onto the atlas. The deforming algorithms perform linear (scaling, rotating, translation and shearing) and/or nonlinear (warping) alignment of individual brains and their structures to the standard spatial reference systems.

Digital atlases of the human brain are used to visualize detailed brain structure and serve for orientation of clinicians prior to surgery (Kikinis et al., 1996). Population-based brain atlases (Evans et al., 1992; Mazziotta et al., 1995) provide an expandable framework to synthesize the results of disparate imaging studies. These atlases use analytic tools to combine data across subjects, modalities and time to detect group-specific features not apparent in individual scans. In chemoarchitectural maps the molecular compositions of certain brain regions are visualized. Different distribution patterns, such as expression of transmitter receptors can be revealed for subdivisions of the brain (Vogt et al., 1990).
Expression patterns of genes and proteins can be visualized with in-situ hybridization or immunostainings. For mouse, as a model system for neuronal development, reference systems are published for the neonatal (Lee et al., 2005, 2007) and the adult mouse brain (MacKenzie-Graham et al., 2004). Gene expression data can be mapped into the anatomical frameworks to compare data derived from histological slices or studies of single brain parts from several studies.
In Drosophila large amounts of expression data has yielded gene networks for embryonic axis formation and segmental pattering (Nuesslein-Volhard and Wieschaus, 1980). It would be very useful to register expression patterns from genetic model systems into standard atlases to relate gene expression to neuroanatomy, functions of various brain parts, and to unravel potential yet unknown interactions between gene products by co-localization analysis in a standardadized references atlas. Through the enhancer trap technique (Bellen et al., 1989) expression patterns of genes in the embryo can be visualized. Several methods were proposed to display the spatial patterns of genes and proteins in a standardized way not only for the nervous

system but for the whole embryo. Image data for the spatial patterns of several reference genes in the Drosophila blastoderm were averaged in one of these models (Fowlkes et al., 2008). Integration of further gene expression data can be achieved through registration based on the reference patterns. In a similar model (FlyEx, Pisarev et al., 2009), data on expression of segmentation genes are available as reference data base. Both methods offer ways for integration of data from other labs and therefore make comparison of gene expression data within a reference system possible.

Drosophila as an insects offers many advantages to study basic principles of nervous system function and development. With about 100,000 neurons the CNS of Drosophila has ∼1000-fold fewer neurons than the mouse brain. Nevertheless, Drosophila shows complex behaviors like flying, walking, mating, aggression (Baier et al., 2002), and learning and memory (Wolf and Heisenberg, 1991). For the central nervous system of adult Drosophila and other insects species, morphological atlases are available for specific brain parts (Rein et al., 2002; Brandt et al., 2005; Kurylas et al., 2008; Berg et al., 2002; Huetteroth and Schachtner, 2005; Laissue et al., 1999). Insect brains are small enough to ensure a good penetration of the neuronal tissue with antibodies. Virtual image stacks can be gathered from whole mount preparations with confocal microscopy. The neuropils of the brains are segmented based on the confocal image stacks of antibody stainings for synaptically localized proteins. Different brain areas are integrated into the insect standards as landmarks. In some brain regions, sub-structures can be recognized through different neuropil staining intensities, and compartment boundaries are demarked by glia tissue or tracts which lack staining with specific markers. All of the named standard atlases resemble averages derived from populations. The standardized staining methods allow for integration of further data based on a neuropil label. Differences in volume of brain regions between male and female flies and volume differences for several brain regions between two wild-type strains could be shown with standardized brain anatomy in Drosophila (Rein et al., 2002). In Manduca brain sexual dimorphism is investigated (el Jundi et al., in revision) with standardized mapping methods.
These existing frameworks can potentially be extended with functional data derived from calcium imaging recordings, imaging of voltage-sensitive dyes or spatial expression patterns of genes and proteins. Positions of cell bodies, tracts, commissures, and single neurons, or classes of neurons can be mapped into the reference space. In Drosophila the UAS/GAL4 system is a powerful tool that allows for targeted gene expression (Brand and Perrimon, 1993). Subpopulations of cells can be visualized through expression of reporter genes like green fluorescent protein (GFP).

With the labeling of secondary neuron lineages (Ito and Hotta, 1992), groups of neurons derived from one neuroblast during postembryonic development can be located within the brain. For the larval brain Pereanu and Hartenstein (2006) generated a three-dimensional digital atlas for the spatial pattern of all secondary lineages and secondary linage tracts. Mapping of gene expression patterns can reveal lineage-specific patterns for the investigated genes by this atlas.

Investigations of axonal and dendritic projections for single identified neurons are also possible through standard registration. In Drosophila, like in other insect nervous systems, some neurons can be identified across preparations. Registration of single identified neurons into a standard might be a powerful tool for mapping components of neuronal circuits to visualize their spatial location to each other. Central projections areas and connections between the neurons can be displayed in 3D. The common mapping methods are precise enough to accomplish this, as was shown for 3D reconstructions of single neurons in honey bee (Brandt et al., 2005) and locust (Kurylas et al., 2008). Although single neurons can be identified with intracellular staining techniques in locust and honey bee brains, data acquisition is these systems is time consuming. In Drosophila the mosaic analysis with a repressive cell marker (MARCM) technique (Lee and Luo, 1999) allows for generation of enhancer trap GAL4 lines for many individual cell types. By using GFP as a reporter in these lines, single neurons can be visualized for many individual samples and fast data acquisition is possible. With the help of genetic analysis methods single components of different behavioral circuits were identified (Jefferis et al., 2002; Lin et al., 2007; Morante and Desplan, 2008). Despite the description of these circuit components, no mapping of entire circuits into a standard brain has been shown to date.

Labeling of pre- and postsynaptic partners simultaneously in one preparation is too time-consuming for random screens of synaptic contacts. Therefore, another approach proposed by Jefferis et al. (2007) might be useful to identify putative synaptic contacts. In these experiments the central projection areas of single neurons were mapped to a reference space from several individuals. The MARCM clone technique allowed for fluorescence labeling of single projection neurons (PNs) in the Drosophila brain. With a counterstaining for presynaptically localized proteins, they created quantitative synaptic densities maps of the mushroom body and lateral horn for projections of the PNs. Through registration of traced PNs of several samples on one reference brain, an overlay of all stained PN presynaptic terminals resulted in a synaptic density map. Mapping of other neurons into these density maps makes a prediction of putative connectivity possible. Defining neuropil regions

within a standard for the probability of containing axons or dendrites of one neuron is theoretically possible for every identified neuron.

In the insect ventral nerve cord (VNC) monosynaptic connections between neurons participating in walking (Burrows et al., 1988; Laurent and Burrows, 1988), flying (Peters et al., 1985; Burrows, 1975; Reye and Pearson, 1987), and larval crawling (Sandstrom and Weeks, 1991) have been identified anatomically and physiologically, but standardized atlases for the insect VNC are still missing. Landgraf et al. (2003) proposed standardized labeling of a set of evenly distributed landmarks in Drosophila embryos and larva. Counterstaining of tracts within every preparation was used for mapping of neurites to identify pre- and postsynaptic elements and to investigate circuit formation. In adult Drosophila expression of GFP in a subset of sensory neurons was used as reference labels (Tyrer et al., 2000). Together with labeling of the ganglion architecture individual cells and neuron projections derived from different samples were related to each other. However, labeling of landmarks within the neuropil cannot serve as comprehensive framework for the VNC. A standardized atlas for the whole VNC would offer a good reference system for integration of single parts of known circuits and could result in a comprehensive 3D wiring diagram for the VNC.

In the VNC of adult Drosophila only a few synaptic connections and complete circuits are identified (e.g. the Giant Fiber system; see Allen et al., 2006 for review). Intracellular staining techniques are not feasible for most of the central neurons in adult Drosophila and even though many genetic techniques are available for visualization of single neurons, most of the published GAL4-lines used in Drosophila brain research are not described for their expression pattern in the VNC.
Well investigated are the synaptic connections of the giant fiber system (GFs). The GFs controls the escape behavior in Drosophila. Mono- and polysynaptic connections between interneurons and leg and flight motoneurons have been described (King and Wyman, 1980). Further, the morphology and physiology of one flight motoneuron, MN5 (Coggshall, 1978; Ikeda and Koenig, 1988), participating in this network has been investigated in detail. The soma of the MN5 lies on the dorsal surface of the VNC and is thus good accessible for intracellular staining techniques and electrophysiological recordings (Duch et al., 2008). Together with 4 other motoneurons (MN1-4) the MN5 innervates the dorsal longitudinal flight muscle (DLM).

Flying, walking, and crawling, as any other rhythmic motor behavior is controlled by central pattern generators (CPGs, see Marder and Bucher, 2001 for review). Proprioceptive feedback plays a critical role for the coordination of rhythmic body movements (Reye and Pearson, 1988; Johnston and Levine, 1996). Sensory

feedback from external (bristles, campaniform sensilla) and internal (stretch receptors, chordotonal organs) sensors can alter the motor output of the central networks. So far no monosynaptic connection between sensory neurons and the central components of the flight motor system is identified for adult Drosophila.
Identification of such monosynaptic connections would enable new tools to investigate the impact of sensory feedback on the cellular level. Registration of candidate presynaptic neurons into a reference space could indicate such contacts to identified central neurons. Several GAL4 driver lines were investigated in this study to reveal such putative monosynaptic connections. P0163 (Hummel et al., 2000), atonal-GAL (Jarman et al., 1993, 1995), and Pickpocket-GAL4 (PPK) (Adams et al., 1998) are described for their expression patterns in peripheral neurons. GFP expression in P0163 and atonal-GAL4 can be detected in many sensory neurons and their central projections. These lines might be useful to identify and map sensory neuropils within the VNC standard. PPK expression is restricted to a subset of sensory neurons (Adams et al., 1998; Haesemeyer et al., 2009). The ppk gene encodes a Drosophila degenerin/epithelial sodium channel (DEG/ENaC) subunit that is expressed in mechanosensory neurons (Adams et al., 1998). It was shown that loss of the PPK1 protein in ppk1 null mutants enhanced locomotion in the larva and its role for controlling rhythmic locomotion was suggested (Ainsley et al., 2003). Single central axon projections of PPK positive neurons can be detected in the VNC. Therefore, the PPK line was a good candidate for providing sensory feedback on identified central neurons of the flight network. With the identification of synaptic contacts between two neurons the feasibility of standard registration for revealing connectivity could be tested. In double labeling experiments for both putative synaptic partners it was investigate whether such connections may really exist.

In summary, the specific aims of this study are:

- Generate a standard for the ventral nerve cord neuropil of adult *Drosophila melanogaster*.
- Expand the atlas by registration of tracts, commissures, and the ganglionic cortex.
- Test the feasibility of registration of expression patterns of different GAL4 lines.
- Register individual neurons. Test whether an overlay of the registered neuron structures can yield in a good probability map of average projection areas for identified neurons.
- Test whether standard registration of individual neurons can be used to reveal possible connectivity between neurons.
- Through registration into a standard the image data are transformed affine and non-rigid. In some cases e.g. high resolution confocal image scans a deformation of the images is not desired. Test how the standard can be used to analyze such image data derived from individual samples to make comparative studies possible.
- Make the atlas available to the scientific community via the web and provide a detailed protocol for standard registration for the users.

2 Materials and Methods

2.1 Animals

Drosophila melanogaster strains were kept on a standard cornmeal medium at 25°C (12/12 light/dark cycle). Female adult flies were used for experiments one to three days after eclosion. The ventral nerve cord standard was generated from wild-type Berlin (wtb) flies. Several GAL4-driver and GFP-reporter lines were used to visualize neuroanatomical features of the ventral nerve cord. Membrane-targeted GFP and cytoplasmic GFP (yw; UAS-CD8-GFP; UAS-GFP/CyO) was expressed under the control of specific drivers to visualize the positions of somata and neuritic projections. With a repo-GAL4 driver (reverse polarity, citealtXiong1994) glia of the cortex and nerves were marked with GFP. Different driver lines with restricted expression to neurons of specific functional classes were used. The TDC line expresses GAL4 under the control of tyrosine decarboxylase (Cole et al., 2005) and labeled octopaminergic and tyraminergic neurons. For expression of GFP in neurons of selected transmitter classes the GAD-GAL4, the OK371, and the cha-GAL4 were used. GAD-GAL4 drives expression of UAS transgenes under the control of the promoter for glutamic acid decarboxylase (GAD) (Chude et al., 1979; Jackson et al., 1990), an enzyme that catalyses the decarboxylation of glutamate to γ-aminobutyric acid (GABA). The GAL4 driver line OK371 has been reported to drive expression under the control of the vesicular glutamate transporter (DVGLUT), and thus, has been used as marker for glutamatergic neurons (Mahr and Aberle, 2006). Cha-GAL4 drives expression of UAS transgenes under the control of the promoter for choline acetyltransferase, thus expressing in cholinergic neurons. Two recombinant motoneuron driver lines were used to determine the positions of the expressing cells in the ventral nerve cord. C380-GAL expresses in most larval motoneurons (Sanyal et al., 2003; Sanyal, 2009). With UAS-CD8-GFP as a reporter the somata could be visualized. To avoid expressions of GAL4 in interneurons, the Cha-GAL80 was used (choline-acetyl transferase promoter driven GAL80), which has been shown to suppress GAL4 activity in all cholinergic neurons (Aberle et al., 2002). The recombinante C380-GAL4, UAS-CD8-GFP; Cha-GAL4 line was received from Dr. S. Sanyal (Emory University, Atlanta, GA, C380-GAL4, UAS-CD8-GFP; +; cha-GAL80). D42-GAL4 (Yeh et al., 1995) expresses in motoneurons of the ventral nerve cord in larva (Sanyal, 2009). With the recombinant UAS-mCD8-GFP; D42-GAL4, Cha-GAL80UAS-mCD8-GFP line the position of somata and dendrites could be visualized. Cha-GAL80 was used to restrict the expression. Expression of GFP in presynaptic terminals was visualized for cholinergic neurons with an

UAS-Synapsine1-GFP line crossed to a cha-GAL4 driver line. A subset of peripheral sensory neurons and their central axon projections were labeled by expressing GFP under the control of the pickpocket (ppk) gene (Adams et al., 1998). The ppk gene encodes a Drosophila degenerin/epithelial sodium channel (DEG/ENaC) subunit that is expressed in mechanosensory neurons (Adams et al., 1998). The PPK-EGFP reporter line was used (Grueber et al., 2003) to investigate these neurons. With the recombinant PPK-GFP; UAS-dsRed line the fluorescent dye dsRed could be expressed in motonoeurons for crosses with a C380-GAL4; Cha-GAL80 line (Budnik et al., 1996).

2.2 Histology

Dissection

The animals were anesthetized by chilling on ice in a vial. After cutting the legs and wings the flies were pinned with dorsal side up on Sylgard-coated (Dow Corning Co., Midland, MI) Petri dishes. In standard saline (Jan and Jan, 1976) an incision was made on the dorsal midline from the abdomen to the cervical connective. To open the thorax fine pins were pierced through the flight muscles on each side. The head was cut and the ovaries, the gut and the heart were removed and the glands between the nervous system and the flight muscles on each side.

Retrograde staining technique

Intact animals were immobilized and pinned dorsal side up in a dish without removing the wings. The left wing was stretched in a 90% angle to the body axis an fixed with Vaseline. An incision through the wing blade close to the wing base was made to cut the axons of the sensory cells. After placing a Vaseline well around the incision the well was filled with a 10% w/v Neurobiotin (Linaris GmbH, Wertheim-Bettingen, Germany) solution in distilled water and covered with Vaseline to avoid evaporation. The preparation was flooded with saline. Incubation was performed for 2-4 h at room temperature. The Vaseline well was removed and the animals were dissected as described above.

Intracellular staining of the flight motoneuron 5

Intracellular staining was performed as described in Duch et al. 2008. Briefly, dissected animals were mounted onto a Zeiss fluorescence microscope. A thin sheath lying above the MN5 was removed enzymatically by applying a 2% protease solution locally with a glass microelectrode for 2 minutes. The preparation was rinsed with

saline for 2 minutes before the staining. A thin-walled glass microelectrode (75-95 MΩ tip resistance) was filled with a mixture of 7% Neurobiotin and rhodamine-dextran (Invitrogen, Carlsbad, CA) in 2 M potassium acetate. An air bubble was left between the dye-filled tip and the shaft filled with 2 M potassium acetate to avoid dye dilution. Following intracellular penetration of MN5, the dyes were injected iontophoretically by a constant depolarizing current of 0.5 nA for 10-12 minutes. The electrode was removed and the samples were fixed for histology.

Immunocytochemistry

Fixation was performed in 4% PFA in phosphate buffer solution (PBS, Calbiochem) for 30-45 minutes at room temperature. Samples were rinsed in PBS for 1 hours and in PBS with 0.5% TritonX (TX, Sigma) for 9x20 min at room temperature before incubation with the primary antibody solution for two nights at 4°C. The primary antibodies were diluted in PBS TX 0.3% and 10% albumin from bovine serum (BSA, Sigma) in different concentrations as following: NC82 (mouse) 1:100 and 22c10 (mouse) 1:50 (the monoclonal antibody NC82 developed by Erich Buchner and the monoclonal antibody 22c10 developed by Seymour Benzer were both obtained from the Developmental Studies Hybridoma Bank developed under the auspices of the NICHD and maintained by The University of Iowa, Department of Biological Science Iowa City, IA, 52242), anti-GFP (rabbit, Sigma) 1:400, anti-GABA (rabbit, Abcam), and the alpha-Tubulin antibody (rabbit, Abcam) 1:200. Before application of the secondary antibodies the samples were rinsed for 8x15 minutes in PBS. Incubation with the secondary antibodies was performed in PBS for 1 night at 4°C. All secondary antibodies against mouse and rabbit were used in a concentration of 1:500. The secondary antibodies were conjugated to either Cy2, Cy3 or Cy5 (Jackson ImmunoResearch). The intracellular stainings with neurobiotin were labeled with streptavidin-Cy2 (Jackson ImmunoResearch) in a concentration of 1:750. Before mounting the samples in methyl salicylate they were rinsed for 6x15 min in PBS, dehydrated in a ascending ethanol series and incubated for 5 min treatment in a 1:1 mixture of pure ethanol and methyl salicylate. The flight muscles were removed.

2.3 Confocal microscopy

The whole ventral nerve cord was visualized by scanning several stacks of optical sections with a Leica (Bensheim, Germany) SP2 laser scanning microscope using a 40x oil immersion objective (numerical aperture 1.25). The zoom factor was set to

1.5x and resulted in an image resolution of 1024x1024 with a step size of 0.7 μm. The obtained images had a voxel size of 0.3x0.3x0.7 μm. Each sample consisted of 2 to 4 fields of view. For high resolution scans the zoom factor was set to 3.5x and resulted in a approx. 0.1x0.1 μm pixel size with a step size of 0.3 μm.

2.4 Standard generation and registration

Preparation of confocal image stacks

Confocal image stacks used for standard generation and mapping were preprocessed in Amira 4.0 (Mercury Systems). After resampling the image stacks laterally to 512x512 the single fields of view of one sample were merged to one image stack.

Segmentation

For further processing the gray scale image stacks were converted into labelfields in Amira. NC82 stainings for the neuropil were segmented semi-automatically with the LabelVoxel tool. The threshold between background and staining was verified by blotting the number of pixels for each gray value. The value were the curve had its steepest negative slope was chosen as the threshold. The entire ventral nerve cord neuropil staining was defined as one material of a Labelfield. The resulting Labelfield was modified in the label editor by removing islands (voxel size 15) in 3 dimensions and smoothing the label. False labeled structures like autoflourescent cuticle or glands were removed from the labelfield manually. The segmentation of tracts, somata clusters, and retrograde stainings was performed manually or automatically with a global thresholding criterion in the label editor.

Standard generation

The neuropil standard of the ventral nerve cord for adult Drosophila was generated as an average shaped standard as described by Brandt et al. (2005) through subsequent affine and elastic registration in Amira 3.1 of 24 wtb samples. As reference for the affine registration one sample was chosen which showed little obvious deformation caused by the histological procedure. All other 23 samples were registered affine onto this reference. Labelfield averaging (in the ZIB.2007-version of Amira, Konrad-Zuse-Zentrum für Informationstechnik Berlin) of all 24 affine transformed samples resulted in a new average shaped reference for the elastic registration. Only pixel with an overlay of 50% and more for all 24 samples were chosen for the new reference. After the elastic registration of all 24 affine transformed samples on this

reference averaging of the labelfields resulted in the average shaped ventral nerve cord neuropil.

2.5 Standard application

Mapping of sub-neuropils

For any anatomical information of the ventral nerve cord derived from immunostainings a counterstaining with NC82 was performed. The segmented neuropil labelfield (see above) was registered affine and elastic onto the standard and the transformation was applied subsequently onto the second structure. With the registration tools in Amira labelfields, gray scale image stacks, and geometric reconstructions could be transformed onto the standard. Structures of interest were segmented manually and automatically to create labelfields for the transformation process. The generation of three-dimensional geometric reconstruction is described below. The sensory axon projections of neurons from the wing blade were visualized by retrograde stainings (see above). The central projections were segmented automatically with a local thresholding criterion for 4 preparations. After registration of all 4 samples into the standard, an average label for the sensory wing neuropil was calculated in Amira. For the generation of the dendritic neuropil for the flight motoneurons the GFP-signal of 5 preparations of the UAS-mCD8-GFP; D42-GAL4, Cha-GAL80 line was segmented automatically with a local thresholding criterion. The somata were excluded from the labelfield. Registration into the neuropil standard and averaging of the labelfileds resulted in a averaged dendritic neuropil.

Backwards application of the standard

Immunstainings for NC82 was combined with GABA-immunstainings in wtb flies amd with GFP-stainings in Cha-GAL4 lines crossed to UAS-Synapsin1-GFP respectively. The entire ventral nerve cord was scanned with a zoom factor of 1.5. The dorsal most 20 μm of the transition from prothoracic to mesothoracic neuromere, the ventral 25 μm in the region of the left accessory mesothoracic neuromere, and the median neuropil of the right prothoracic neuropil were scanned with a zoom factor of 3.5. The entire neuropil staining was segmented automatically. For localization of neuropil regions within the confocal image stacks the average shaped standard neuropil was registered affine and elastic onto the sample neuropil label. Two previously defined sub-neuropils (wing sensory and dendritic neuropil, see above) were subsequently transformed onto the neuropil. The transformed sub-neuropils could be be displayed simultaneous within the high resolution confocal image stacks. The

image stacks were cropped to several non-overlapping regions of interest with a size of 143x143 pixels localized inside the sub-neuropils.

Analysis of presynaptic terminal area

From each cropped image stack single images in steps sizes of 1.5 μm were collected. Analysis of the single images was performed in MATLAB R2007a (The MathWorks). A graphical user interface (GUI) was programed to analyze both channels of one optical slice simultaneously. Thresholds for both channels (NC82 and GABA or Cha) were adjusted by hand in the GUI for each image separately. For the set thresholds contours, outlining all pixels with a gray value above the threshold, were generated and displayed as a contour image. An overlay of both channel contours was calculated and a new contour image for the overlay areas was calculated. For all resulting overlay images the number of areas inside the contours and the size of the single areas were calculated. All data from one neuropil region of one sample were summed up and normalized to the total area of the images.

2.6 Geometric reconstructions

For three-dimensional reconstructions of dendritic segments of the MN5 software plugins for Amira were used as published previously (Schmitt et al., 2004; Evers et al., 2005). These deliver precise quantification of midline and diameter as well as triangulated surface definitions fully exploiting optical resolution. To address the distribution of putative input synapses of sensory neurons onto the dendritic tree of the MN5, GFP expression was driven under the control of the pickpocket gene (Adams et al., 1998). The stainings were combined with NC82 immunstainings to visualize active zones (Wagh et al., 2006) within the PPK positive terminals. For quantification of the distribution of immunolabeled profiles along dendrites, the generated surface description was used to calculate the staining density within 300 nm from each surface element, a triangle. The position of the triangle was determined perpendicular to the midline of the corresponding reconstructed segment (for details see Evers et al. 2005). An electron microscopy study demonstrated that this procedure accounted for all synaptic terminals located in the thoracic motor neuropils of Manduca, but that it produced approximately 20% false positive synapses if only one immunolabel was used (Hohensee et al., 2008). The surface calculation was performed for the PPK staining and the NC82 staining separately. The correlation of both calculated surfaces was used to indicate sites of putative

sensory input synapses on the dendrite. For statistical analysis, morphological data exported as CSV-tables generated in Amira were imported into MATLAB.

Identification of dendritic subtrees

Subtree identification was performed in cooperation with Fernando Vonhoff (unpublished data). From the primary neurite of the MN5 subtrees were projecting predominantly anteriorly and posteriorly. Ten posteriorly projecting subtrees and one anteriorly projecting subtree were identified in all preparations. Since subtree shape can differ between the single preparations, identification of subtrees was according to the sequence of their branching from the primary neurite. The first subtree branches at the distal side of the neurite and the last subtree branches at the proximal end of the neurite close to the soma.

3 The Drosophila ventral nerve cord standard

Standardized neuroanatomy allows for comparison and combination of anatomical and functional data acquired from individual samples. In insect nervous systems behavior can be studied on the level of single neurons, small neural circuits and specific brain parts. Drosophila, as a genetic model system, offers the possibility to relate neuroanatomical data to gene expression data and to use targeted genetic manipulations. With the generation of a standardized neuroanatomical atlas for the ventral nerve cord of adult Drosophila, data derived from different samples and modalities can be analyzed in a common framework. Standardized staining methods with a commercially available antibody and automatic registration procedures make the ventral nerve cord standard applicable for the whole scientific community. Single neurons, gene expression patterns, and anatomical structures can be integrated into the standard, as will be shown here.

In insect ventral ganglia the neuropil forms the inner core of the nervous system and is surrounded by a layer of cell bodies, the cortex. The neuropil is densely packed with synapses and can thus be visualized by immunostainings with synaptic markers. Stainings of the neuropil with synaptic markers are commonly used for the generation of standard atlases of insect brains (Honey bee, Brandt et al. 2005); Drosophila, Rein et al. (2002); locust, Kurylas et al. (2008)). Here the commercially available monoclonal Drosophila antibody NC82 (HybridomaBank) was used which is highly specific for the Bruchpilot protein localized at the presynaptic active zone (Wagh et al., 2006). NC82 immunostaining marked the entire neuropil of the ventral nerve cord (Fig. 1A). With a refined immunostaining protocol (see methods) homogeneous antibody penetration throughout the entire ventral nerve cord in whole mount preparations (Fig. 1A) could be ensured. This enabled definition of the whole neuropil for standard generation by a global threshold criterion (Fig. 1B). To distinguish between staining and background the number of pixels of a confocal image stack were plotted for each gray value in a histogram (Fig. 1B1). The value where the curve showed the steepest negative slope was defined as threshold value (arrow in Fig. 1B1). All pixels of the image stack with a value equal to or higher than the threshold were assigned to the label field (Figs. 1B2, B3). By this procedure the gray scale images resulting from NC82 confocal image stacks were automatically segmented into a label field in Amira (Fig. 1B2-B3). The Drosophila ventral nerve cord is small enough to acquire confocal image stacks with a high resolution 40x oil immersion lens (NA 1.2), so that labeled active zones appeared as distinct puncta on the light microscopy level. Despite high resolution confocal scanning, no obvious borders were observed between different neuropil regions, but tracts could clearly be

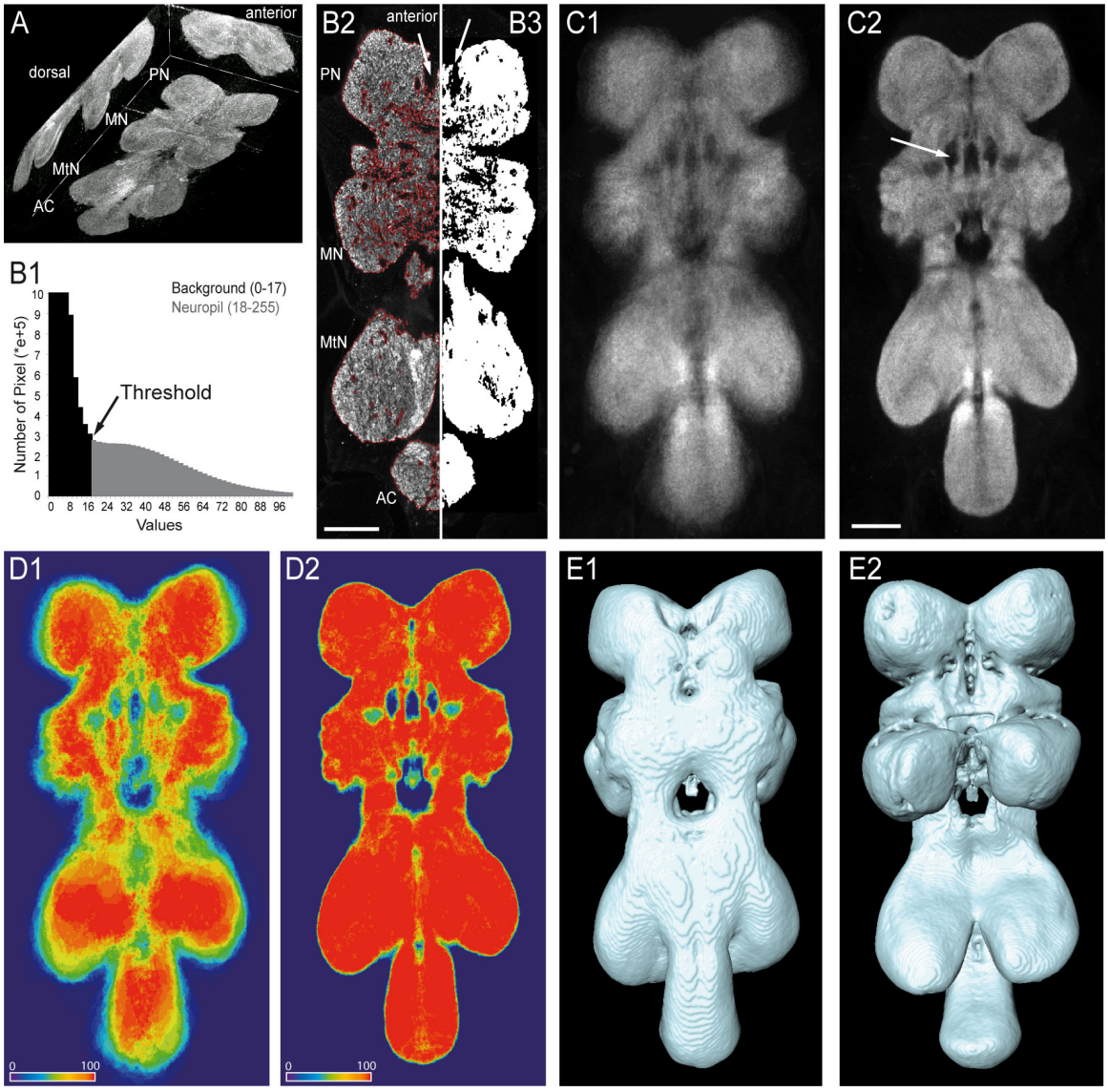
A
anterior
dorsal
PN
MN
MtN
AC
B1
Background (0-17)
Neuropil (18-255)
Threshold
Number of Pixel (*e+5)
Values
B2
anterior
B3
PN
MN
MtN
AC
C1
C2
D1
D2
E1
E2

identified by the absence of synaptic marker staining (Figs. 1A, B2). Consequently, for standard generation the whole neuropil was regarded as one structure and was not further divided into sub-neuropils. Areas with no NC82 inside the neuropil staining marked the positions of tracts and commissures (arrows in 1B2 and B3) and were excluded from the neuropil label. Neuropils of 24 adult female Drosophila wild type Berlin ventral nerve cords were segmented in this way. The standard was generated in two steps. First all original label fields were registered affine on one reference label. The reference label was chosen from a large number of pre-selected preparations that showed little deformation caused by the histological procedure. Affine registration corrected for positioning and global size differences between the individual images, i.e. translation, rotation, and global isotropic scaling (Brandt et al., 2005). Averaging of all labels after affine transformation (Fig. 1D1) resulted in a blurred image when the transformation was applied to the original gray scale images of the confocal stacks (Fig. 1C1). Only pixels with 50% or more overlap

Figure 1 *(preceding page)*: **Generation of the average shaped neuropil standard for the ventral nerve cord of adult *Drosophila melanogaster*: A**: Projection views of a confocal image stack along the x-, y- and z-axis of the thoracic-abdominal neuropil. NC82 stains the neuropil homogeneous through the whole ventral nerve cord. Although the segmental organization is visible and the pro-, meso-, meta-thoracic neuromer (PN, MN, MtN) and the abdominal center (AC) can be identified, no clear boundaries between these segments can be drawn. In the x-projection the ventral swellings of the thoracic neuromers are visible. **B**: The gray scale image stack is converted into a label field with one material representing the entire neuropil. **B1**: For the threshold based labeling the number of pixels for each gray value are plotted. The x-axis is restricted from 0 to 100 for a better resolution between background (black) and staining (gray). For accepting a pixel as an unit of the label field the threshold is set to the value of the steepest negative slope (arrow). **B2/B3**: The split view shows the transformation of the gray scale image into the label field image. **B2** All pixels with a value between the threshold and 255 are assigned to the label field. Here the positive pixels of one gray scale image are outlined in red in the label mode of Amira. Structures with no NC82 staining, like tracts, are thus excluded from the label. The arrow indicates one example for a tract, the ventral median tract of ventral cervical fasciculus (VTV). **B3**: The resulting label field does not encode the staining intensities, the information is reduced to a binary code. Structures with no synapse staining like the VTV (arrow) are excluded from the neuropil but their position is still encoded through their boundaries. **C**: Single slices of averaged gray images after affine and elastic registration. The transformation based on the label fields is applied to the gray image stacks and an average image stack is calculated. **C1**: The average of all affine transformed stacks gives a blurred average shaped image. **C2**: After the second registration step the averaged neuropil shows more distinct boundaries, and tracts (arrow) are still clearly visible. Differences in staining intensities are conserved in the averaged gray image. **D**: Single slices of the probability maps of 24 averaged label fields after affine and elastic registration of all 24 preparations. The linear scale is color coded from 0% overlap (blue) to 100% overlap (red). **D1** Only pixels which locate to the same position in 50% (green) to 100% (red) of label fields after affine registration are counted for the averaged label which is the new reference for the next registration step. **D2**: The probability map computed from all 24 labels after the elastic registration shows a higher probability of overlap then the one in D1 and the transition is less broad. **E**: 3D views of the neuropil standard as a surface reconstruction of the label field from dorsal (**E1**) and ventral (**E2**). Scale bar, 50 μm.

(yellow to red in Fig. 1D1) were assigned to the average shaped label field. This average included the entire range of shape differences of all 24 individual samples. In the second step each affine registered label field was registered non-rigidly (elastic registration) onto the average shaped label. This procedure corrected for local shape differences and anisotropic scaling (Brandt et al., 2005). As for affine registration the resulting labels were averaged (Fig. 1D2). Only pixels with 50% or more overlap (yellow to red in 1D1) were assigned to the average shaped label field. The color map demonstrated that non-rigid registration (Fig. 1D2) increased the overlay of all 24 individual samples considerably as compared to affine registration only (Fig. 1D1). Applying the same transformation to the original gray scale images resulted in a sharp gray image with clear borders in which the tracts and commissures were preserved (Fig. 1C2, see arrow). Therefore, affine and non-rigid registration were used sequentially for standard generation. Surface representations of the resulting standard Drosophila ventral nerve cord neuropil are depicted in figures 1E1 (dorsal view) and 1E2 (ventral view).

To analyze the degree of deviation of each individual sample from the standard, the overall spatial dimensions of all 24 original neuropil labels were compared to the standard. Measured dimensions included: The anterior to posterior length of the entire ventral nerve cord neuropil as well as the length of pro- and mesothoracic neuromere, the widths of the pro-, the meso- and the metathoric neuromere, and the thicknesses (z-dimension) of the pro- and the mesothoracic neuromeres. All measures were normalized to the values of the standard neuropil. The relative deviations from the standard were plotted for all 24 samples (Fig. 2A). For dimensions in x (length) and in y (width) the individual samples scatter around the standard by up to plus and minus 10%. In the z-dimension (thickness) the individual samples scatter around the standard by up to 20%. For each of the 24 samples the different overall spatial dimensions differed with respect to the distance and direction of deviation from the standard. As an example preparation number 17 is labeled with an asterisk in figure 2A. In this sample total neuropil length, prothoracic neuropil width and mesothoracic neuropil thickness were smaller than the standard, whereas combined pro- and mesothoracic neuropil length as well as meso- and metathoracic neuropil width and prothoracic neuropil thickness were larger as compared to the standard. Therefore, the standard is not simply a result of rescaling of all samples to an average size, but by contrast, during standard generation all samples are transformed individually in different areas of the neuropil. The sample that was chosen as starting reference for the affine registration (marked by an arrow in Fig. 2A) strongly affected the total length of the resulting standard but not the other neuropil features. With

A Normalized shape differences of individual neuropiles to the standard

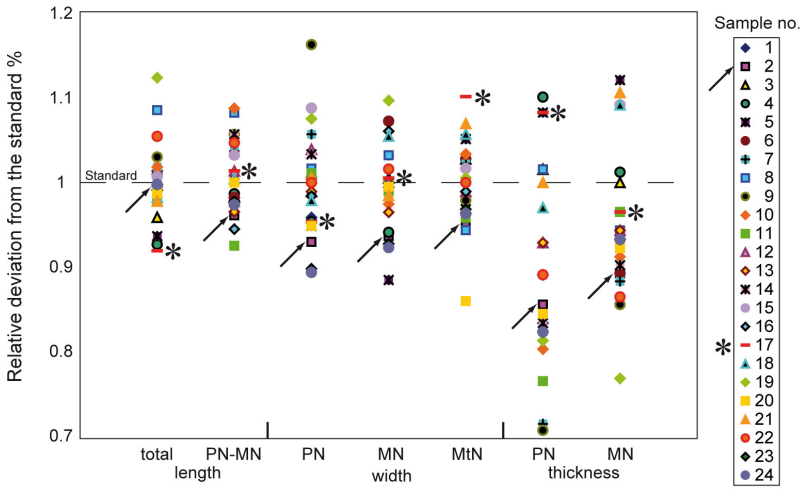

B Relative neuropile volume changes after transformations

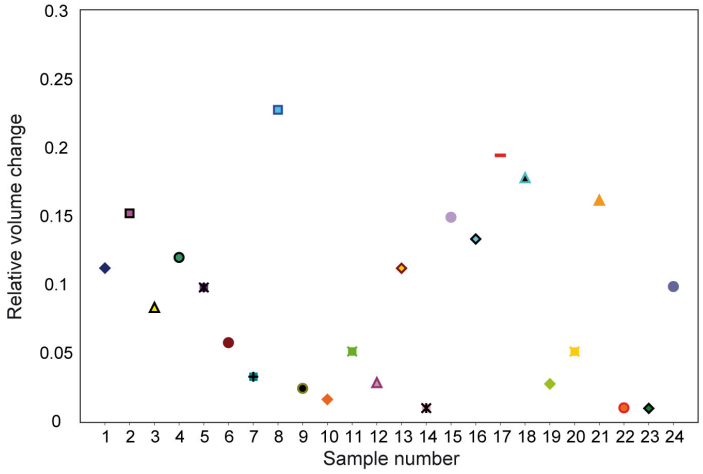

C Average deviation of the 24 samples to the standard and to each other

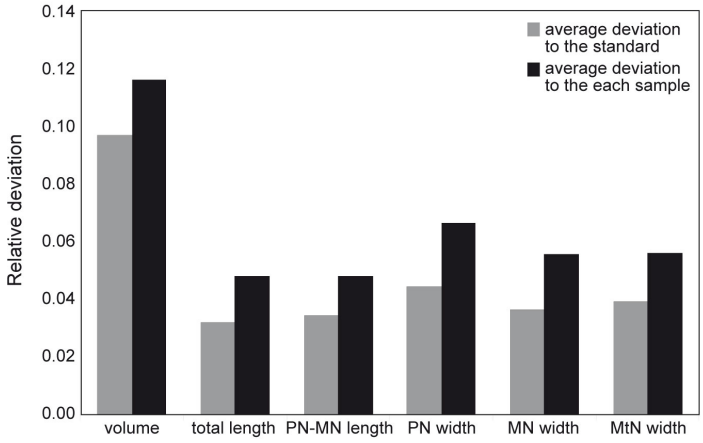

regard to volume, the sample that was used as starting reference differed by 15% from the standard (sample 2 in Fig. 2B). Overall, volume changes of all individual samples with regard to the standard ranged from 1% to 23% (Fig. 2B), whereby for 9 out of 24 samples volume changes were smaller than 5%. Consequently, relative changes of the neuropil volume during transformations were approximately twice as large as changes of one dimensional measures (Fig. 2A). One important requirement of a standard is that the difference of each individual sample to the standard should be smaller than the average distance of all samples to each other (see Rohlfing et al. 2004). This was tested by comparing the average deviation of all 24 samples from the standard (Fig. 2A, gray bars) with the average deviation of these 24 samples from each other (Fig. 2C, black bars) with respect to volume, length and width. For all 6 parameters tested, the deviation from the standard was smaller than the deviation between the different samples, demonstrating that the performed registration and transformation procedures generated a standard that fulfills the above mentioned requirement. Additional non-rigid registration steps did not further decrease the average distance of all samples to the standard, nor did it markedly decrease the numbers of voxels that were assigned with intermediate probabilities for belonging to the standard (see Fig. 1D2).

As mentioned above, in insect ventral nerve cord, neuronal somata are located outside the neuropil in the ganglionic cortex. To include the ganglionic cortex into the standard atlas, it had to be labeled selectively. Since ganglionic cortex consists of neuronal cell bodies and glia tissue (Power, 1948), the glia specific promoter, repo-GAL4 (Xiong et al., 1994) was used to drive the expression of GFP in cortex only (Fig. 3A, green). In all preparations GFP expression under the control of repo- was combined with NC82 immunostaining (Fig. 3A, red). As described above the

Figure 2 *(preceding page)*: **Comparison of shape differences between individual neuropils and the neuropil standard: A**: The neuropil proportions of all original label fields used for the standard generation are measured in all three dimensions. The total length, the length of the prothoracic (PN) and mesothoracic (MN) neuromeres, the width of PN, MN and metathoracic neuromeres (MtN) and the thickness of PN and MN of the 24 samples are normalized to the dimensions of the average shaped standard label. The relative deviation of each sample to the standard (at 1) is plotted for these parameters. For length and width the standard is almost in the center, the most variable parameter is thickness. Sample 2 (arrows), as the reference for the affine registrations, equals only in length with the resulting standard. Sample 17 (asterisk) is another example for size variations in both directions. The standard is not simply a result of rescaling of all samples to a certain size. **B**: The amount of relative neuropil volume change after elastic transformations is plotted for each sample. The volume change is calculated for each sample by normalizing the initial label field volume to the volume of the transformed label field. Only one sample (8) undergoes a volume change of more than 20%. 8 samples undergo a volume change of less then 5%. **C**: The average deviation of all 24 samples from the standard (gray bars) is plotted against the average deviation of all 24 samples to each other (black bars). The compared parameters were volume, neuropil length and width.

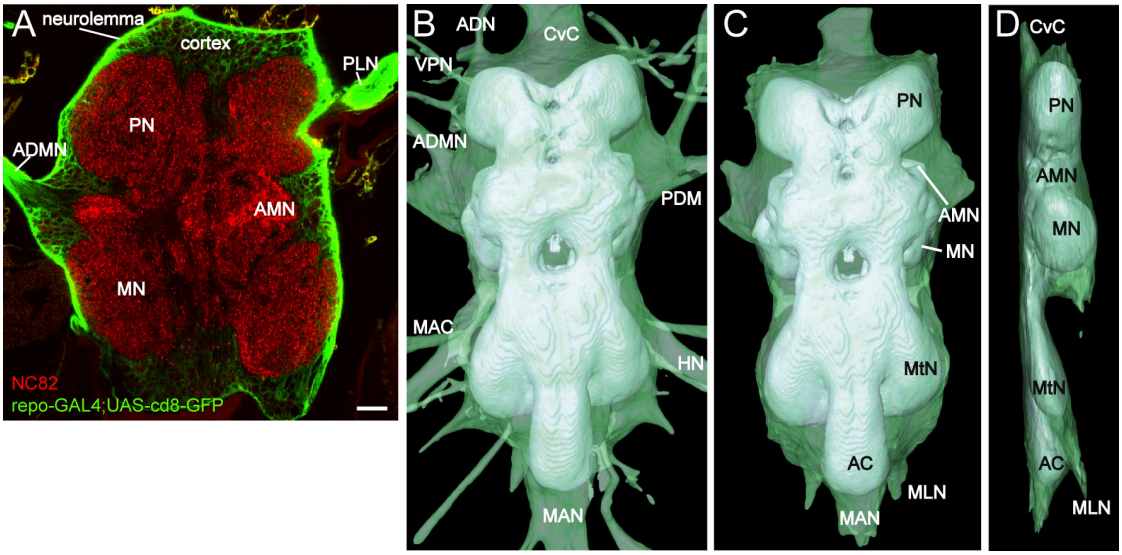

Figure 3: **Registration of the cortex onto the neuropil standard:** **A**: Single slice of a confocal image stack through the prothoracic (PN), accessory mesothoracic (AMN) and the mesothoracic neuromers (MN) of the ventral nerve cord. The neuropil is labeled with NC82 (red) and glia cells are labeled by using a repo-Gal4;UAS-cd8-GFP construct (green). The cellular cortex surrounds the whole neuropil and is enclosed in a neurolemma. The neurolemma extends over the anterior dorsal mesothoracic nerve (ADMN) and the prothoracic leg nerve (PLN). **B**: Surface view of the cortex and the nerves (light green, transparent) from one registered sample enclosing the neuropil standard (gray). Based on the GFP signal (A) a label field of the cortex and the associated nerves is created and registered on the standard. Some of the bigger nerves named by Power 1948 are labeled. ADMN, anterior dorsal mesothoracic nerve; ADN, anterior dorsal nerve; CvC, cervical connective; HN, haltere nerve; MAC, mesothoracic accessory nerve; MAN, median abdominal nerve; PDM, posterior dorsal mesothoracic nerve; VPN, ventral prothoracic nerve. **C**: Dorsal surface view of the averaged cortex of four samples enclosing the neuropil standard. The cortex forms a closed sheath around the neuropil. Only a few stumps of the bigger nerves are left after averaging because the orientation of the nerves varies among preparations. **D**: Lateral surface view of the cortex and the standard. Scale bar, 20 μm.

neuropil staining was converted into a label field (see Figs. 1A, B) and registered onto the neuropil standard (see Figs. 1C to E). On the basis of the GFP staining a separate cortex label field was generated by a global threshold criterion. User interaction was required to ensure that cortex label field segmentation yielded a continuous closed structure, including the roots of all major lateral nerves (Fig. 3B). Affine and nonrigid transformation parameters obtained form neuropil registration were applied to the cortex label field. Averaging of four transformed cortex labels resulted in a standard cortex label enclosing the neuropil standard (Figs. 3C, D). The lateral nerve roots were lost during the averaging procedure, because their localization was strongly depended on dissection during histology. Only the stumps of the thicker nerves and the cervical connective (CvC) were visible after averaging.

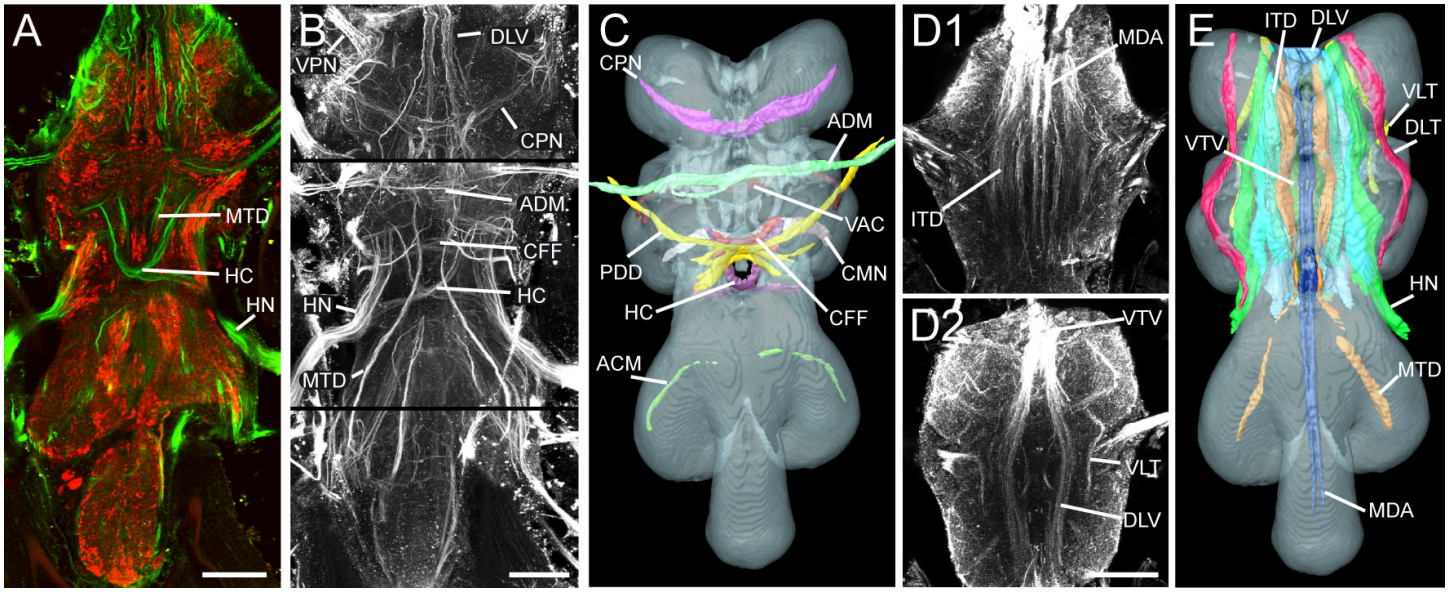

Figure 4: **Registration of tracts and commissures into the neuropil standard:** **A**: Single optical section from a confocal image stack of an immuno staining in the ventral nerve cord of a UAS-Synapsin1-GFP;Cha-GAL4 fly. GFP expression (red) marks the neuropil. Tracts and commissures are labeled with a monoclonal antibody against the Futsch protein (antibody 22c10) (green) (HC, haltere chiasma; HN, haltere nerve; MTD, median tract of dorsal cervical fasciculus). **B**: Z-projections of 3 to 5 μm in different depth of the Futsch staining. Distinct bundles of neurites that form tracts and commissures can be recognized and are named after Power 1948 (ADM, anterior dorsal mesothoracic decussation; CFF, chiasma of fine fibers of the intermediate tracts of the dorsal cervical fasciculi; CPN, commissure of prothoracic neuromeres; DLV, dorsal lateral tract of ventral cervical fasciculus; VPN, ventral prothoracic nerve). **C**: All clear identifiable commissures are labeled as separate materials (different colors) of one label field in AMIRA and registered into the standard (gray) (ACM, accessory commissure of metathoracic neuromeres, dark green; ADM, light green; CFF, red; CMN, commissure of mesothoracic neuromeres, light pink; CPN, dark pink; HC, purple; PDD, posterior dorsal mesothoracic decussation, yellow; VAC, ventral accessory commissure of mesothoracic neuromeres, brown). **D**: Staining with an anti Tubulin antibody in wtb Drosophila labels the tracts as diffuse bundles. **D1**: A single optical section in the dorsal part of the confocal image stack shows the MDA and the broad intermediate tract of dorsal cervical fasciculus (ITD). **D2**: The VTV (ventral median tract of ventral cervical fasciculus), VLT (ventral lateral tract) and DLV are located in the ventral part of the ventral nerve cord. For better visualization the image is a z-projection of 4 μm. **E**: The tracts are converted into a label field and registered into the standard (DLT, dorsal lateral tract of dorsal cervical fasciculus, pink; DLV, light blue; HN, green; ITD, turquoise; MDA, median dorsal abdominal tract, dark blue; MTD, orange; VLT, yellow; VTV, dark green). Scale bars, 50 μm.

Another basic neuroanatomic feature of insect ventral ganglia are tracts and commissures (Braeunig et al., 1981; Pflueger et al., 1988). A tract comprises the axon fascicles of intersegmentally projecting neurons, and the commissures contain axon fascicles of neurons projecting across the ganglionic midline. Neuronal processes, including axons and dendrites contain high levels of tubulin. Consequently, densely packed axons as occurring in fascicles can be labeled with antibodies recognizing tubulin protein. Two different antibodies were used to stain tracts and commissures. First, antibody 22C10 has been widely used to label neuronal morophology and axonal projections (Estes et al., 1996). 22C10 recognizes the Drosophila Futsch protein, a MAP1B-like protein which localizes to the microtubule compartment of the cell (Hummel et al., 2000). Second, tubulin was labeled with an anti alpha Tubulin antibody (Abcam). For the adult ventral nerve cord anti-Futsch was a good marker for all commissures and some tracts (Figs. 4A,B). Since 22C10 is generated in mouse, it was not possible to counterstain the neuropil with the mouse monoclonal NC82 antibody. To obtain a neuropil label that can be used for registration onto the standard, UAS-Synapsin1-GFP was expressed in all cholinergic neurons under the control of the Cha promoter. This yielded a representative neuropil staining similar to NC82 staining (Fig. 4A, red), which can be used for the registration procedure, and is distinct from 22C10 label in commissures . The anti-tubulin antibody was a more useful marker for all tracts. By contrast, anti-tubulin staining of the commissures is weak (Figs. 4D1, D2). Commissures and tracts of both staining were segmented in Amira as label fields. Within each label field individual tracts or commissures can be defined as separate materials. Due to partial de-fasciculation of axons in tracts and commissures within specific regions of the ventral nerve cord and due to additional staining outside tracts and commissures, automated global threshold segmentation was not possible, but label fields and materials had to be defined manually. The commissures and tracts were identified based on the work of Power (1948). In most samples the commissures formed thick bundles (HC in Figs. 4A, B). Staining for tracts were more diffuse as compared to commissure stainings, the tracts were loose broad bundles with blurred boundaries (for an example see ITD in Fig. 4D1). Segmentation of the tracts is strongly dependent on the quality of the immunostaining. Therefore, transformation of tracts of a few samples on the standard and subsequent averaging could not reproduce a representative average tract. In Fig. 4 eight identified and registered commissures (4B) and eight tracts (4D) are shown exemplary for one anti-Futsch sample and one anti-Tubulin sample together with the neuropil standard.

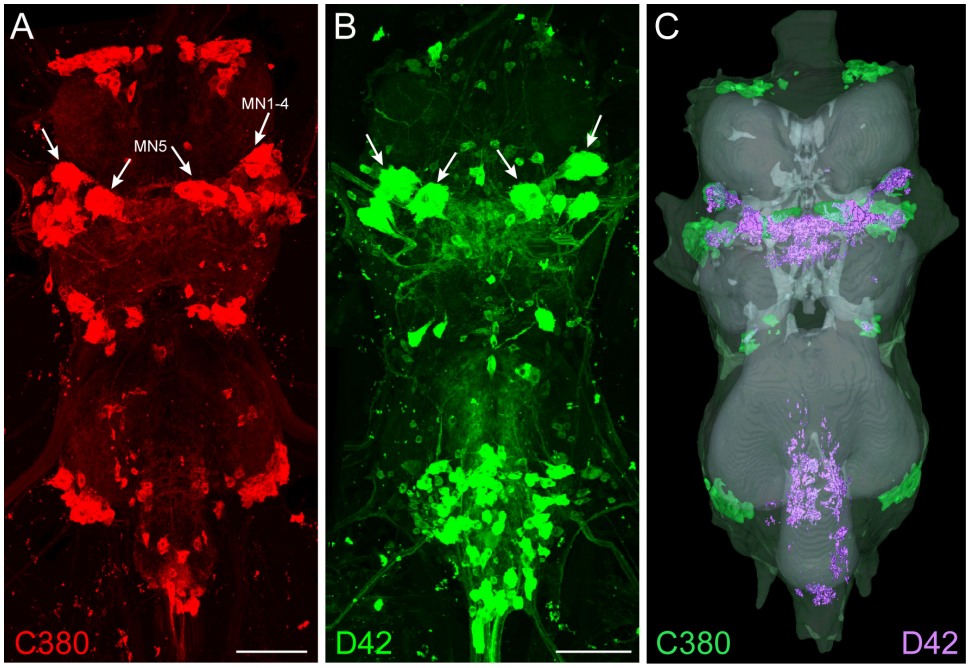

Figure 5: **Registration of expression patterns as revealed by different motoneuron GAL4 driver lines: A**:Projection view of a confocal image stack of the ventral nerve cord of GFP expression under the control of the C380-driver (red). **B**: Projection view of a confocal image stack of the ventral nerve cord of the GFP expression under the control of the D42-driver (green). Both motoneuron drivers express predominantly in adult motoneurons. The depressor flight motoneurons are marked by arrows and could be clearly identified in both lines. Distinct cell body clusters on the edges of the pro-, meso- and methathoracic neuromeres were only GFP-labeled under the control of C380 and not D42. GFP expressing small cell bodies on the dorsal surface of the abdominal neuromere were only detected for the D42 driver. **C**: Prominent cell clusters of the C380 expression were segmented by hand for 5 samples and registered, the average label (green) is displayed in the standard (gray). One threshold based segmented D42 label is displayed exemplarily after registration (purple) to compare it to the C380 clusters. Clear overlap of C380 and D42 can only be seen for the big cell bodies of motoneurons of the mesothoracic neuromer. Scale bar, 50 μm.

In Drosophila the UAS-GAL4 system can be used to label neurons fluorescently. Expression of GFP under the control of GAL-drivers for genes with special functions can be used to report position of somata in the cortex. Some GAL4 lines as commonly used to drive expression of transgenes in motoneurons have been characterized in the larval CNS (Sanyal et al., 2003), but it remains unclear whether these fly lines also express in large overlapping populations of adult motoneurons. Standardized neuroanatomy might be a useful tool to gather a fast and comprehensive overview of the similarities of the expression patterns of GAL4 lines. As an example GFP was expressed under the control of the motoneuron drivers C380 and D42. In both cases expression was restricted by recombination with the Cha-GAL80 transgene. Projections views of C380 and D42 driven GFP expression in the ventral nerve cord are shown in figures 5A and B. A number of neurons could

clearly be identified in both driver lines, including the depressor flight motoneurons MN1-5 (arrows), but also large non-overlapping expression patterns could be observed (Figs. 5A, B). GFP expression in both driver lines was counterstained with NC82 for registration into the standard. For the C380 expression prominent cell clusters were segmented by hand and an average label of 5 samples was calculated after registration (in green 5C) into the standard. Dendrites and other neuronal processes were omitted from the registration process. The D42 driven GFP signal showed many single neuronal somata not forming dense clusters. For this line the GFP signal was automatically segmented by a threshold based criterion that included strongly labeled dendrites and registered into the standard (purple 5C). Within the standard, D42 and C380 expression patterns overlap in the large somata of depressor flight motoneurons. However, most other smaller neurons as revealed by D42 expression were not part of the C380 clusters. Combined 3-dimensional visualization within the standard allows for a comprehensive judgment of the degree of similarities and differences in expression patterns of multiple GAL4 lines. This does not yield significant advantages for the comparison of two lines, such as C380 and D42, which can be accomplished by a simply side by side comparison of different preparations. However, the standard allows for registration of hundreds of GAL4 lines and web based 3 dimensional display, thus providing a tool for quick comparison of expression patterns based on staining derived from different laboratories. A quantitative database on the exact numbers and positions of neuronal cell bodies as revealed by GFP expression in different GAL4 lines was not attempted. First, the position of individual cell bodies was different between individuals, and spatial transformation during affine and non-rigid registration did not correct sufficiently for this. Second, the total numbers of neurons expressing GAL4 in either of the two lines was too large to uniquely identify all individual neurons, and thus, to judge whether expression varied between different preparations. In summary, registration of GAL4 lines is straight forward and not time consuming if expression is restricted to small numbers of neurons. Neuron identification and neuron counts are easy if somata do not overlap to a large degree (e.g. many small single neuronal somata in D42, see Fig. 5B). Although clusters of neuronal cell bodies can be hand registered, large numbers of neurons with strong overlap can not be automatically registered without allowing large errors. Manual registration can in principle be applied to virtually every GAL4 line, but is becomes increasingly time consuming the more neurons are labeled.

Examples for GAL4 lines that are commonly used to drive expression of transgenes in large numbers of neurons of selected neurotransmitter classes are shown in

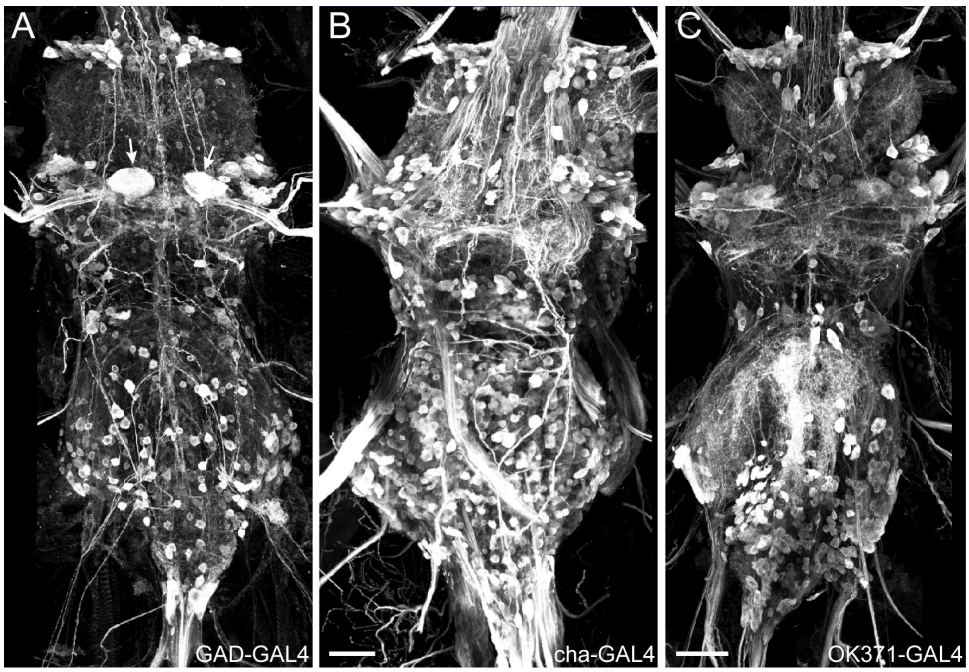

Figure 6: **Expression patterns of commonly used transmitter driver lines:** Projection views of confocal image stacks of the ventral nerve cords of GFP expressions under the control of the GAD-driver (**A**), the cha-driver (**B**) and the OK371-driver (**C**). **A**: GFP-expression driven by GAD could be detected in the depressor flight motoneuron MN5 (arrows), single small cell bodies distributed over the whole ventral nerve cord and small bundles and single axons projecting through some nerves. **B**: A high number of small cell bodies were GFP positive when GFP-expression was driven by cha. Most of the nerves had thick bundles with GFP staining and many neurites inside the neuropil were stained. **C**: Expression of GFP under the OK371-driver labels cluster of small and bigger cell bodies in the pro- and mesothoracic neuromere and smaller cell bodies in the metathoracic and abdominal neuromere. Most nerves contain GFP expressing axon bundles. Scale bar, 20 μm.

figure 6. GAD-GAL4 drives expression of UAS transgenes under the control of the promoter for glutamate decarboxylase (GAD) (Chude et al., 1979; Jackson et al., 1990), an enzyme that catalyses the decarboxylation of glutamate to GABA. GAD is, therefore, assumed to express in GABAergic neurons. However, expression occurs in a large number of neurons and is not restricted to GABAergic neurons because a number of glutamatergic motoneurons, including MN5, can unambiguously be identifiedin by expressing GFP under the control of GAD-GAL4 (Fig. 6A, arrows). Cha-GAL4 drives expression of UAS transgenes under the control of the promoter for choline acetyltransferase, thus expressing in cholinergic neurons (Fig. 6B). The GAL4 driver line OK371 has been reported to drive expression under the control of the vesicular glutamate transporter (DVGLUT), and thus, has been used as a pan motoneuronal marker (Mahr and Aberle, 2006). Projection views of representative confocal image stacks resulting from driving GFP expression under the control of each of these three drivers reveal largely non-overlapping expression patterns

(Fig. 6). Due to the large number of overlapping neuronal somata, and the different levels of expression in different neurons as observed in each of the three lines, registration of transmitter specific expression patterns into a standard can not be achieved by automated or semi-automatic procedures, and thus, would be extremely time consuming. Another problem is that axons, dendrites and somata may show different levels of expression (Fig. 6). Furthermore, the data indicate that at least GAD-GAL4 does not restrict expression to GABAergic neurons only, because some glutamatergic motoneurons clearly show expression, and double labeling with anti-GABA reveled largely non-overlapping staining patterns (not shown). Furthermore, expression of OK371 shows clear differences from expression as revealed by other GAL4 driver lines that have been used to restrict expression to motoneurons (see Fig. 5A, B). Therefore, it was not attempted to register these lines manually into the standard.

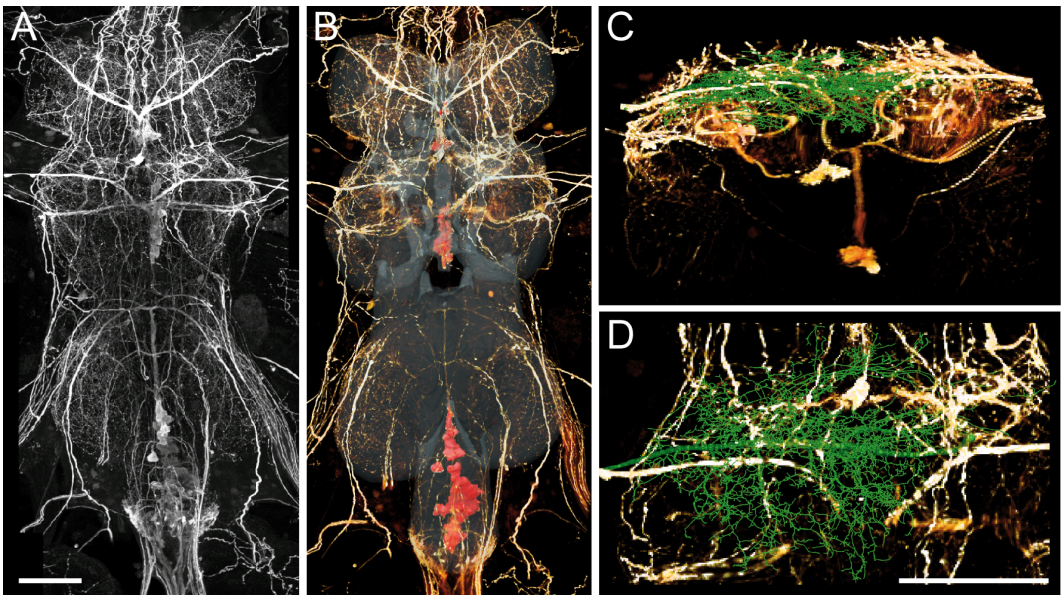

Figure 7: **Registration of putative neuronal connectivity maps into the standard: A:** Projection view of a confocal image stack of GFP expression under the control of TDC-GAL4 in the ventral nerve cord. **B:** The GFP positive cell bodies (red) were manually labeled and registered into the standard (gray). The gray scale image stack of the GFP expression was transformed onto the standard and is displayed as a volume rendering together with the standard to visualize the projections of the octopaminergic and tyraminergic neurons. **C, D:** Comparison of the transformed TDC2 label with a previously registered geometric reconstructions of an identified neuron (green). C Part of the mesothoracic neuromere in a transversal view from anterior. The somata of 2 TDC2 positive cells are on the ventral side of the ventral nerve cord their primary neurites project dorsally. D Dorsal view of the same area as in C. C and D show that the projections of the TDC2 positive processes overlap with the dendritic field of the MN5. Scale bars, 50 μm.

A number of GAL4 lines available in Drosophila restrict expression to small numbers of central neurons of specific functional classes. Among these are, for example, lines that express GAL4 under the control of tyrosine decarboxylase (TDC,

Cole et al. 2005), so that all octopaminergic and tyraminergic neurons are labeled (Fig. 7A). TDC2 positive cell bodies are located in the midline on the ventral side of the VNC (Fig. 7A). The primary neurites project dorsally, bifurcate, and give rise to branches in the dorsal part of the neuropil before exiting the vnc through the nerves. The somata of all octopaminergic/tyraminergic neurons could easily be registered into the standard (Fig. 7B, red). However, in order to use the standard to retrieve information about the possible central targets of aminergic modulation as resulting form the activity of TDC2 expressing neurons, one needs to relate the neuronal projections of TDC2 expressing neurons to the arborizations of other registered neurons. A segmentation of the whole TDC2 network (Fig. 7A) would be time consuming, but registration of the NC82 label field of the same sample provides transformation information to locate the TDC2 in the standard. Therefore, this approach was proposed here to retrieve information about possible connectivity between neuron populations stained in different preparations using the standard. In the example shown in figure 7, TDC2-GAL4 was used to express GFP in all octopaminergic/tyraminergic neurons (Fig. 7A), and the ventral nerve cord was counterstained with NC82. The NC82 neuropil label was registered onto the standard, and the resulting transformation was applied to the original grey scale image stack of the TCD2/GFP staining (Fig. 7B, white-yellow). This procedure resulted in transformation of the TDC2 label to allow comparison with other structures that had previously been registered into the standard, e.g. geometric reconstructions of identified neurons (Figs. 7C, D). This revealed that TDC2 positive neuronal processes (shown as voltex view in Figs. 7B, C, D) overlap with the dendritic tree of the depressor flight motoneuron, MN5 (see next chapter for registration of MN5 geometric reconstruction). Therefore, transformation of the TDC2/GFP grey scale image stack revealed information as to whether octopaminergic/tyraminergic neurons might potentially modulate the depressor flight motoneuron via paracrine release of biogenic amines, without having stained both in one preparation.

The ventral nerve cord standard, as a real averaged shape of wild-type Drosophila neuropils, can be used for registration of confocal image data. Potentially any structure that is counter stained with NC82 can be transformed onto the standard. Image data can be integrated into the standard as segmented label fields or as gray scale image stacks by transforming the original data. Structures from different samples can thus be displayed together in the standard and spatial relations for expression and projection patterns can be compared. The neuropil standard can now serve as reference system for further data analysis.

4 Investigation of neuropil structure in the standard reference space

The insect ventral nerve cord contains neuronal networks to produce different rhythmic behaviors, like walking and flying. Central projections of sensory organs providing feedback to these networks terminate in different regions of the ventral nerve cord as could be shown for locusts (Hustert et al., 1981; Braeunig et al., 1981, 1983; Pflueger et al., 1981, 1988) and flies (Merritt and Murphey, 1992). This spatial projections in specific neuropil areas related to different functions offers a good system to study internal neuropil structure, e.g. synapse densities or the composition of neurotransmitters and expression patterns of specific genes, and might reveal function related neuropil differences. Further, registration of identified neurons allows for identification of overlapping projection areas with these neuropils and makes a prediction of putative connectivity possible.

Since the homogeneous structure of the Drosophila neuropil did not allow subdividing different parts of the ventral nerve cord neuropil regions on the basis of NC82 immunostaining, different methods had to be used to define distinct regions within the neuropil standard. One approach is to identify projection volumes of defined classes of neurons to chart functionally different parts within the neuropil standard. On the one hand it was attempted to define regions within the ventral nerve cord neuropil standard that are associated with the computation of sensory information from the wings, and on the other hand the neuropil regions that are associated with passing flight motor information onto the final neural output relays, the flight motoneuron were charted. The central projections of all wing sensory cells located on the wing blade were labeled anterogradely with neurobiotin (Fig. 8A, white). A counter staining with NC82 (Fig 8A, red) allowed for registration into the standard. The axon terminals of these sensory neurons entered the neuropil through the anterior dorsal mesothoracic nerve (ADMN) and branched in a distinct neuropil area, the accessory mesothoracic neuromere (AMN, after Power (1948)). AMN was first described by Power (1948) on the basis of classical histology from sections, but could also be seen in confocal images from NC82 immunostainings (encircled in Fig. 8A). Four backfill preparations of the wing were segmented as a label field and registered into the neuropil standard through the NC82 staining. An average label field of the registered projections was calculated. The probability map (Fig. 8B1) shows that the projection areas of four individual stainings overlapped to a high degree. The areas where the overlap was less than 50% (blue to green) were excluded from the averaged sensory wing neuropil (Fig. 8B2). The

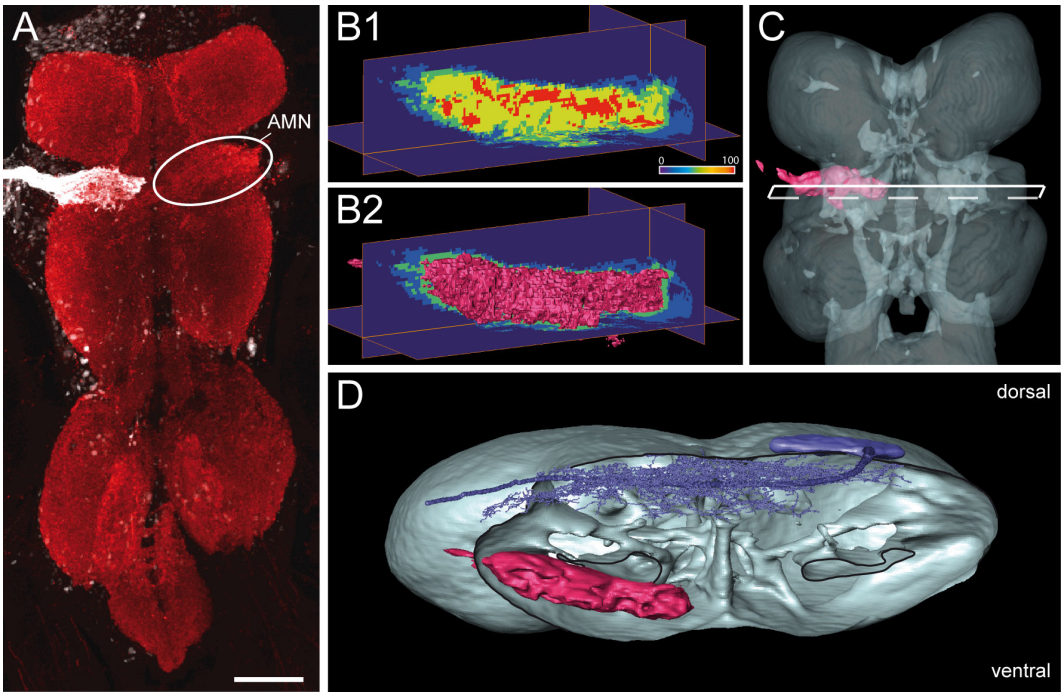

Figure 8: **Identification of the sensory neuropil of the wing in the ventral nerve cord:** **A**: Z-projection of 20m of the VNC from a confocal image stack. The neuropil is stained with NC82 (red). In a backfill experiment the sensory cells of the wing blade are anterograd filled with neurobiotin and visualized with a fluorescent dye (white). The sensory cells project into a small distinct area localized in the accessory mesothoracic neuromere (AMN). In the NC82 staining the AMN is visible through its higher staining intensity (encirceled). **B**: The projections of four backfills are registered into the standard by label field based registration and an average sensory wing neuropil is calculated. **B1**: Single slices in the three dimensions of the probability map for the sensory wing neuropil show a good overlap in a distinct area (red and yellow). The linear scale is color coded from 0% overlap (blue) to 100% overlap (red). **B2**: Only areas with an overlap of 50% and more are counted for the wing neuropil here visualized as a surface reconstruction in the probability map of B1. The area with less then 50% overlap is relative small (green and blue). **C**: Surface reconstruction of the averaged sensory wing neuropil (pink) in the neuropil standard (gray). Only the pro- and mesothoracic part of the standard are shown. The frame points the cutting plane for D out. **D**: For a better 3D visualization, the standard is cut along the AMN (frame in C) and tilted. The sensory wing neuropil (pink) lays on the ventral side of the neuropil. By visualizing one MN5-reconstruction (purple) in the standard it is clear that the dendrites of the MN5 and the projections of the wing sensory cells occupy different areas which do not overlap. Scale bar, 50 μm.

resulting charted volume is characterized by high probabilities for containing the terminals of wing blade sensory neurons. It can, therefore, be defined as wing sensory neuropil and displayed as an average 3-dimensional surface reconstruction within the standard (Fig. 8C). As described below, geometric reconstructions of the dendritic trees of flight motoneurons can also be registered into the standard if the original preparation was counterstained with NC82. This allows for simultaneous 3-dimensional display of standardized average wing sensory projections and flight motoneuron dendrites within the neuropil standard (Fig. 8D). The wing blade sensory projections within the AMN were localized in the ventral part of the neuropil between the pro- and mesothoracic neuromeres (Figs. 8C, D). No overlap of this neuropil areas with dendrites from flight motoneurons was observed, demonstrating that sensory information from the wing must be processed by interneurons before it is passed onto flight motoneurons. Mapping data form several different preparations into the standard allows for visualizing possible network connectivity with neuron populations that have been labeled in different experiments. The only prerequisite for standardized 3-dimensional visualization is that each experiment contains NC82 counterstaining.

The analysis depicted in figure 8 requires the registration of geometric 3 dimensional reconstructions of identified neurons into the standard. An AMIRA based tool set for quantitative geometric single neuron reconstructions from confocal image stacks has been published previously (Schmitt et al., 2004; Evers et al., 2005). These tools can be used to reconstruct the dendritic trees of individually labeled neurons (Fig. 9A), and are fully compatible with the AMIRA based standard registration tools used in this study. Geometric reconstructions yield precise 3-dimensional representations of the dendritic structure of individual neurons (Fig. 9B, white), and dendritic structure is conserved with respect to multiple metric parameters among different animals (Duch et al. 2008; Vonhoff and Duch, personal communication). However, to relate the structure of individual neurons to other structures revealed by labels in different preparations, geometric reconstructions had to be registered into a standard, because manual alignment of 4 representative ventral nerve cord preparations in which MN5 was stained and reconstructed resulted in a large spatial offset of all 4 single neuron reconstructions (Fig. 9D). By contrast, applying affine and non-rigid transformations as obtained by registering NC82 counterstaining onto the standard yielded much better overlap between the MN5 geometric reconstructions (Fig. 9E). Neuropil regions within the dendritic field, prominent for a lack of dendrites, were conserved by standard registration (Fig. 9E, asterisks). Therefore, the transformation procedures allowed for registration of individually labeled single

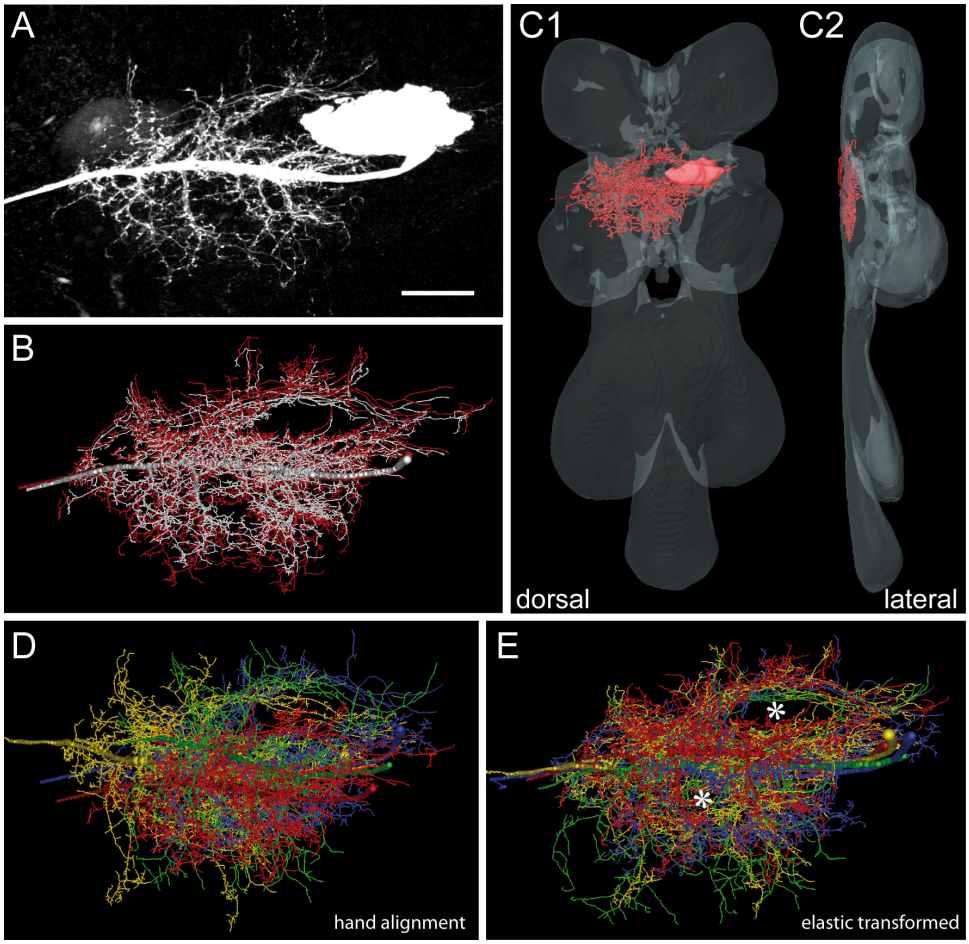

Figure 9: **Registration of geometric reconstructions of identified neurons into the standard: A:** Projection view of a confocal image stack of an intracellular stained motoneuron MN5, of a control animal W1118 crossed to C380-GAL4; UAS-mCD8-GFP, Cha-GAL80. **B**: The 3-dimensional reconstruction of the MN5 (white) was transformed (red) by registration onto the standard. **C**: Through transformation of a neuropil counter staining onto the standard the reconstructed MN5 could be registered into the standard. **C1**: Location of the registered MN5 (red) in the neuropil standard (gray) in a dorsal view. **C2**: In the lateral view of the transparent standard surface reconstruction the very dorsal position of the MN5 is visible. **D**: In the registration steps the original neuron reconstruction (white) is transformed (red) into the standard. Both versions are aligned manually by the position of their primary neurites to visualize the size and shape change due to transformation. **E**: Four single MN5 3-dimensional reconstructions of animals with different genetic background were aligned to each other manually by transforming their NC82 labels to a best fit in all three dimensions. **E:** The elastic transformed MN5s after registration of the according NC82 labels onto the standard. Red and yellow: W1118x C380-GAL4; UAS-mCD8-GFP, Cha-GAL80. Blue: D42xwtb. Green: C380-GAL4; UAS-mCD8-GFP, Cha-GAL80. Scale bar, 20 μm.

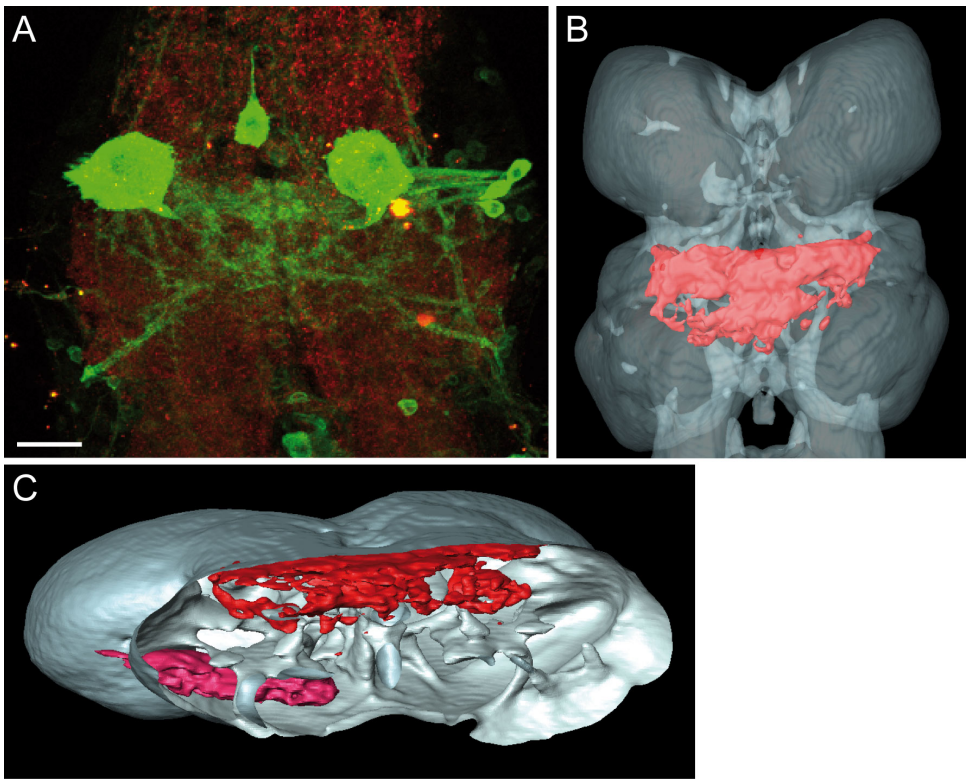

Figure 10: **Identification of the dendritic wing depressor motoneuron neuropil in the ventral nerve cord: A:** 20 μm projection view of the dorsal part of a confocal image stack of the mesothoracic neuromer of the ventral nerve cord. GFP expression of the D42-GAL4, Cha-GAL80, UAS-GFP line (green) was counterstained with NC82 (red). The cell bodies of the MN5s and the dendritic field of the motoneurons 1-5 are visible. **B:** For six samples the area of the dendritic field was transformed into a label field, registration and averaging of the six labels resulted in the dendritic wing depressor motoneuron neuropil (red) in the standard (gray). **C**: The tilted view of the standard shows that the wing neuropil (pink) is spatially separated from the dendritic motoneuron neuropil. Scale bar, 20 μm.

neurons into the standard, so that first hints towards putative neural connectivity maps could be obtained from registration of multiple different single neurons, or neuron populations into the standard. The difference of MN5 geometric structure as resulting from the transformation steps is depicted for one example reconstruction in figure 9B (white to red). The location of one transformed MN5 geometric reconstruction in the neuropil standard is shown in figure 9C1 and C2.

The example shown in figure 8 is based on combinatorial registration of retrograde labeling of sensory cells and geometric reconstruction of an intracellularly labeled motoneuron into the standard. The Drosophila system provides a large number of GAL4 driver lines which show predominant expression in specific classes of neurons (Sanyal, 2009). Examples for GAL4 lines that are commonly used to drive expression of transgenes in motoneurons are C380 (Sanyal et al., 2003; Sanyal, 2009), D42 (Parkes et al., 1998; Sanyal, 2009), OK6 (Sanyal, 2009), OK371 (Mahr

and Aberle, 2006) and RRA (Fujioka et al., 2003). These lines express predominantly in motoneurons, but also in a large number of other unidentified neurons. Expression can be further restricted by co-expression of the GAL4 inhibitor, GAL80, in all cholinergic interneurons under the control of the promoter for acetylcholine transferase (Kitamoto et al., 1992). Such a recombinant line, D42-GAL4, Cha-GAL80, UAS-GFP, was used to drive the expression of GFP predominantly in adult motoneurons. This yielded GFP expression in a large number of motoneurons (see below), among which are the depressor flight motoneurons innervating the dorsal longitudinal flight muscle (Fig. 10A, Consoulas et al. 2002). Segmentation of six individual stainings and their registration, as described above for the wing sensory projections, resulted in a probability volume representing the dendritic wing depressor motoneuron neuropil (Fig. 10B, red). Segmentation of the depressor motoneuron dendritic neuropil was not based on geometric reconstructions of the dendritic tree, but on a procedure that accepted all voxels above a set threshold that were interconnected (AMIRA magic wand tool). This resulting depressor motoneuron dendritic neuropil region was located in the dorsal part of the VNC (Power, 1948), and showed no overlapping volume with the sensory wing neuropil (Fig. 10C). This demonstrated a low probability for monosynaptic connection between wing sensory projections and any of the wing depressor flight motoneurons.

The neuropil standard could be sub-divided into different functional regions by registration of the projections of populations of neurons as demonstrated in figure 8, or by registration of GAL4 expression patterns that were obtained from preparations counterstained with NC82 (Fig. 10). Defining functionally different regions within the neuropil standard allowed for locating these regions in every preparation (Fig. 11A, yellow and white) that was counterstained with NC82 (Fig. 11A, red) without having to mark these regions by specific labeling. The standard neuropil label was therefore registered affine and elastic onto the segmented neuropil label of the sample and allowed for subsequent transformation of the defined sub-neuropils. Consequently, immunostainings derived from individual samples (Fig. 11B and C) could be compared by standardized anatomy to further analyze the structure of specific parts of the ventral nerve cord. One application of this was to test whether different neuropil regions of the standard contained similar compositions of synaptic terminals of specific transmitter classes. Terminals belonging to neurons of specific transmitter classes could be identified by pairing NC82 staining with immunostainings for the respective neurotransmitter (Fig. 11B and C). Labeling of GABAergic terminals was achieved with a GABA antibody (Fig. 11B, blue). To visualize cholinergic terminals of the neuropil GFP tagged Synapsine1 was expressed under the

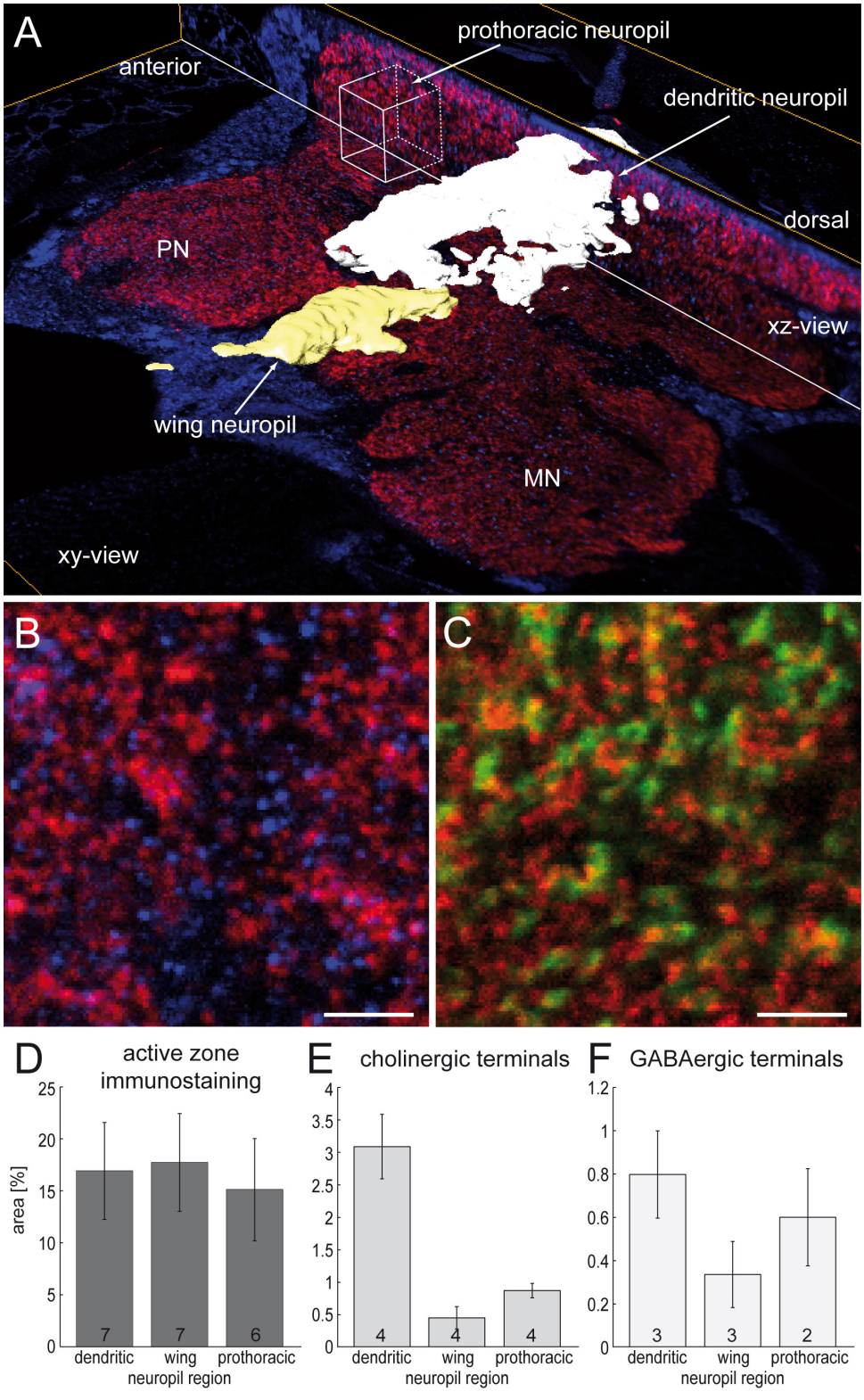
A
anterior
prothoracic neuropil
dendritic neuropil
dorsal
PN
xz-view
wing neuropil
MN
xy-view
B
C
D
active zone immunostaining
area [%]
25
20
15
10
5
0
7
7
6
dendritic
wing
prothoracic
neuropil region
E
cholinergic terminals
4
3.5
3
2.5
2
1.5
1
0.5
0
4
4
4
dendritic
wing
prothoracic
neuropil region
F
GABAergic terminals
1.2
1
0.8
0.6
0.4
0.2
0
3
3
2
dendritic
wing
prothoracic
neuropil region

control of the gene for choline acetyltransferase (cha) (Fig. 11C, green). Standard registration onto the samples then allowed for identification of specific neuropil areas. From high resolution confocal image stacks regions of interest could be defined which were positioned inside the sub-neuropil regions. Additionally one unidentified neuropil of the prothoracic neuromere was analyzed (see cube in Fig. 11A). For all samples single images from the regions of interest were analyzed separately for colocalization of transmitter staining and NC82 staining. About 17% of the analyzed neuropil area showed staining with NC82 in all 3 sub-neuropils (Fig. 11D). No obvious differences in active zone densities could be observed between the three neuropil regions for immunostainings. The depressor flight motoneuron neuropil showed higher densities for cholinergic (Fig. 11E) and GABAergic (Fig. 11F) terminals compared to the sensory wing neuropil. Cholinergic terminals covered 3% of the analyzed dendritic area and GABAergic terminals could be found in 0.8% of the analyzed depressor dendrite neuropil area.

Figure 11 *(preceding page)*: **GABAergic and cholinergic terminal densities in identified sub-neuropils: A:** Registration of the neuropil standard onto the neuropil staining of an individual sample allowed for subsequent transformation of identified sub-neuropils into the sample. The sensory wing neuropil (yellow) and the depressor flight motoneuron neuropil (white) could be localized within confocal image stacks of immunstainings for NC82 (red) and anti-GABA (blue). Single optical slices in xy- and xz-orientation show the prothoracic (PN) and mesothoracic neuromere (MN) of the ventral nerve cord. With the visualization of these sub-neuropils in individual samples regions of interest could be chosen from high resolution scans. Additionally one unidentified region of the PN was used for analysis (see cube). Colocalization of immunostainings for NC82 (red) and GABA (**B**, blue) and cha/Syn-GFP (**C**, green) were analyzed in single optical slices. Expression of Synapsin1-GFP under the control of the cha-driver allowed for visualization of cholinergic terminals. Colocalization of NC82 and anti-GABA is depicted in purple (B). Pixels with overlay for NC82 staining and Synapsin1-GFP-staining in cholinergic terminals is depicted in yellow (C). **D:** The relative areas with NC82 staining derived from the single image analysis for three different sub-neuropils were plotted with error bars. **E:** Areas with colocalization of cha/Synapsine1-GFP and NC82 were plotted relatively to the whole image area for all three sub-neuropils. **F:** Relative areas with colcoalization of NC82 and anti-GABA were plotted for all three sub-neuropils. Scale bars, 3μm.

5 User manual for standard registration

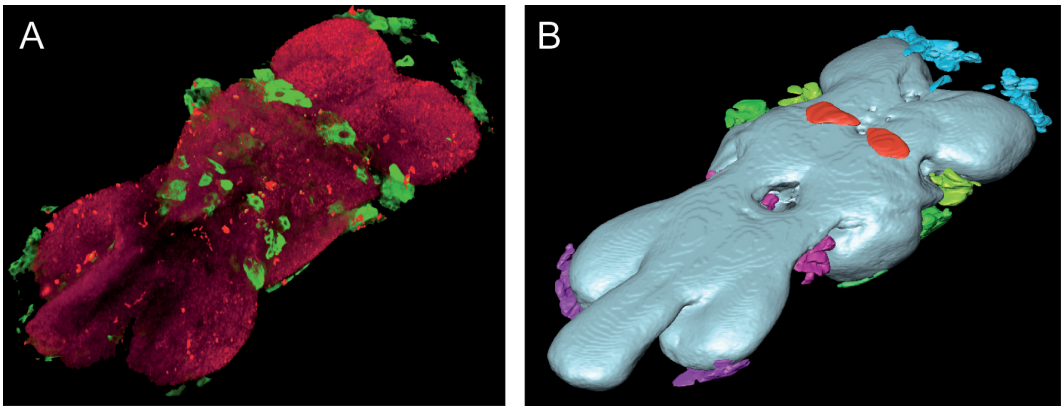

Figure 12: **Registration of GFP stainings into the ventral nerve cord standard:** A: Volume rendered view of a confocal image stack of immuno staining in the ventral nerve cord. GFP expression is driven in somata under the control of the C380 driver (green). The neuropil is counter stained with NC82 (red). B: Position of segmented somata (blue, red, green and purple) after the registration onto the standard (gray), surface reconstruction.

This is a protocol describing the usage of the ventral nerve cord neuropil standard of adult Drosophila for registration of anatomical data. Any structure of the ventral nerve cord can be mapped onto the standard in a standardized procedure. The structure of interest (Figure 12A, green) has to be counter stained with the commercially available antibody NC82 to label the entire neuropil (Figure 12A, red). The neuropil serves as the reference structure for the registration onto the standard (Figure 12B, gray) and the transformation can be applied onto the second structure successively (Figure 12B, blue, red, green and purple). All steps from dissection and data acquisition to registration and transformation onto the standard will be described in detail. Processing of the confocal image data and the registration steps are performed in Amira 4.1.1 (Mercury Computer Systems).

5.1 Immunostaining protocol for NC82

5.1.1 Dissection

5.1.2 Fixation

5.1.3 Primary antibody for NC82 counterstaining

5.1.4 Secondary antibody for NC82 label

5.1.5 Dehydration and embedding

5.2 Scan settings

5.3 Processing of image stacks

5.3.1 Transformation

5.4 Segmentation

5.1 Immunostaining protocol for NC82

Dissection

Immobilize female Drosophila in a vial on ice. After removing legs and wings pin the fly in a sylgarde dish with the dorsal side up. Make an incision along the dorsal midline from the abdomen to the cervical connective. Open the thorax by piercing fine pins through the flight muscles. Remove the head, gut, hart and glands to expose the ventral nerve cord.

Fixation

Fixate the samples in 4% PFA in phosphate buffer solution (PBS, Calbiochem) for 30-45 minutes at room temperature. Rinse the samples for 1 hour in PBS.

Primary antibody for NC82 counterstaining

Rinse the samples in PBS with 0.5% Triton X-100 (TX, Sigma) for 9x20 minutes at room temperature. Dilute the monoclonal antibody NC82 (mouse, developed by Erich Buchner obtained from the Developmental Studies Hybridoma Bank developed under the auspices of the NICHD and maintained by The University of Iowa, Department of Biological Science Iowa City, IA, 52242) at a concentration of 1:100 in PBS 0.3% TX with 10% albumin from bovine serum (BSA, Invitrogen). Apply antibodies for a second label together with NC82. In case you want to use expression of GFP for visualization of a second structure, you should enhance the GFP signal with a GFP-antibody (e.g. anti-GFP produced in rabbit, 1:400, Sigma). Incubate the samples in the antibody solution for 2 nights at 4 °C.

Secondary antibody for NC82 label

Rinse the samples for 8x15 minutes in PBS. Dilute a Cy5 Goat Anti-Mouse (Jackson ImmunoResearch) antibody 1:500 in PBS to label NC82. Choose another fluorescent dye coupled secondary antibody for your second label (e.g. Cy2 Goat Anti-Rabbit, 1:500). Incubate the samples for one night in the secondary antibody at 4 °C in the dark.

Dehydration and embedding

Rinse the samples for 6x15 min in PBS. Perform a ascending ethanol series with 50%, 70%, 90% and 100% ethanol in 10 minute steps. Remove the flight muscles and transfer the samples on a object slide in a 1:1 mixture of pure ethanol and methyl salicylate. Replace the solution after 5 minutes with pure methyl salicylate. To avoid squeezing of samples it is best to use customized object slides. For example a 100 μm thick metal slide (7.5 x 2.5 cm) with a whole (1 cm in diameter) in the center. One cover slip (22 mm x 22 mm) glued on one side of the slide as the bottom. Cover the samples with a cover slip (18 mm x 18 mm, 0.1 mm thick). Seal the sides with clear nail polish.

5.2 Scan settings

The confocal image stacks should have a voxel size of approx 0.3 x 0.3 x 0.7 μm. With a Leica SP2 and a 40x oil lens (NA 1.25) this resolution can be achieved by setting the scan format to 1024x1024 with a 1.5x zoom and a step size of 0.7 μm. Orientate the samples dorsal side up in a straight angle for scanning and set the scan direction from dorsal to ventral, to avoid bleaching of dorsal sections while scanning the ventral part. Scan the whole ventral nerve cord in slightly overlapping fields of view.

5.3 Processing of image stacks

Resample the stacks to a pixel size of 0.4 x 0.4 μm with the 'Resample' tool in Amira. Align the stacks of different fields of view in Amira in x, y and z. (see transformation) Merge the stacks with the 'Merge' module choose 'Standard' interpolation and the 'blend Options'. Make sure to process all channels of one stack in the same way.

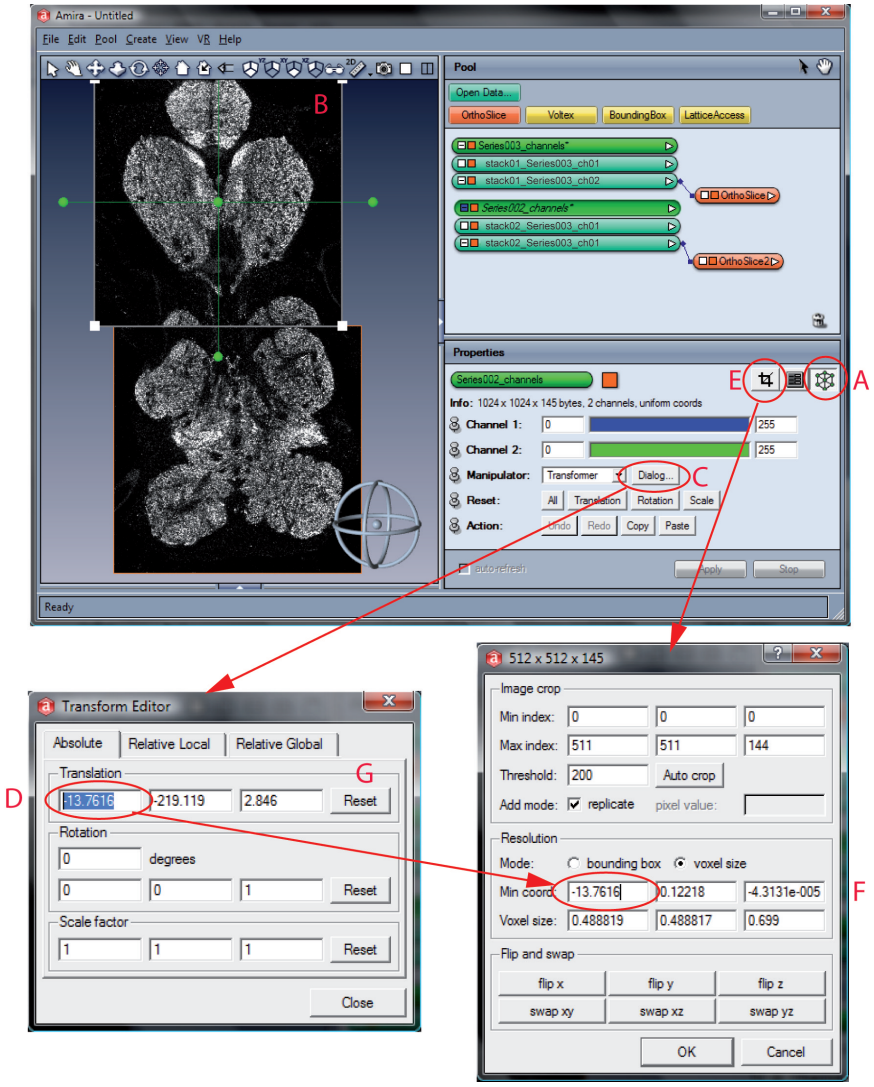

Figure 13: **Transformation of confocal image stacks in Amira:** Activation of the Transform Editor (A) allows the positioning of stacks in x, y and z in the Viewer (B). The new coordinats (D) are copied from the Transform Editor (activated with the Dialoge (C) button) to the Crop Editor (E, F). With the Reset button (G) the new coordinates are applied to the stack.

Transformation

Activate the 'transform editor' for the stack that has to be transformed (Figure 13A). Drag the stack in the viewer to the right position (Figure 13B) in x, y and z. To apply the new location to the file open the 'dialog' box in the transform editor (Figure 13C). Copy the values for x, y and z separately from the 'Translation' panel (Figure 13D) into the 'Resolution' panel of the crop editor (Fig. 13 E) and replace the 'Min coord' values (Figure 13F). Set the values in the dialog box to 0 with the 'Reset' button (Figure 2G). Save the transformed stack.

5.4 Segmentation

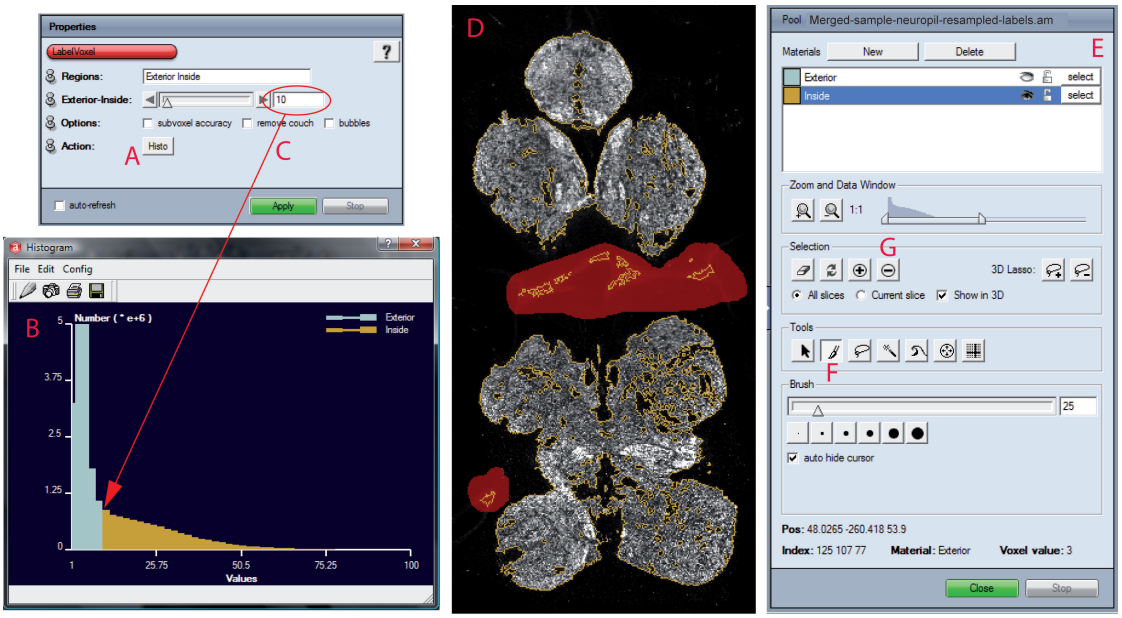

Figure 14: **Segmentation of the neuropil staining:** With the 'Histo' button (A) in the 'LabelVoxel' module a histogram for all gray values is generated (B). The value where the curve has its steepest negative slope (arrow) is set as the threshold (C). In the segmentation editor (D, E) the label field can be modified manually. With the brush tool (F) areas can be selcted (D, red) an deleted from the material (G).

For segmentation of the neuropil staining into a label field in Amira, connect the 'label voxel' tool with your neuropil stack. The option 'Histo' in the 'label voxel' properties (Figure 14A) blots the distribution of all pixels for the values 0 to 255. Set the y-axis on linear and adjusting the range to a reasonable value. A clear step should be visible in the histogram. Apply this value as the threshold (Figure 14C) between 'Exterior' and 'Interior'. Process the resulting label field in the 'label editor' (Figure 14D/E). The border between interior and exterior is visualized by the yellow line (Figure 14D). Remove smaller islands with the 'remove islands' function from the menu bar under 'Segmentation'. Set the 'size' to 15 and select the option 'all stacks'. Apply a 'smoothing' of 2 for 'all stacks' with the smooth function. Remove mislabeled structures like auto fluorescent cuticle outside the neuropil boundaries (Figure 14D, marked red) with the 'Brush' tool in the label editor (Figure 14F, red areas) from the material 'Interior' (Figure 14G).

Incorporation of the second structure

For segmentation of expression patterns (e.g. GFP staining) create a 'LabelField' connect to your image stack. Use the tools in the segmentation editor for the generation of the label field. Alternatively use the 'LabelVoxel' module. Intracellular

stainings of single neurons can be transformed into a geometric reconstruction for the registration (see Schmitt et al. 2004). Confocal image stacks do not need to be processed for registration.

5.5 Affine registration

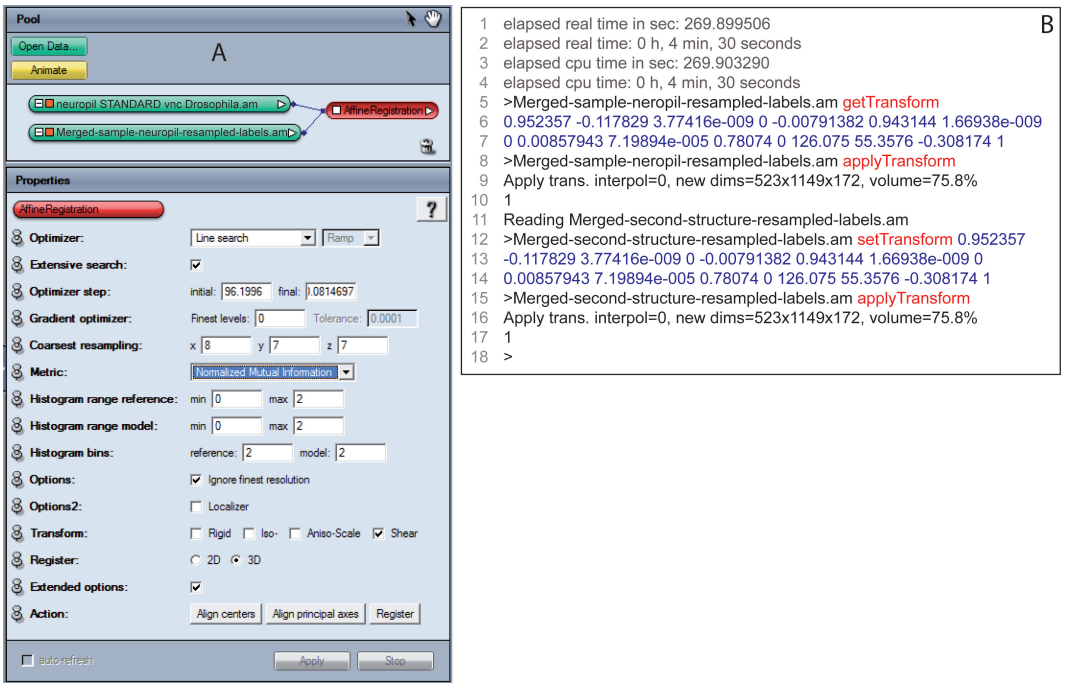

Figure 15: **Affine registration of lable fields onto the standard:** A: The 'AffineRegistration' module is connected to the reference and the sample label field. Registration settings can be set in the 'Properties'-window. B: Part from the command window to show the commands for the transformation of files. The commands to access, apply and set the matrix are highlighted in red, the matrix is highlighted in blue.

Connect the neuropil label field to the AffineRegistration tool in Amira and to the standard label as the reference (see Figure 15A, Pool-window). The properties for the affine registration are shown in Figure 15A (Properties-window). All values depend on the resolution of the label fields and can differ from this example. Some of the settings can be adjusted to get a more precise registration (see 'help' for this module in Amira). Align the labels to each other with the 'Align centers' button before using the 'Register' button. After the affine registration the transformation matrix can be accessed with the 'getTransform' command. Figure 15B shows an example for the steps done after the registration in the Command-window. Choose the transformed label in the Pool-window, by pressing the 'Tab'-key the file name can be copied into the command line of the Command-window (line 5). Enter 'getTransform' (line 5, red) to display the 12 values of the matrix (line 6-7, blue).

To apply the matrix to the label, enter behind the file name the 'applyTransform' command (line 8, red). Save the affine transformed neuropil label.

Affine transformation of the second label

Open the label of the second structure. Enter the file name of your second label in the Command-window (Figure 4B, line 12). Type 'setTransform' and enter the 12 numbers of the matrix (without a line break) behind the file name (line 12-14) of your label field. Apply the matrix with the 'applyTransform' command (line 15). Save the transformed label field. Transformations of image stacks and geometric reconstructions can be performed in the same way.

5.6 Elastic registration

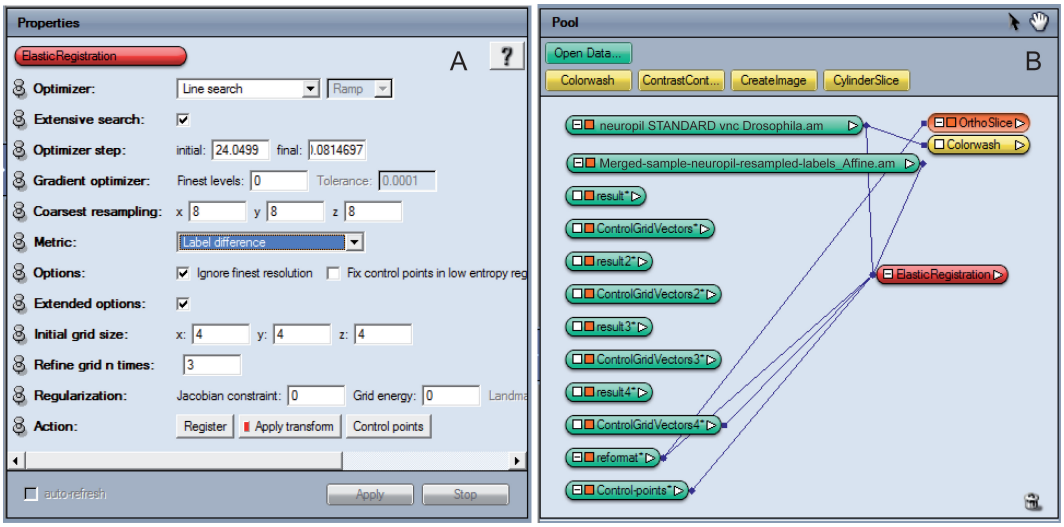

Figure 16: **Elastic registration of lable fields onto the standard:** A: Paramters for the registration can be set in the 'Properties'-window of the 'ElasticRegistration' module. B: The 'Pool'-window after the registration. The standard and the affine transformed label are connected to the module. The result of the registration are a 'reformat' file and the 'Control-points'.

Registration and settings

Connected the affine transformed neuropil label to the ElasticRegistration modul and to the standard as the reference. The settings are shown in Figure 16A. Use the 'Register' button to start the registration. The 'reformat' file is the result of the registration (Figure 16B). Save the reformat.

Apply the transformation onto a second label or image stack

To apply the registration onto another label field or image stack it is necessary to continue right after the elastic registration. A later transformation after restarting the Amira software is not possible. For the transformation of a label or image stack open the ControlPoints with the button 'Control points' in the elastic registration properties (Figure 16A). Open your label or image stack and connect it to the 'ElasticRegistration' module as the 'Data', this disconnects it from the neuropil label. Disconnected the reformat from the 'ElasticRegistration' module. Keep the connection to the control points (see Figure 16B). Use the 'Apply transform' button in the Properties-window to apply the transformation. You get a new reformat in the Pool-window. Save this file.

Apply transformation onto a geometric reconstruction

For transformation of skeleton trees the vector field will be needed instead of the control points. Open the vector field with the button in the Properties-window after the elastic registration. Connect the skeleton tree to the ApplyDeformation module and the vector field and apply the transformation. Save the elastic transformed file.

6 Distribution of putative monosynaptic sensory inputs on the Drosophila MN5 dendrite

Proprioceptive feedback from sensory neurons can influence centrally generated motor rhythms (Pearson et al., 1983; Reye and Pearson, 1988). Monosynaptic connections between the wing hinge stretch receptors and flight motoneurons have been shown in locust (Burrows, 1975; Peters et al., 1985). In double stainings of sensory and motoneurons first estimations were made about the quantity of synaptic contacts between both neurons (Peters et al., 1985). With new staining, imaging, and computational techniques putative synaptic contacts on the dendrite of a motoneuron can be visualized in three dimensions and make fast quantitative analyses possible (Duch and Mentel, 2004; Evers et al., 2006; Meseke et al., 2009b). For Drosophila monosynaptic contacts between the dendrite of the flight motoneuron MN5 and its presynaptic partners have never be shown. With GFP-targeting of a subset of sensory neurons and intracellular staining of the MN5 in the same preparation, putative presynaptic input sites on the MN5 dendrite could be indicated.

The pickpocket gene (ppk) encodes for a degenerin/epithelial sodium channel (DEG/ENaC) subunit that is expressed in mechanosensory neurons (Adams et al., 1998). A PPK-EGFP reporter line (Grueber et al., 2003) was used to investigate peripheral soma locations (Fig. 17C, E, F) and central axon projections (Fig. 17A, green) of PPK expressing neurons. The neuropil of the VNC was counterstained with NC82, an antibody against the synaptic localized protein Bruchpilot (Wagh et al., 2006). In confocal image scans it could be verified that no PPK positive somata were located in the ganglionic cortex surrounding the neuropil (Fig. 17A). The expression is restricted to neurons with somata locations in the periphery (not shown). The majority of PPK positive central projections entered the VNC via the leg nerves, the abdominal nerves and the anterior dorsal mesothoracic nerve (ADMN, named after Power (1948)) and posterior dorsal mesothoracic nerve (PDM) of the mesothoracic neuromere (MN, Fig. 17A). Most abdominal trunk afferents terminated in the abdominal center (AC, Fig. 17A). The number of axons, entering the VNC via the ADMN and the PDM were counted for 4 preparations. Four axons projecting to the mesothoracic neuromere were identified in the ADMN and 4-5 axons in the PDM. In a transversal view of the mesothoracic neuromere (Fig. 17B, from the region of interest as depicted in A) it was noticeable that these PPK positive axons have two distinct projection areas within the mesothoracic neuropil. The majority of the projections could be observed in more ventral neuropil areas (Fig. 17B, white arrow), only a few axons were projecting to the very dorsal neuropil

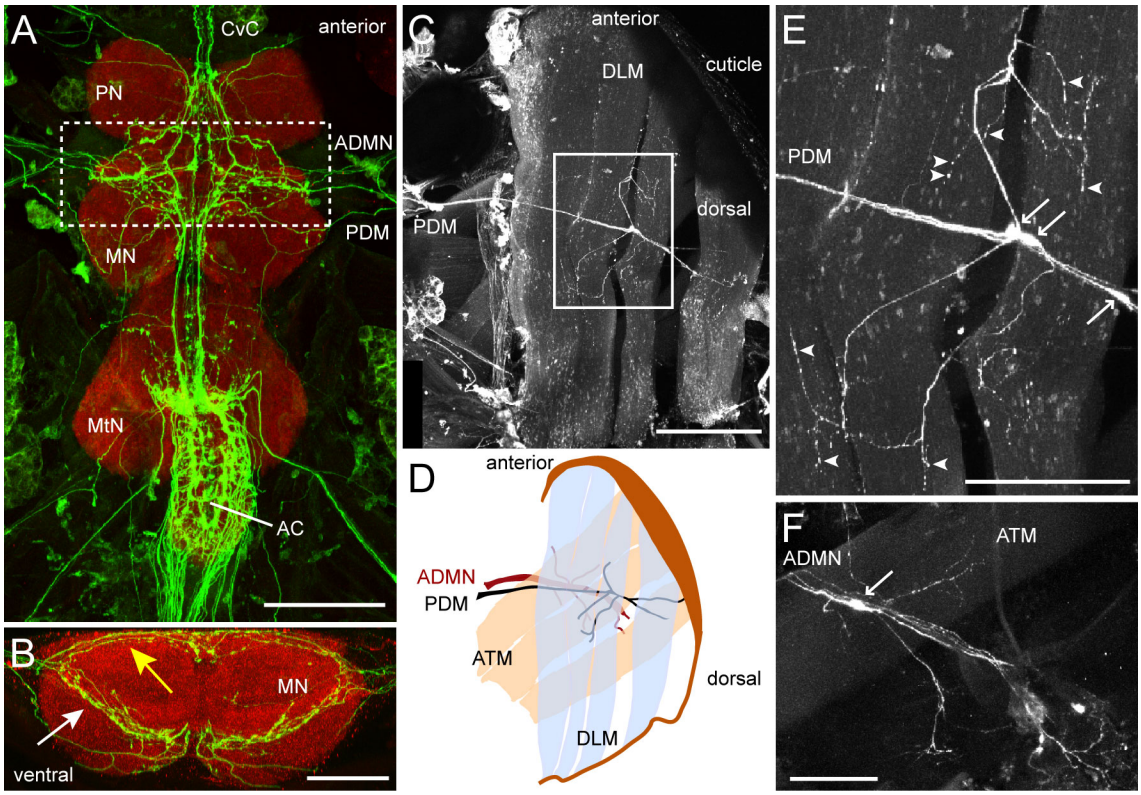

Figure 17: **Expression pattern of PPK in the ventral nerve cord and the thoracic muscles of adult Drosophila: A**: Dorsal view of a projection along the dorso-lateral-axis from confocal image stacks of immuno stainings in the ventral nerve cord (VNC) of Drosophila. Expression of PPK as revealed by a PPK-GFP reporter (green) is restricted to neurons in the periphery, no somata are located in the cortex of the VNC. The neuropil of the VNC is counterstained with NC82 (red). Axonal projections enter the mesothoracic neuromere (MN) through the anterior dorsal mesothoracic nerve (ADMN) and the posterior dorsal mesothoracic nerve (PDM). Some fibers project from the abdominal center (AC) median through the metathoracic neuromere (MtN), the MN and the prothoracic neuromere (PN) to the cervical connective (CvC). The frame depicts the region of interest for **B**: Transversal view from posterior of the MN as a maximum projection view. PPK positive axons entering the MN project to ventral (white arrow) and dorsal neuropil regions (yellow arrow) within the neuromere. **C/E/F**: Lateral projection views from parts of the right thorax. Muscles and cuticle are visible due to autofluorescence. **C**: Sensory axons in the PDM can be followed back to the dorsolongitudinal indirect flight muscle (DLM) fibers. On the lateral side of the DLM, PPK positive processes leave the main nerve and branch onto the muscle fibers (frame). **D**: Schematic drawing of the muscle fibers and the nerve branches containing PPK positive axons from the preparation in C. The PDM (black) projects laterally on the DLM (light blue). The ADMN (red) projects to areas close to the body wall, branches leave the main nerve laterally of the anterior tergosternal muscle (ATM). **E**: Close up from C. Projection view of 50 μm from the DLM muscle fibers. Within the nerve branch spindle shaped cell bodies are visible (open arrows). Varicosities can be observed along the processes on the muscle (arrow heads). **F**: PPK positive axons, entering the VNC via the PDM, can be followed back to an area lateral of the ATM, close to the body wall. One spindle shaped soma along the nerve is marked with an arrow. Scale bar, 100 μm (A, E, F); 50 μm (B); 200 μm (C).

(Fig. 17B, yellow arrow). Both projection areas had a small dorso-lateral extension and no branching into neighboring dorsal and lateral neuropil areas. The ADMN and the PDM were projecting to the muscle fibers of the thorax (Power, 1948). In muscle preparations where the nerve connections to the VNC were left intact (Fig. 17A, C), the nerves containing PPK positive axons could be followed to the periphery. PPK positive axons in the PDM were observed in nerve branches close to the dorsal longitudinal flight muscle (DLM, Fig. 17C, D) and axons in the ADMN were seen in nerve branches close to the anterior tergosternal muscle fibers (ATM, Fig. 17F). For a better visualization of the position of the thoracic muscles relative to one another and to the nerve projections, a schematic drawing is shown in figure 17D. The DLM lies medial in the dorsal thorax and is composed of 6 fibers. Not all 6 fibers could be kept intact in this sample. The ATM lies lateral to the DLM and is composed of 3 fibers. The peripheral projections of the PDM branches (black) and the ADMN branches (red) containing PPK positive axons are indicated schematically. In close up views from the termination area of the PDM, PPK positive spindle shaped somata could be observed in the nerve (Fig. 17E, arrows). From these somata dendritic processes extend anteriorly and posteriorly onto the muscle fibers of the DLM. The processes arborized on the muscle and along the dendritic processes varicosities were present (Fig. 17E, arrow heads). Axon projections in the ADMN could be followed to the periphery to more lateral areas in the thorax. Three axons originated in an area between the body wall and the fibers of the ATM. Close to one ATM fiber a spindle shaped soma in the ADMN nerve branch was detected (Fig. 17F, arrow).

The fibers of the DLM are innervated by 5 flight motoneurons (MN1-MN5, Coggshall 1978; Ikeda and Koenig 1988; Consoulas et al. 2002). Postembryonic development, morphology, and physiology of the MN5 are well investigated (Consoulas et al., 2002; Duch et al., 2008). The soma of the MN5 lies on the dorsal surface of the VNC and is easyly identifiable, what makes the MN5 accessible for intracellular staining methods. Most of the MN5 dendrites branch in the dorsal-most 20 μm of the mesothoracic neuromere (Coggshall, 1978). As shown in figure 17B, central axon projections of PPK positive neurons could be detected in the dorsal neuropil. To verify a possible contact between the axon terminals of the PPK expressing neurons and the dendrites of the MN5, double stainings for both structures were performed within the same preparation. A PPK-GFP;UAS-dsRed line was crossed to a motoneuron specific GAL4 line (C380, Budnik et al. 1996). The dsRed signal in the soma of the MN5 was necessary for identification of the soma location for intracellular dye injections into the MN5. The GFP-signal of PPK expression was enhanced with a GFP-antibody. In the heterozygous PPK-GFP animals GFP expression was

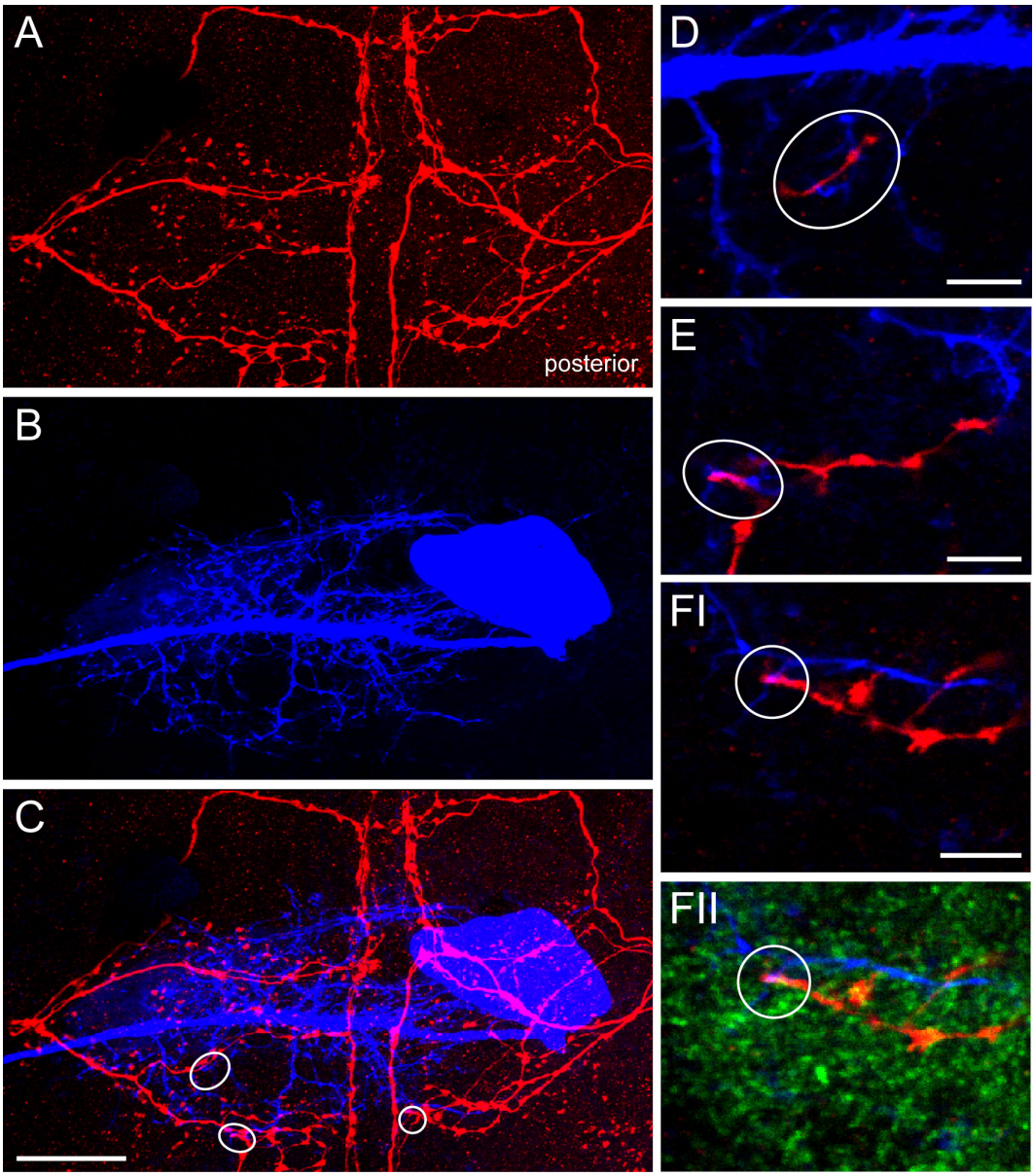

Figure 18: **Axonal projections of Pickpocket positive neurons colocalize with dendrites of the MN5: A-C**: Dorso-lateral-projections of confocal image stacks for 20 μm of the dorsal neuropil in the mesothoracic neuromere. **D-F**: Single optical slices from the same confocal image stacks as in A-C. **A**: Immuno staining of GFP-expression under the control of ppk (red). PPK positive axon projections enter the mesothoracic neuromere from the periphery of both body sides and branch in the mesothoracic neuromere. The processes do not cross the midline. **B**: Intracellular staining of the flight motoneuron MN5 in the same preparation (blue). The dendrites occupy the same area in the mesothoracic neuromere as the PPK positive axons as revealed in **C**: Overlay of both stainings from A and B. The encircled areas depict regions of overlap of both stainings. These regions are enlarged in D-F. **D-FI**: Areas with overlap (purple) from different parts of the dendritic tree. **FII**: The same view as in FI. In a third channel (green) the active zones are labeled with the NC82 antibody. Putative presynaptic terminals on the MN5 are visible as an overlay of all three stainings. Scale bar, 20 μm (C); 5 μm (D, E, FI).

visible in 3 axons in the PDM and 1-2 axons in the ADMN. The central axon projections are displayed in figure 18A as a maximum projection view from the dorsal area of the mesothoracic neuromere (same ganglion region as depicted in figure 17A, frame). No axon branches crossing the midline could be observed. The soma, axon, and dendritic field of the MN5 in the same field of view is visible in figure 18B. The soma lies contralateral to the target muscle, dendritic branches project anteriorly and posteriorly from the primary neurite into both hemisegments. In an overlay view of both stainings the overlapping projection areas of MN5 and PPK positive neurons were noticeable. In closeup views from different areas of the dendritic tree in high resolution confocal images (Fig. 18D-F) colocalizations of both stainings could be seen as purple areas (see circles). Contacts between axon terminals and dendrites were restricted to small patches, they did not extend over large areas. For a verification of presynaptic sites a counterstaining for active zones with NC82 was performed in the same preparation (Fig. 18FII, green). With a scanning resolution of 100x100x300 nm, overlay of all three channels showed a close proximity of axon, pre-synaptically localized protein and dendrite and could therefore be interpreted as putative presynaptic terminals on the MN5 dendrites (Evers et al., 2005; Hohensee et al., 2008).

For a better three dimensional visualization of the branching areas for PPK positive axons and dendrites of the MN5, geometric reconstructions (Schmitt et al., 2004; Evers et al., 2005) were generated exemplarily for one preparation (Fig. 19). The soma of the MN5 was excluded from the reconstruction and its position is pointed out by an asterisk (Fig. 19). PPK positive branches (Fig. 19, red) from both body sides are interweaved with the dendrites of the MN5 (blue). On the posterior side of the dendritic field, both projections terminated in the same area (Fig. 19A). In a transversal view from posterior (Fig. 19B) it was visible that transversal branching axons were projecting to areas dorsally to the MN5 dendrites, whereas medially projecting axon fibers proceeded on the ventral side of the dendritic field.

For 4 preparations with triple stainings for PPK-GFP, MN5, and NC82 the dendritic trees of the MN5s were geometrically reconstructed. To test how many putative presynaptic PPK positive terminals have contact with MN5 dendrites, colocalization analysis was performed as described in Evers et al. (2005). Briefly, the staining intensity for all PPK-GFP positive voxles in close proximity (300 nm) to the reconstructed dendrite were measured and projected onto the surface of the reconstruction. The same measurements were performed for the NC82 stainings separately (not shown). Correlation of both measured intensity resulted in an intensity map for the dendrite surface (Fig. 20). Warmer colors indicated higher staining

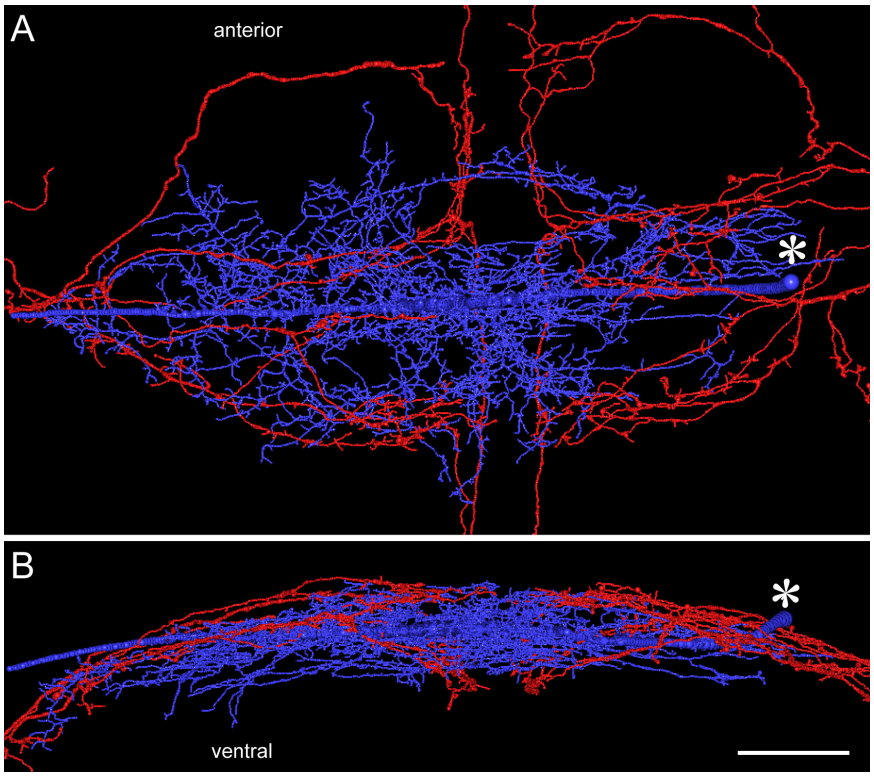

Figure 19: **Geometric reconstructions for PPK positive axons and MN5 dendrites in the ventral nerve cord:** A: Dorsal view of geometric reconstructions of PPK positive axons (red) and the dendritic tree of the flight motoneuron MN5 (blue) in the mesothoracic neuromere of adult Drosophila. The approximate position of the cell body is marked by an asterisk. Axons and dendrites share the same projection areas. B: Transversal view from posterior from the same preparation as in A. Most of the axon projections are located dorsally to the MN5 dendrites. Median axon fibers proceeded on the ventral side of the dendritic field. Scale bar, 20 μm.

intensities for both stainings, and colder colors indicated lower correlated staining intensities. For analysis only areas with high colocalized staining intensities were counted. The described mapping method can result in a good approximation for sites of chemical output synapses as demonstrated in a correlative electron and confocal microscopy study (Hohensee et al., 2008). The threshold was adjusted to a value, where colocalization of all 3 stainings could be verified in the original image data (see Fig. 18FII). The somata of the MN5s were excluded from the surface for all analyses. High staining intensities of the somata made a mapping of immuno stanings onto the surface imprecise. Since the PPK positive axons do not cross the midline, the dendritic tree of the MN5 could be analyzed for putative input sites from both body sides separately. The midline of the ganglion is depicted by a line in the example in figure 20.

Each dendritic segment that showed a colocalization on its surface resulting from the correlated intensity maps (see red areas in Fig. 20) was counted as one presynaptic input site. The numbers of input sites were counted for all 4 samples on

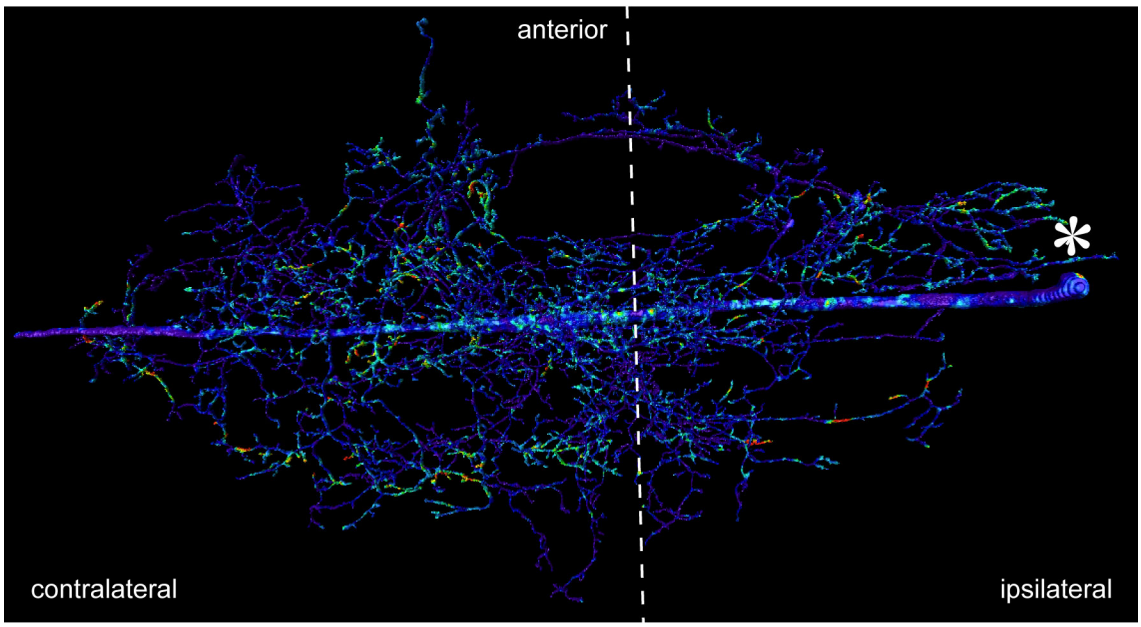

Figure 20: **Putative presynaptic sensory inputs on the MN5 dendrite:** Surface reconstruction of one MN5 from a dorsal point of view. High colocalized staining intensities of NC82 and PPK-GFP stainings in close proximity ($\leq$ 300 nm) to the dendrite surface are visualized color coded on the surface. Warmer colors indicated higher staining intensities for both stainings, and colder colors indicated lower correlated staining intensities. The ganglionic midline is depicted by a dashed line. The soma is located on the ipsilateral ganglion side and its position is pointed out by an asterisk.

the whole dendritic tree, the contra-, and ipsilateral dendritic tree part. The total amount of putative presynaptic input sites on the dendritic trees of the MN5s were 119±22. Summation of surface areas with colocalization resulted in an average area of 0.5937±0.3289% of the total dendritic surface. On average 3/4 of putative input regions were located on the contralateral side of the dendritic tree, the side of the target muscle. With the used staining and analysis methods putative presynaptic input sites could be localized on the MN5 dendrite, based on contacts of dendrites with PPK positive axons that were also NC82 positive at the contact site. This did not allow for estimations of numbers of active zones or strength of synapses. Within presynaptic terminals several chemical synapses can be found (Hohensee et al., 2008). Large areas of colocalization might therefore display several synaptic contacts. Furthermore, several terminals might be to close to each other to get a good separation with the resolution of confocal images from immunostainings. Putative presynaptic input areas on the dendrites varied from 0.004 to 5.9 μm^2 in all 4 preparations.

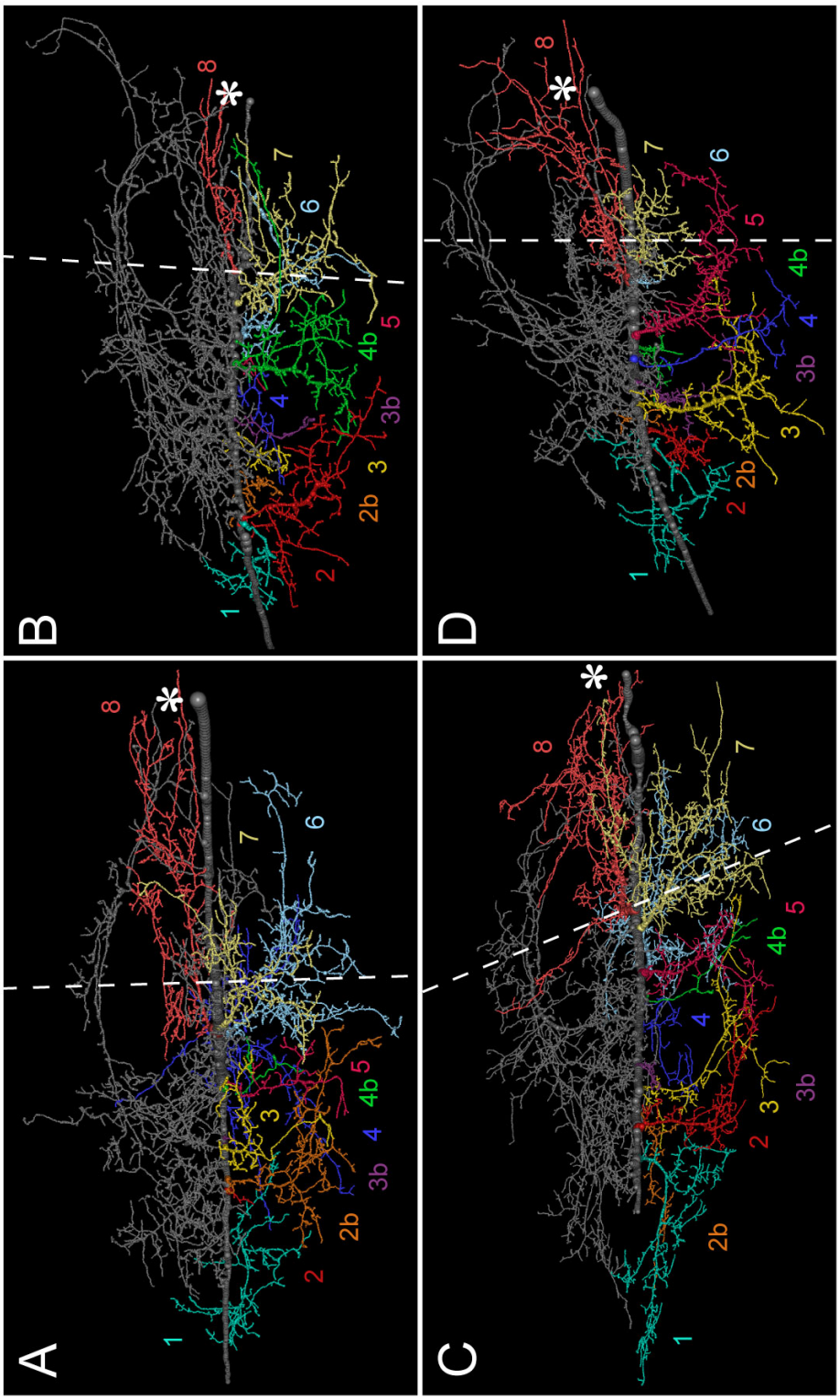

Figure 21: **Identification of dendritic subtrees for 4 MN5s:** Dorsal view of geometric reconstructions of 4 MN5s. Eleven subtrees that could be identified in each sample are displayed color coded, same colors were assigned to same subtrees between the preparations. The subtrees were labeled with numbers starting on the contalateral side of the tree. Ten subtrees were projecting posteriorly and one subtree was projecting anteriorly. Not all dendrites of the MN5s were identified the remaining tree parts are shown in gray. The position of the somata is indicated by an asterisk. The ganglionic midline is depicted by a dashed line.

The dendrites of the adult MN5 showed typical projection patterns (Coggshall, 1978) that could be observed during metamorphosis (Consoulas et al., 2002). In crickets it was shown that sensory neurons innervating hairs on the cerci which are sensitive to specific wind directions projected on specific branches of their post-synaptic interneurons (Murphey et al., 1984; Miller and Jacobs, 1984). To test for the hypothesis that axonal projections of PPK positive neurons made contact with specific dendritic subtrees, the dendritic tree of the MN5 was subdivided into subtrees. Subtree identification was performed in cooperation with Fernando Vonhoff (unpublished data). Ten posteriorly and one anteriorly projecting branch were identified and are displayed color coded in figure 21 for the 4 MN5s separately. The subtrees were originating from the primary neurite of the MN5 reconstructions and were numbered from the contralateral to the ipsilateral end of the primary neurite. These subtrees could be identified in all 4 reconstructions. Subtrees where a classification was not possible are depicted in gray. Thus, most of the posterior dendritic field could be analyzed for location of presynaptic input sites on subtrees. The analyzed surface covered on average 51.5±8.4% of the whole dendritic surface.

The numbers of putative input sites derived from the correlated mapping were calculated for each of the 11 identified subtrees. A summery for all counts is plotted in figure 22A. Colors of the single bars accord to the subtree colors in figure 21. The MN5 identity is according to the figure numbers (21A, 21B, 21C and 21D). Subtrees 1, 2, 2b, 3, 7 and 8 had high numbers of input sites compared to the other subtrees. The highest number of input sites (28) was observed for subtree 2b in sample 21D. Subtrees 4 and 5 had no input sites in sample 21B and 5C. The size of single subtrees varied between preparations (see Fig. 22B), but the number of input sites was not simply depending on subtree size (Fig. 22C). The relative surface area of each subtree to the whole dendritic tree is plotted in figure 22B. Subtrees with relatively large surface areas (see subtree 6 of 21C and subtree 4 of 21A) did not necessarily have high numbers of input sites. Small subtrees had relatively low numbers of input sites. The relation of number of input sites on subtrees to relative surface area of the subtrees is plotted in figure 22C, revealing that subtree 3 had relatively high numbers of input sites relatively to its surface. Summation of all input sites on the identified subtrees showed that on average 63.2±7.5% of all input sites of the whole dendritic tree were located on the identified subtrees.

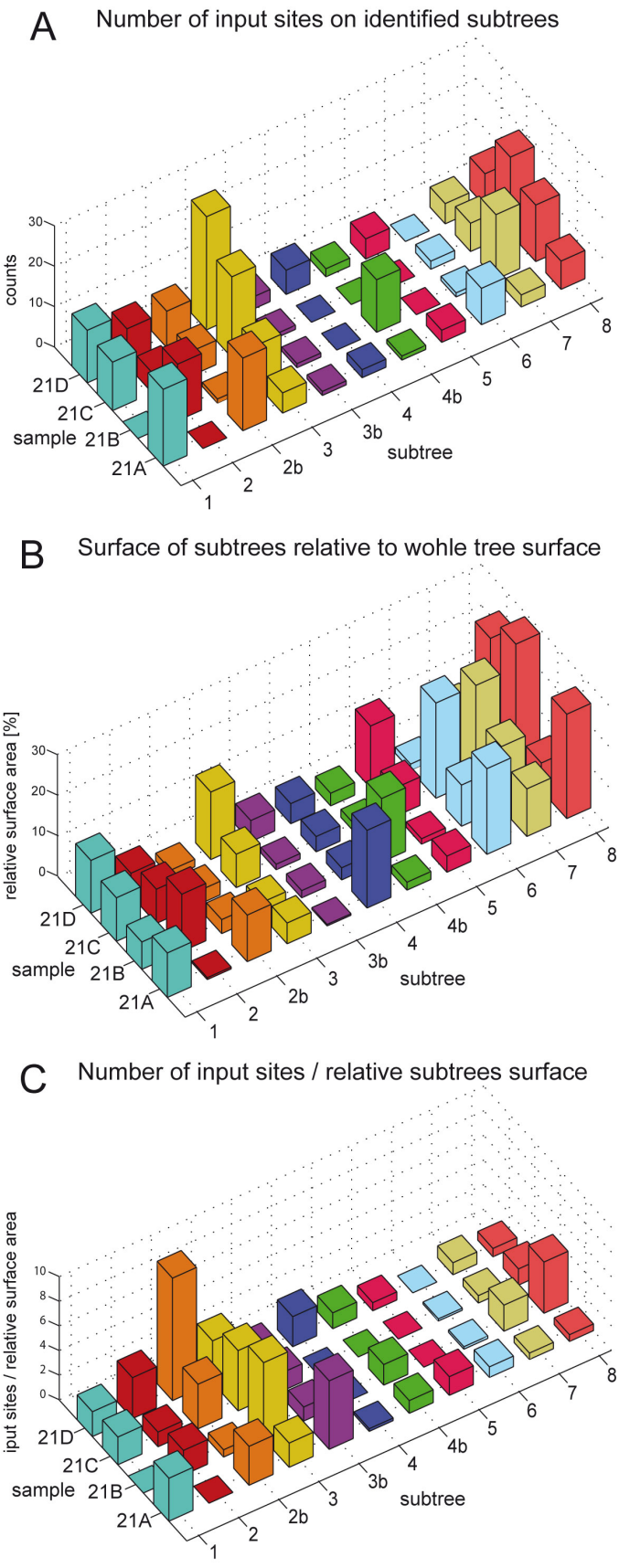

Figure 22: **Putative presynaptic input sites on identified subtrees of the MN5 and relative size of the subtrees: A:** For 11 identified subtrees putative input sites are plotted separately. The subtree ID is indicated by different colors. The 4 samples accord to the 4 different MN5 reconstructions (A, B, C, and D) in figure 21. **B:** Relative surface area of each identified subtree to the whole dendritic tree surface for all 4 samples. **C:** Relation of number of input sites on the identified subtrees to the relative surface area.

7 Discussion

For the ventral nerve cord of adult Drosophila melanogaster a standard atlas was generated, which will be available to the scientific community at http://sols.asu.edu/ people/ faculty/ cduch.php. This webpage will contain the standardized ventral nerve cord for download, as well as detailed instructions for the histological protocols needed to prepare specimen for standardization, the segmentation, and the registration processes. Below the quality of this standard and its validity for various applications is discussed.

Quality of the ventral nerve cord standard

For the standard generation a shape-averaging procedure, similar to the iterative shape-averaging (ISA) protocol, described for the honey bee (Brandt et al., 2005) and the locust brain (Kurylas et al., 2008) was used. The ISA protocol yields into a standard that compensates for individual differences and allows combining of data from individual samples. One sample serves as the reference for the affine transformation. This start sample was chosen based on two criteria. First, it showed a high NC82 immunostaining quality, i.e. full and even antibody penetration throughout the tissue. Second, it showed little obvious deformation of the ventral nerve cord as sometimes caused by the histological procedure. The resulting average from 24 affine transformations of wild type ventral nerve cords served as the new reference for the subsequent non-rigid registration steps (see methods for re-sampling of image resolution and step size of elastic registration). This resulted in a reliable overlay of all samples that can be characterized as follows: only 20% of all pixels from all samples showed less than 50% overlay, and 77.6% of all pixels from all samples showed 100% overlay. Compared to the honey bee brain standard 100% overlay was achieved for 57.9% voxels after one nonrigid registration, and had to be improofed by iterative nonrigid registration steps. Iterative non-rigid registration steps did not significantly increase the reliability of the Drosophila VNC standard, and were thus omitted. The resulting standard showed a smaller distance to all 24 individual samples than the individual samples to each other. This demonstrates that the average ventral nerve cord is more similar to each of the input samples than any of the individual samples are to each other. Therefore, the standard fulfills the major positive criterion for the validity of the average shape properties of a standard (Brandt et al., 2005; Kurylas et al., 2008), and thus, represents a real average for wild type Drosophila ventral nerve cords.

The generation of the Drosophila ventral nerve cord standard bears one major methodological difference when compared to previously published insect brain atlases (Rein et al., 2002; Brandt et al., 2005; Kurylas et al., 2008). It is based on one material only, the NC82 neuropil staining, which contained enough spatial information for standard generation. Within the neuropil staining, the positions of tracts are marked by areas lacking NC82-staining and are excluded from the neuropil material. This creates internal boundaries which provide spatial information to increase the accuracy of the registration process. Therefore, the use of only one material still results in a standard with a high percentage of pixel overlap from all samples and a minimized shape difference of the standard to the input samples. The use of only one material bears multiple important advantages: First, the entire neuropil staining can be transformed into a label field with a global thresholding criterion, in a non time consuming way. Second, the segmentation process does not depend on extensive user knowledge of the nervous system anatomy. The segmentation process for currently available insect brain atlases materials (Rein et al., 2002; Brandt et al., 2005; Kurylas et al., 2008) requires the user to identify multiple distinct brain structures and assign different materials to these. By contrast, the registration process for Drosophila ventral nerve cord relies only on user decisions as to whether NC82 immuno-positive staining belongs to neuropil or not. The histology for standardizations depends entirely on stainings with the commercially available NC82 synaptic marker (Wagh et al., 2006), and the histological procedure is explained in the protocol. Therefore, the Drosophila ventral nerve cords standard can readily be used by a broad spectrum of users for manifold applications. However, it was not test whether the quality of the standard would be improved by including additional materials. Dividing the NC82 staining into several distinct materials is difficult, because it is is not possible to make out clear boundaries within the neuropil in a reliable and repeatable manner in different preparations. Potentially, one could include a second staining for further landmarks, but this would complicate the application, and it would occupy one fluorescent channel that can be used for the registration of other labeled structures into the standard. Therefore, it was judged ventral nerve cord standard generation to be optimal with one material only deriving from NC82 neuropil staining. Below the applicability and the limits of this standard for the registration of additional structures, expression lines, single neuron geometries and neural networks will be discussed.

Registration of tracts, commissures and ganglionic cortex

Additional coordinates can be defined by integrating more anatomical structures

into the standard. These coordinates can help to describe mapped data within the standard. Classical features of insect ventral ganglia are conserved positions of tracts and commissures (Pflueger et al., 1981, 1988; Braeunig et al., 1981; Nassif et al., 1998, 2003; Landgraf et al., 2003; Kuehn and Duch, 2008). Information about the positions of tracts and commissures which have originally been described and named by Power (1948) were included. Tracts and commissures could be identified in immunstainings with antibodies against Tubulin and Futsch. However, immunstainings of tracts and commissures showed fuzzy borders, and some were characterized by de-fasciculation of axon bundles in parts of the ganglia. This made the segmentation strongly dependent from staining quality, manual segmentation precision, and user judgment. Therefore, only well stained examples were register but no averages are produced for the localization of tracts and commissures in the atlas. This problem can potentially be solved by increasing the sample size to create prominent average tracts and include them in the standard as landmarks. An alternative approach could be to take advantage of expression lines which selectively label only distinct tracts or commissures. These will most likely become available over time due to the continuous effort of screening for postembryonic lineages (Truman et al., 2004; Cornbrooks et al., 2007; Boone and Doe, 2008) and the invention of novel screening strategies (Pfeiffer et al., 2008). In all insect ganglia, neuronal somata lay outside the neuropil, and somata in turn, are surrounded by a ganglionic sheath composed out of glia cells (Hartenstein et al., 1998; Awasaki et al., 2008), often refered to as ganglionic cortex (Power, 1948). This ganglionic cortex was labeled by expression of GFP under the control of the glia specific GAL-4 driver reverse polarity (repo, Xiong et al. 1994). Co-labeling of NC82 allowed for registration of the cortex into the standard, further completing the web based atlas and providing additional coordinated for the future registration of additional structures.

Registration of GAL4 expression lines into the standard

One of the reasons that Drosophila has become a valuable model for neuroscientific research is the availability of a large number of fly lines that show distinct spatial and temporal patterns of gene expression. A growing number of databases (*Flybase*, the *Interactive Fly*, *FlyEx*, *FlyView*) makes these expression lines available to the scientific community, and new screening methods are constantly being developed (Boone and Doe, 2008). The number of available GAL4 enhancer trap lines outnumbers the number of structural genes as there exist more enhancers than genes coding for proteins (Levine and Tjian, 2003). One major aim of this study was to determine what attributes such GAL4 lines must have to be successfully registered

into a web based standard without excessive time investment. Towards this goal the registration process for two general motoneuron driver lines (D42-GAL4, Parkes et al. 1998; C380-GAL4, Sanyal et al. 2003), a GAL4 line that drives expression in all octopaminergic/tyraminergic neurons (TDC2, Cole et al. (2005)), and lines that drive GAL4 expression specifically in neurons containing distinct classical fast neurotransmitters (Cha-GAL4, cholinergic neurons; OK371-GAL4, glutamatergic neurons; GAD-GAL4, GABAergic neurons) were tested. In principle, the classical label field based registration of all of these driver lines into the standard is possible, but it was found that specific features of expression patterns make the registration process straight forward and, whereas others make the process less feasible and very time consuming. All drivers that express in distinct clusters of neuronal somata can easily be labeled as materials and registered, as was the case for clusters of somata in C380-GAL4 and TDC2-GAL4. By contrast, many individual somata with GAL4 expression appeared in Cha-GAL4, OK371-GAL4, and GAD-GAL4. First, it is time consuming to label all individual somata by hand, and second, neuronal somata positions vary between animals much stronger than the locations of clusters of somata, making the averaging of single neuron positions highly variable. Similarly, dense dendritic fields with clear borders deriving from multiple neurons can easily be labeled (see dendritic field of DLM flight motoneurons as revealed by D42-GAL42 expression), but the labeling of distributed individual neurites projecting to different neuropil regions requires time consuming segmentation prior to registration, and is thus far less feasible (see distributed processes as revealed by TDC2 expression). Therefore, the registration of a large number of GAL4 lines as materials into the standard revealed to be extremely time consuming. One suggestion was to restrict this approach to lines that express in defined clusters of neurons that give rise to dense dendritic fields with sharp borders. This is certainly the case for somata in postembryonic lineages because Drosophila neuroblasts and their progeny remain within one cluster (Doe, 1992; Truman et al., 2004). However, it is not the case in many other expression lines which might be of great functional interest. Therefore, an alternative method to solve this problem is suggested here. For any expression patterns in a first fluorescent channel that was co-labeled with NC82 immunostaining, the neuropil material can be defined (see above) and registered into the standard. The resulting values for the NC82 transformation steps can subsequently be applied to the stack of gray scale TIFF images of the first channel. Thereby, any confocal image stack can be registered into the standard without defining any materials. As an example the overlap of the dendritic field of the identified flight motoneuron, MN5, with the central projection patterns of aminergic neurons is determined, both

of which derived from different preparations, each of which was counterstained with NC82 for registration. This approach potentially allows for quantitative comparison of image data from different preparations and different laboratories worldwide, and might thus produce a very valuable database.

Localization of defined regions in original image stacks by applying standard information backwards

Detailed analysis of specific structures within the ventral nerve cord often requires high resolution confocal microscopy with a limited field of view. The standard can be used to find the same regions within different preparations, so that these can be compared. For this it is necessary to define specific sub-regions within the standard up front. For example, this can be done by the registration of retrogradely labeled sensory projections, or the dendritic fields of GFP expressing flight motoneurons. These sub-regions can be detected in any additional dataset that was counterstained with NC82 by transformation of the standard neuropil label onto the dataset neuropil label. As an example for this application, the backwards registration of the standard and hence the sub-neuropils defined by wing sensory neuron axon terminals and by flight motoneuron dendritic fields is applied onto an individual preparation, to analyze the densities of GABAergic and cholinergic terminals within these neuropil regions. Importantly, GABAergic and cholinergic terminals were stained in different animals, but yet, their densities could be compared in the same functional neuropil areas by using the standard. This revealed that the overall density of labeled active zones was similar in both sub-neuropils, but the sub-neuropli defined by flight motoneuron dendrites as contained 6 times more cholinergic and 2 times more GABAergic as compared to the one defined by the axon terminals of wing sensory neurons. This indicated that functionally different neuropil regions within the motor circuitry underlying flight behavior might contain different densities of excitatory and inhibitory synapses. The comparison of GABAergic and cholinergic terminals relied on immunolabels from different preparations, which could be compared by using backwards registration of the standard.

Registration of individual identified neurons

One distinct advantage of many invertebrate preparations is the existence of individually identified neurons, that can unequivocally be recognized from animal to animal and between different developmental stages. Registration of many such identified neurons might result in future neural network maps, or at least in maps of putative connectivity. It was tested how applicable the standard is for registration of single

identified neurons. The individually identified flight motoneuron, MN5, was chosen because it comprises a very complex dendritic tree with more than 6000 microns total dendritic length and more than 1500 dendritic branches (Duch et al., 2008). The geometry of MN5 was reconstructed in 3 dimensions from confocal image stacks with previously published customized tools (Schmitt et al., 2004; Evers et al., 2005, 2006; Duch et al., 2008) which also incorporate into AMIRA, and are freely available via the internet (http://www.neurobiologie.fu-berlin.de/pflueger/evers.html). The registration of MN5 geometric reconstructions from four different animals resulted in strong overlay of the dendritic branches. This overlay was improved by the transformation steps during registration, and could not be achieved to the same degree by an experimenter moving the MN5 reconstructions in 3 dimensional space. However, it is clear that the detailed dendritic branching patterns differ between preparations, and thus, identification of individual synaptic contacts will not be possible by the registration of multiple neurons into the standard. However, registration will allow determining whether neurons labeled in different preparations have the potential projection fields for synaptic connections.

Identification of putative monosynaptic connections to the flight motoneuron 5

This study is the first description of putative monosynaptic connections from sensory neurons onto the dendrites of a Drosophila flight motoneuron. The combination of GFP expression, intracellular staining methods, and immunostainings in this model organism made the identification of putative synaptic contacts on the light microscopy level possible. In high resolution confocal image stacks the entire dendritic tree of the MN5 could be investigated to quantify the number of contacts. Confocal microscopy has been used in various studies for high resolution analysis of connections between labeled neurons (Gan et al., 1999; Cabirol-Pol et al., 2000; Jacoby et al., 2000; Hiesinger et al., 2001; Nakagawa and Mulloney, 2001; Gray and Weeks, 2003; Zhang et al., 2003). In some cases contacts found on the light microscopy level could be verified as synapses with electron microscopy (Peters et al., 1985). Further, monosynaptic connections between sensory neuron and motoneuron contacts have been proofed in electrophysiology experiments (Gray and Weeks, 2003; Zhang et al., 2003). With a NC82 counterstaining for the Bruchpilot protein that localizes to the active zone (Wagh et al., 2006) the putative presynaptic input sites from pickpocket (ppk) expressing neuron terminals onto the MN5 dendrite could be narrowed to areas of synaptic transmitter release. A recent study in Manduca (Meseke et al., 2009a) used the combination of two antibodies to identify GABAergic presynaptic terminals on the intracellular stained dendrite of the flight motoneuron 5.

For a precise quantitative analysis of presynaptic sites, the MN5 was geometrically reconstructed (Schmitt et al., 2004; Evers et al., 2005). With the generation of staining intensity maps for NC82 and PPK on the dendrite surface and their subsequently correlation (Evers et al., 2005), the putative presynaptic input sites could be displayed on the surface of the dendrites and counted automatically. In a correlative electron and confocal microscopy study (Hohensee et al., 2008) it was shown, that immunostaining for presynaptic proteins can yield in a good estimate of synaptic contacts along reconstructed dendritic surfaces. Thus, the staining with NC82 was a sufficient criterion to identify synaptic contacts with a high likelihood.
The used methods allowed for estimation of numbers for dendritic segments for having contact with PPK positive sensory cells. With 119 22 synaptic contacts between sensory axons and the dendrite the PPK positive input sites covered 0.59±0.33% of the whole surface of the MN5 dendritic tree. In Manduca (Gray and Weeks, 2003), Aplysia (Zhang et al., 2003), and crayfish (Nakagawa and Mulloney, 2001) 9, 24, and, 42 contacts respectively could be observed between sensory neurons and motoneurons. Peters et al. (1985) showed that at every identified contact between the hindwing stretch receptor and the motoneuron 127, a number of separate anatomical synapses, each defined by a single presynaptic density, was present. For eight identified contacts they found a total of 20 synapses. The size of putative input sites on the MN5 dendrite varied between 0.004 and 5.9 μm^2 what leads to the suggestion, that the number of anatomical synapses might be higher than the actual counted contact sites. In two studies it has been shown that the number of contacts between sensory neurons and the postsynaptic motoneurons were proportional to the amplitude of the evoked excitatory postsynaptic potentials (EPSPs) (Zhang et al., 2003). A developmental decrease in EPSP amplitude results from a decrease in the number of contacts of release sites (Gray and Weeks, 2003). The precise localization of presynaptic input sites on the MN5 of Drosophila offers a good model for computer simulations to test for the impact of sensory feedback from the periphery onto the dendrite of this flight motoneuron and the integration of the presynaptic signal.

Expression of GFP under the control of the ppk gene resulted in a strong continuous staining of sensory neurons and their central axon projections. Approximately 2-3 PPK positive neurons terminated in the very dorsal neuropil and showed an overlap with the dendritic field of the MN5. It was not possible to verify the number of sensory neurons which had contact with the MN5 dendrites. Further in the heterozygous animals used for the co-localization analysis not all of the PPK positive axons that were visible in the homozygous PPK-GFP line could be observed. This is most likely caused by the lower expression of GFP tagged channels in the

heterozygous animals. Here, half of the endogenous channels were expressed by the wildtype chromosome and the other half is expressed by the transgene chromosome. However, the appearance of projections in the dorsal neuropil seemed to be similar for both lines (data not shown).

The location of the ppk expressing neurons suggests that they provide sensory feedback upon flight muscle contractions and supposedly other deformations of the thorax. The ppk gene, encoding for a degenerin/epithelial sodium channel (DEG/ENaC) subunit, is expressed in mechanosensory multi dendritic (md) neurons (Adams et al., 1998). The position of the somata in close proximity to the dorsal longitudinal flight muscle (DLM) fibers and dendrites projecting onto the fibers make a function as muscle stretch receptors possible (Schrader and Merritt 2007). An exact classification to a distinct subclass of md neurons (Bodmer and Jan, 1987; Grueber et al., 2002) was not possible, and it is not clear whether the classification derived from the larval body wall can be applied to the adult.

The DLM is composed of 6 muscle fibers. The two dorsal-most fibers are innervated by the MN5. Each of the ventral-most four fibers is innervated by one motoneuron (MN1-4) (Coggshall, 1978; Ikeda and Koenig, 1988). The dendrites of MN1-4 branch in the same neuropil region as the MN5 (Ikeda and Koenig, 1988), thus, it is possible that PPK positive axons provide sensory input onto MN1-4 as well. Stainings for all 5 motoneurons combined with GFP expression in PPK positive neurons is difficult within one preparation. First estimations on possible contacts of axons and dendrites could potentially be achieved through registration into a common reference space. Registration of MN5 reconstructions into the ventral nerve cord standard for Drosophila resulted in a dendritic density map within the standard. The same method could be used for the axonal projections of PPK positive neurons and the possibility for contacts with the MNs could be calculated. This would test the feasibility of standard registration for identification of synaptic contacts.

Since the axonal projections of PPK positive neurons seemed to be very similar between preparations, standard registration could also allow for precise description of axonal branching patterns in the VNC. Studies by Killian et al. (1993) showed that axons of transplanted sensory neurons follow a stereotype projection pattern within the VNC, resembling their usual projections. The transplanted sensory neurons could form ectopic synapses with neurons in the host ganglion. They concluded that the common projection areas of axons and dendrites was sufficient for the establishment of a synaptic contact. In the late Drosophila embryo dendrites of motoneurons can adjust their size and geometry to the level and the distribution of input received from presynaptic partners (Tripodi et al., 2008).

The well described dendritic structure of the Drosophila MN5 (Duch et al., 2008) offers a good system to analyze the relationship of dendrite geometry and synaptic targeting. With the available tools for precise geometric reconstructions (Schmitt et al., 2004; Evers et al., 2005) the 3D structure of the MN5 could be investigated. Comparison of many reconstructed MN5 allowed for identification of dendritic sub-trees (Vonhoff, personal communication). This study analyzed PPK positive contacts on an identified subset of dendritic sub-trees of MN5, comprising about 50% of the whole dendritic tree of the MN5. This study did not analyze the whole tree, because across animal identification was difficult for some dendritic sub-trees. The localization of input sites showed an accumulation on more lateral positioned sub-trees. The median sub-trees showed less putative sensory inputs. These results gave first insights on the arrangement of putative synaptic contacts of PPK positive neurons on the MN5. In the cercal system of crickets it is known that each branch of the postsynaptic interneuron overlaps with a separate class of sensory afferents which are sensitive to a different wind direction (Miller and Jacobs, 1984). By contrast, the PPK positive axons were contacting multiple branches of the MN5, suggesting that sensory inputs to MN5 are not organized in a functional topographic manner. However, it is clear that most wing sensory neurons project into the ventral neuropil, and that MN5 must receive input from flight pro-motor neurons. Therefore, a strict topographic sensory organization was not expected. Nevertheless, the data showed that PPK positive terminals targeted the same neuropil areas in different preparations, and that these areas were targeted by identified dendritic sub-trees of MN5. Thereby, the total number of contacts remains relatively constant (119±22), but different MN5 sub-trees might compete for PPK input synapses. For example, large numbers of inputs to sub-tree 1 coincide with low numbers of inputs in sub-tree 2, and vice versa. Intermediate numbers of inputs to subtree 1 coincide with intermediate numbers of input to sub-tree 2. MN5 sub-trees can have variable projections spaces (Vonhoff and Duch, personal communication), but they never overlap with each other within such a projection space. These are indications for competition of central dendrites for synaptic inputs, with a first comes first serves mechanisms at place. For a statistical analysis of possible competitive interactions during motoneuron dendritc field development more data will be needed. The data also show that PPK positive axonal projections never cross the ganglionic midline. By contrast MN5 dendrites project to both sides of the ganglion. Consequently, MN5 received synaptic input from ppk expressing mechanoreceptors from both the left and the right muscle. Approximately 75% input sites were from the MN5 target DLM, whereas only 25% projected onto the MN5 from the other side. It remains to

be shown whether the observed segregation of sensory feedback from the right and left DLMs onto different parts of the MN5 dendritic field has functional relevance, for instance during steering maneuvers. In combination with the genetic tools of Drosophila the interaction between central projections of sensory neurons and the MN5 dendrites can now be investigated in future studies. With ectopic gene expression (Brand and Perrimon, 1993) under the control of the ppk gene a subset of peripheral neurons could be genetically modified (White et al., 1994; Li et al., 2005; Sweeney et al., 1995). Investigations on the structure of the MN5 in these animals could reveal dendritic adjustments to altered presynaptic input.

8 Abstract

Modern neuroanatomy requires quantification of neural structures, i. e. neurons, circuits and brain parts. The increased computational power that has become available during recent years makes electronic knowledge bases possible, which can serve as common platforms for the incorporation of anatomical and physiological data. In this study a standardized neuroanatomical atlas for the ventral nerve cord of the genetic model system, *Drosophila melanogaster* was generated. By testing the quality of the standard it could be confirmed that the neuropil standard can serve as real average of wild-type Drosophila. A standardized staining protocol with a commercially available antibody ensures that the standard is applicable for any user. Standard generation was based on the entire neuropil structure and internal neuropil boundaries could be defined. With a global thresholding criterion user interaction for the segmentation process could be minimized and therefore, offers an easy and non time-consuming way for standard registration. The standard will be made available on the web together with a detail protocol for the histological methods, the segmentation, and the registration process. Ganglionic cortex, tracts, and commissures were registered into the standard to define additional landmarks. The feasibility for standard registration for managing gene expression data was tested for several GAL4 lines. Theoretically any structure that was counterstained with the neuropil marker can be registered into the standard. However, standard registration was not useful for every expression pattern to display similarities or differences between GAL4 lines.

Registration of anatomical structures derived from individual samples into the reference space yielded in a good overlay and allowed for defining of sub-neuropils within the standard. In a new approach it could be shown that these defined sub-regions can be applied onto individual samples by backwards application of the standard. This allowed for comparative studies of ventral nerve cord neuropils, i.e. transmitter compositions of neuropil regions with defined functions.

Spatial relationships of registered structures can be investigated within the common reference space. An overlap of axonal and dendritic projections could indicate connectivity of identified neurons stained in individual samples. With the identification of the putative monosynaptic connection of sensory neurons and the flight motoneuron of Drosophila the feasibility of standard registration can now be tested for revealing synaptic connectivity.

9 Zusammenfassung

Eine Quantifiezierung von neuronalen Strukturen wie Nervenzellen, Netzwerke und Gehirnteile ist für moderne Neuroanatomie von grosser Bedeutung. Mit zunehmender Rechnerleistung, die in den letzten Jahren verfügbar wurde, können elektronische Datenbanken generiert werden. Diese dienen als öffentliche Plattformen in die neuroanatomische und physiologische Daten integriert werden können. In der vorliegenden Arbeit wurde ein standardisierter neuroanatomischer Atlas für das ventrale Nervensystem von adulten Drosophila melanogaster generiert. Mit der Überprüfung der Qualität des Standards konnte bestätigt werden, dass dieser einen Durchschnitt von wildtypischen Drosophila bildet. Durch die Anwendung eines standardisierten Färbeprotokolls mit einem kommerziell erwerblichen Antikörper kann dieser Standard von jedem Nutzer angewendet werden. Die gesamte Neuropilstruktur des ventralen Nervensystems ist in diesem Standard enthalten und interne Neuropilgrenzen wurden integriert. Der Segmentierungsprozess der Neuropilstruktur basierte auf einem globalen Schwellenwert, dieses führte zu einer einfachen und zeitsparenden Anwendung. Der Standard wird auf einer Internetseite zusammen mit einem detailierten Protokoll für die histologischen Methoden, der Segmentierung und des Registrierungsvorgangs veröffentlicht werden. Die Ganglionrinde, Trakte und Kommissuren wurden als zusätzliche Landmarken in den Standard integriert.
Eine Anwendung des Standards für die Verwaltung von Genexpressionsdaten wurde mit der Integration von verschiedenen GAL4 Linien getestet. Jede Struktur, die mit einem Neuropilmarker gegengefärbt wird, kann theoretischer weise in den Standard registriert werden. Für einige der getesteten GAL4 Linien war eine Registrierung in den Standard jedoch nicht sinnvoll, um Ähnlichkeiten oder Unterschiede zwischen den Expressionsmustern verschiedener Linien festzustellen.
Mit der Registrierung von anatomischen Strukturen aus individuellen Tieren und dem anschliessenden Übereinanderlagern dieser Strukturen im Standard konnten interne Einzelneuropile abgegrenzt werden. Diese zuvor definierten Unterstrukturen konnten in Einzelpraeparate definiert werden, indem der Standard auf diese Präparate registriert wurde. Mit dieser neuen Methode können Informationen über die Feinstruktur von Neuropilregionen untersucht werden und zwischen individuellen Präparaten verglichen werden. Die Lage von registrierten Strukturen zueinander kann innerhalb des gemeinsamen Referenzatlasses überprüft werden. Eine Überlagerung von Axonen und Dendriten von registrierten Neuronen kann auf eine mögliche Konnektivität zwischen beiden Komponenten hindeuten. Mit der Identifizierung einer monosynaptischen Verbindung von sensorischen Neuronen und dem

Flugmotoneuron in Drosophila, kann nun die Anwendung des Standards für die Identifizierung solcher Kontakte durch Standardregistrierung getestet werden.

References

Aberle, H., Haghighi, A. P., Fetter, R. D., McCabe, B. D., Magalhes, T. R., and Goodman, C. S. (2002). wishful thinking encodes a bmp type ii receptor that regulates synaptic growth in drosophila. *Neuron*, 33(4):545–558.

Adams, C. M., Anderson, M. G., Motto, D. G., Price, M. P., Johnson, W. A., and Welsh, M. J. (1998). Ripped pocket and pickpocket, novel drosophila deg/enac subunits expressed in early development and in mechanosensory neurons. *J Cell Biol*, 140(1):143–152.

Ainsley, J. A., Pettus, J. M., Bosenko, D., Gerstein, C. E., Zinkevich, N., Anderson, M. G., Adams, C. M., Welsh, M. J., and Johnson, W. A. (2003). Enhanced locomotion caused by loss of the drosophila deg/enac protein pickpocket1. *Curr Biol*, 13(17):1557–1563.

Allen, M. J., Godenschwege, T. A., Tanouye, M. A., and Phelan, P. (2006). Making an escape: development and function of the drosophila giant fibre system. *Semin Cell Dev Biol*, 17(1):31–41.

Awasaki, T., Lai, S.-L., Ito, K., and Lee, T. (2008). Organization and postembryonic development of glial cells in the adult central brain of drosophila. *J Neurosci*, 28(51):13742–13753.

Baier, A., Wittek, B., and Brembs, B. (2002). Drosophila as a new model organism for the neurobiology of aggression? *J Exp Biol*, 205(Pt 9):1233–1240.

Bellen, H. J., O'Kane, C. J., Wilson, C., Grossniklaus, U., Pearson, R. K., and Gehring, W. J. (1989). P-element-mediated enhancer detection: a versatile method to study development in drosophila. *Genes Dev*, 3(9):1288–1300.

Berg, B. G., Galizia, C. G., Brandt, R., and Mustaparta, H. (2002). Digital atlases of the antennal lobe in two species of tobacco budworm moths, the oriental helicoverpa assulta (male) and the american heliothis virescens (male and female). *J Comp Neurol*, 446(2):123–134.

Bodmer, R. and Jan, Y. N. (1987). Morphological differentiation of the embryonic peripheral neurons in drosophila. *Roux's Arch Dev Biol*, 196:69–77.

Boone, J. Q. and Doe, C. Q. (2008). Identification of drosophila type ii neuroblast lineages containing transit amplifying ganglion mother cells. *Dev Neurobiol*, 68(9):1185–1195.

Braeunig, P., Hustert, R., and Pflueger, H. J. (1981). Distribution and specific central projections of mechanoreceptors in the thorax and proximal leg joints of locusts. i. morphology, location and innervation of internal proprioceptors of pro- and metathorax and their central projections. *Cell Tissue Res*, 216(1):57–77.

Braeunig, P., Pflueger, H. J., and Hustert, R. (1983). The specificity of central nervous projections of locust mechanoreceptors. *J Comp Neurol*, 218(2):197–207.

Brand, A. H. and Perrimon, N. (1993). Targeted gene expression as a means of altering cell fates and generating dominant phenotypes. *Development*, 118(2):401–415.

Brandt, R., Rohlfing, T., Rybak, J., Krofczik, S., Maye, A., Westerhoff, M., Hege, H.-C., and Menzel, R. (2005). Three-dimensional average-shape atlas of the honeybee brain and its applications. *J Comp Neurol*, 492(1):1–19.

Budnik, V., Koh, Y. H., Guan, B., Hartmann, B., Hough, C., Woods, D., and Gorczyca, M. (1996). Regulation of synapse structure and function by the drosophila tumor suppressor gene dlg. *Neuron*, 17(4):627–640.

Burrows, M. (1975). Monosynaptic connexions between wing stretch receptors and flight motoneurones of the locust. *J Exp Biol*, 62(1):189–219.

Burrows, M., Laurent, G. J., and Field, L. H. (1988). Proprioceptive inputs to nonspiking local interneurons contribute to local reflexes of a locust hindleg. *J Neurosci*, 8(8):3085–3093.

Cabirol-Pol, M. J., Mizrahi, A., Simmers, J., and Meyrand, P. (2000). Combining laser scanning confocal microscopy and electron microscopy to determine sites of synaptic contact between two identified neurons. *J Neurosci Methods*, 97(2):175–181.

Chiang, A. S., Liu, Y. C., Chiu, S. L., Hu, S. H., Huang, C. Y., and Hsieh, C. H. (2001). Three-dimensional mapping of brain neuropils in the cockroach, diploptera punctata. *J Comp Neurol*, 440(1):1–11.

Chude, O., Roberts, E., and Wu, J. Y. (1979). Partial purification of drosophila glutamate decarboxylase. *J Neurochem*, 32(5):1409–1415.

Coggshall, J. C. (1978). Neurons associated with the dorsal longtitudinal flight muscles of drosophilla melanogaster. *J Comp Neurol*, 177(4):707–720.

Cole, S. H., Carney, G. E., McClung, C. A., Willard, S. S., Taylor, B. J., and Hirsh, J. (2005). Two functional but noncomplementing drosophila tyrosine decarboxylase genes: distinct roles for neural tyramine and octopamine in female fertility. *J Biol Chem*, 280(15):14948–14955.

Consoulas, C., Restifo, L. L., and Levine, R. B. (2002). Dendritic remodeling and growth of motoneurons during metamorphosis of drosophila melanogaster. *J Neurosci*, 22(12):4906–4917.

Cornbrooks, C., Bland, C., Williams, D. W., Truman, J. W., and Rand, M. D. (2007). Delta expression in post-mitotic neurons identifies distinct subsets of adult-specific lineages in drosophila. *Dev Neurobiol*, 67(1):23–38.

Diedrichsen, J. (2006). A spatially unbiased atlas template of the human cerebellum. *Neuroimage*, 33(1):127–138.

Doe, C. Q. (1992). Molecular markers for identified neuroblasts and ganglion mother cells in the drosophila central nervous system. *Development*, 116(4):855–863.

Duch, C. and Mentel, T. (2004). Activity affects dendritic shape and synapse elimination during steroid controlled dendritic retraction in manduca sexta. *J Neurosci*, 24(44):9826–9837.

Duch, C., Vonhoff, F., and Ryglewski, S. (2008). Dendrite elongation and dendritic branching are affected separately by different forms of intrinsic motoneuron excitability. *J Neurophysiol*, 100(5):2525–2536.

el Jundi, B., Huetteroth, W., Kurylas, A. E., and Schachtner, J. (in revision). Anisometric brain dimorphism revisited: implementation of a volumetric 3d standard brain in manduca sexta.

Estes, P. S., Roos, J., van der Bliek, A., Kelly, R. B., Krishnan, K. S., and Ramaswami, M. (1996). Traffic of dynamin within individual drosophila synaptic boutons relative to compartment-specific markers. *J Neurosci*, 16(17):5443–5456.

Evans, A. C., Collins, D. L., and Milner, B. (1992). An mri-based stereotactic brain atlas from 300 young normal subjects. *Soc. Neurosci. Abstr.*, 408.

Evers, J. F., Muench, D., and Duch, C. (2006). Developmental relocation of presynaptic terminals along distinct types of dendritic filopodia. *Dev Biol*, 297(1):214–227.

Evers, J. F., Schmitt, S., Sibila, M., and Duch, C. (2005). Progress in functional neuroanatomy: precise automatic geometric reconstruction of neuronal morphology from confocal image stacks. *J Neurophysiol*, 93(4):2331–2342.

Fowlkes, C. C., Hendriks, C. L. L., Kernen, S. V. E., Weber, G. H., Rbel, O., Huang, M.-Y., Chatoor, S., DePace, A. H., Simirenko, L., Henriquez, C., Beaton, A., Weiszmann, R., Celniker, S., Hamann, B., Knowles, D. W., Biggin, M. D., Eisen, M. B., and Malik, J. (2008). A quantitative spatiotemporal atlas of gene expression in the drosophila blastoderm. *Cell*, 133(2):364–374.

Fujioka, M., Lear, B. C., Landgraf, M., Yusibova, G. L., Zhou, J., Riley, K. M., Patel, N. H., and Jaynes, J. B. (2003). Even-skipped, acting as a repressor, regulates axonal projections in drosophila. *Development*, 130(22):5385–5400.

Gan, W. B., Bishop, D. L., Turney, S. G., and Lichtman, J. W. (1999). Vital imaging and ultrastructural analysis of individual axon terminals labeled by iontophoretic application of lipophilic dye. *J Neurosci Methods*, 93(1):13–20.

Gray, J. R. and Weeks, J. C. (2003). Steroid-induced dendritic regression reduces anatomical contacts between neurons during synaptic weakening and the developmental loss of a behavior. *J Neurosci*, 23(4):1406–1415.

Grueber, W. B., Jan, L. Y., and Jan, Y. N. (2002). Tiling of the drosophila epidermis by multidendritic sensory neurons. *Development*, 129(12):2867–2878.

Grueber, W. B., Ye, B., Moore, A. W., Jan, L. Y., and Jan, Y. N. (2003). Dendrites of distinct classes of drosophila sensory neurons show different capacities for homotypic repulsion. *Curr Biol*, 13(8):618–626.

Haesemeyer, M., Yapici, N., Heberlein, U., and Dickson, B. J. (2009). Sensory neurons in the drosophila genital tract regulate female reproductive behavior. *Neuron*, 61(4):511–518.

Hartenstein, V., Nassif, C., and Lekven, A. (1998). Embryonic development of the drosophila brain. ii. pattern of glial cells. *J Comp Neurol*, 402(1):32–47.

Hiesinger, P. R., Scholz, M., Meinertzhagen, I. A., Fischbach, K. F., and Obermayer, K. (2001). Visualization of synaptic markers in the optic neuropils of drosophila using a new constrained deconvolution method. *J Comp Neurol*, 429(2):277–288.

Hohensee, S., Bleiss, W., and Duch, C. (2008). Correlative electron and confocal microscopy assessment of synapse localization in the central nervous system of an insect. *J Neurosci Methods*, 168(1):64–70.

Huetteroth, W. and Schachtner, J. (2005). Standard three-dimensional glomeruli of the manduca sexta antennal lobe: a tool to study both developmental and adult neuronal plasticity. *Cell Tissue Res*, 319(3):513–524.

Hummel, T., Krukkert, K., Roos, J., Davis, G., and Klaembt, C. (2000). Drosophila futsch/22c10 is a map1b-like protein required for dendritic and axonal development. *Neuron*, 26(2):357–370.

Hustert, R., Pflueger, J. H., and Braeunig, P. (1981). Distribution and specific central projections of mechanoreceptors in the thorax and proximal leg joints of locusts. *Cell Tissue Res*, 216(1):97–111.

Ikeda, K. and Koenig, J. H. (1988). Morphological identification of the motor neurons innervating the dorsal longitudinal flight muscle of drosophila melanogaster. *J Comp Neurol*, 273(3):436–444.

Ito, K. and Hotta, Y. (1992). Proliferation pattern of postembryonic neuroblasts in the brain of drosophila melanogaster. *Dev Biol*, 149(1):134–148.

Jackson, F. R., Newby, L. M., and Kulkarni, S. J. (1990). Drosophila gabaergic systems: sequence and expression of glutamic acid decarboxylase. *J Neurochem*, 54(3):1068–1078.

Jacoby, R. A., Wiechmann, A. F., Amara, S. G., Leighton, B. H., and Marshak, D. W. (2000). Diffuse bipolar cells provide input to off parasol ganglion cells in the macaque retina. *J Comp Neurol*, 416(1):6–18.

Jan, L. Y. and Jan, Y. N. (1976). Properties of the larval neuromuscular junction in drosophila melanogaster. *J Physiol*, 262(1):189–214.

Jarman, A. P., Grau, Y., Jan, L. Y., and Jan, Y. N. (1993). atonal is a proneural gene that directs chordotonal organ formation in the drosophila peripheral nervous system. *Cell*, 73(7):1307–1321.

Jarman, A. P., Sun, Y., Jan, L. Y., and Jan, Y. N. (1995). Role of the proneural gene, atonal, in formation of drosophila chordotonal organs and photoreceptors. *Development*, 121(7):2019–2030.

Jefferis, G. S. X. E., Marin, E. C., Watts, R. J., and Luo, L. (2002). Development of neuronal connectivity in drosophila antennal lobes and mushroom bodies. *Curr Opin Neurobiol*, 12(1):80–86.

Jefferis, G. S. X. E., Potter, C. J., Chan, A. M., Marin, E. C., Rohlfing, T., Maurer, C. R., and Luo, L. (2007). Comprehensive maps of drosophila higher olfactory centers: spatially segregated fruit and pheromone representation. *Cell*, 128(6):1187–1203.

Johnston, R. M. and Levine, R. B. (1996). Crawling motor patterns induced by pilocarpine in isolated larval nerve cords of manduca sexta. *J Neurophysiol*, 76(5):3178–3195.

Kikinis, R., Shenton, M. E., Iosifescu, D. V., McCarley, R. W., Saiviroonporn, P., Hokama, H. H., Robatino, A., Metcalf, D., Wible, C. G., Portas, C. M., Donnino, R., and Jolesz, F. A. (1996). A digital brain atlas for surgical planning, model driven segmentation and teaching. *IEEE Trans. Vis. Comput. Graph*, 2:232–241.

Killian, K. A., Merritt, D. J., and Murphey, R. K. (1993). Transplantation of neurons reveals processing areas and rules for synaptic connectivity in the cricket nervous system. *J Neurobiol*, 24(9):1187–1206.

King, D. G. and Wyman, R. J. (1980). Anatomy of the giant fibre pathway in drosophila. i. three thoracic components of the pathway. *J Neurocytol*, 9(6):753–770.

Kitamoto, T., Ikeda, K., and Salvaterra, P. M. (1992). Analysis of cis-regulatory elements in the 5' flanking region of the drosophila melanogaster choline acetyltransferase gene. *J Neurosci*, 12(5):1628–1639.

Kuehn, C. and Duch, C. (2008). Expression of two different isoforms of fasciclin ii during postembryonic central nervous system remodeling in manduca sexta. *Cell Tissue Res*, 334(3):477–498.

Kurylas, A. E., Rohlfing, T., Krofczik, S., Jenett, A., and Homberg, U. (2008). Standardized atlas of the brain of the desert locust, schistocerca gregaria. *Cell Tissue Res*, 333(1):125–145.

Laissue, P. P., Reiter, C., Hiesinger, P. R., Halter, S., Fischbach, K. F., and Stocker, R. F. (1999). Three-dimensional reconstruction of the antennal lobe in drosophila melanogaster. *J Comp Neurol*, 405(4):543–552.

Landgraf, M., Jeffrey, V., Fujioka, M., Jaynes, J. B., and Bate, M. (2003). Embryonic origins of a motor system: motor dendrites form a myotopic map in drosophila. *PLoS Biol*, 1(2):E41.

Laurent, G. and Burrows, M. (1988). A population of ascending intersegmental interneurones in the locust with mechanosensory inputs from a hind leg. *J Comp Neurol*, 275(1):1–12.

Lee, E.-F., Boline, J., and Toga, A. W. (2007). A high-resolution anatomical framework of the neonatal mouse brain for managing gene expression data. *Front Neuroinformatics*, 1:6.

Lee, E.-F., Jacobs, R. E., Dinov, I., Leow, A., and Toga, A. W. (2005). Standard atlas space for c57bl/6j neonatal mouse brain. *Anat Embryol (Berl)*, 210(4):245–263.

Lee, T. and Luo, L. (1999). Mosaic analysis with a repressible cell marker for studies of gene function in neuronal morphogenesis. *Neuron*, 22(3):451–461.

Levine, M. and Tjian, R. (2003). Transcription regulation and animal diversity. *Nature*, 424(6945):147–151.

Li, X., Gutierrez, D. V., Hanson, M. G., Han, J., Mark, M. D., Chiel, H., Hegemann, P., Landmesser, L. T., and Herlitze, S. (2005). Fast noninvasive activation and inhibition of neural and network activity by vertebrate rhodopsin and green algae channelrhodopsin. *Proc Natl Acad Sci U S A*, 102(49):17816–17821.

Lin, H.-H., Lin, C.-Y., and Chiang, A.-S. (2007). Internal representations of smell in the drosophila brain. *J Biomed Sci*, 14(4):453–459.

MacKenzie-Graham, A., Lee, E.-F., Dinov, I. D., Bota, M., Shattuck, D. W., Ruffins, S., Yuan, H., Konstantinidis, F., Pitiot, A., Ding, Y., Hu, G., Jacobs, R. E., and Toga, A. W. (2004). A multimodal, multidimensional atlas of the c57bl/6j mouse brain. *J Anat*, 204(2):93–102.

Mackenzie-Graham, A. J., Lee, E.-F., Dinov, I. D., Yuan, H., Jacobs, R. E., and Toga, A. W. (2007). Multimodal, multidimensional models of mouse brain. *Epilepsia*, 48 Suppl 4:75–81.

Mahr, A. and Aberle, H. (2006). The expression pattern of the drosophila vesicular glutamate transporter: a marker protein for motoneurons and glutamatergic centers in the brain. *Gene Expr Patterns*, 6(3):299–309.

Marder, E. and Bucher, D. (2001). Central pattern generators and the control of rhythmic movements. *Curr Biol*, 11(23):R986–R996.

Mazziotta, J., Toga, A., Evans, A., Fox, P., Lancaster, J., Zilles, K., Woods, R., Paus, T., Simpson, G., Pike, B., Holmes, C., Collins, L., Thompson, P., MacDonald, D., Iacoboni, M., Schormann, T., Amunts, K., Palomero-Gallagher, N., Geyer, S., Parsons, L., Narr, K., Kabani, N., Goualher, G. L., Boomsma, D., Cannon, T., Kawashima, R., and Mazoyer, B. (2001). A probabilistic atlas and reference system for the human brain: International consortium for brain mapping (icbm). *Philos Trans R Soc Lond B Biol Sci*, 356(1412):1293–1322.

Mazziotta, J. C., Toga, A. W., Evans, A., Fox, P., and Lancaster, J. (1995). A probabilistic atlas of the human brain: theory and rationale for its development. the international consortium for brain mapping (icbm). *Neuroimage*, 2(2):89–101.

Merritt, D. J. and Murphey, R. K. (1992). Projections of leg proprioceptors within the cns of the fly phormia in relation to the generalized insect ganglion. *J Comp Neurol*, 322(1):16–34.

Meseke, M., Evers, J., and Duch, C. (2009a). Ptx-induced hyperexcitability affects dendritic shape and gabaergic synapse density but not synapse distribution during manduca postembryonic motoneuron development. *J Comp Physiol A Neuroethol Sens Neural Behav Physiol*.

Meseke, M., Evers, J. F., and Duch, C. (2009b). Developmental changes in dendritic shape and synapse location tune single neuron computations to changing behavioral functions. *J Neurophysiol*.

Miller, J. P. and Jacobs, G. A. (1984). Relationships between neuronal structure and function. *J Exp Biol*, 112:129–145.

Morante, J. and Desplan, C. (2008). The color-vision circuit in the medulla of drosophila. *Curr Biol*, 18(8):553–565.

Murphey, R. K., Walthall, W. W., and Jacobs, G. A. (1984). Neurospecificity in the cricket cercal system. *J Exp Biol*, 112:7–25.

Nakagawa, H. and Mulloney, B. (2001). Local specification of relative strengths of synapses between different abdominal stretch-receptor axons and their common target neurons. *J Neurosci*, 21(5):1645–1655.

Nassif, C., Noveen, A., and Hartenstein, V. (1998). Embryonic development of the drosophila brain. i. pattern of pioneer tracts. *J Comp Neurol*, 402(1):10–31.

Nassif, C., Noveen, A., and Hartenstein, V. (2003). Early development of the drosophila brain: Iii. the pattern of neuropile founder tracts during the larval period. *J Comp Neurol*, 455(4):417–434.

Nixdorf-Bergweiler, B. and Bischof, H.-J. (2007). *A Stereotaxic Atlas of the Brain of the Zebra Finch Taeniopygia guttataWith Special Emphasis On Telencephalic Visual And Song System Nuclei in Transverse and Sagittal Sections*. National Library of Medicine, NCBI, Bethesda.

Nuesslein-Volhard, C. and Wieschaus, E. (1980). Mutations affecting segment number and polarity in drosophila. *Nature*, 287(5785):795–801.

Oishi, K., Zilles, K., Amunts, K., Faria, A., Jiang, H., Li, X., Akhter, K., Hua, K., Woods, R., Toga, A. W., Pike, G. B., Rosa-Neto, P., Evans, A., Zhang, J., Huang, H., Miller, M. I., van Zijl, P. C. M., Mazziotta, J., and Mori, S. (2008). Human brain white matter atlas: identification and assignment of common anatomical structures in superficial white matter. *Neuroimage*, 43(3):447–457.

Parkes, T. L., Elia, A. J., Dickinson, D., Hilliker, A. J., Phillips, J. P., and Boulianne, G. L. (1998). Extension of drosophila lifespan by overexpression of human sod1 in motorneurons. *Nat Genet*, 19(2):171–174.

Pearson, K. G., Reye, D. N., and Robertson, R. M. (1983). Phase-dependent influences of wing stretch receptors on flight rhythm in the locust. *J Neurophysiol*, 49(5):1168–1181.

Pereanu, W. and Hartenstein, V. (2006). Neural lineages of the drosophila brain: a three-dimensional digital atlas of the pattern of lineage location and projection at the late larval stage. *J Neurosci*, 26(20):5534–5553.

Peters, B. H., Altman, J. S., and Tyrer, N. M. (1985). Synaptic connections between the hindwing stretch receptor and flight motor neurones in the locust revealed by double cobalt labelling for electron microscopy. *J Comp Neurol*, 233(2):269–284.

Pfeiffer, B. D., Jenett, A., Hammonds, A. S., Ngo, T.-T. B., Misra, S., Murphy, C., Scully, A., Carlson, J. W., Wan, K. H., Laverty, T. R., Mungall, C., Svirskas, R., Kadonaga, J. T., Doe, C. Q., Eisen, M. B., Celniker, S. E., and Rubin, G. M. (2008). Tools for neuroanatomy and neurogenetics in drosophila. *Proc Natl Acad Sci U S A*, 105(28):9715–9720.

Pflueger, H. J., Braeunig, P., and Hustert, R. (1981). Distribution and specific central projections of mechanoreceptors in the thorax and proximal leg joints

of locusts. ii. the external mechanoreceptors: hair plates and tactile hairs. *Cell Tissue Res*, 216(1):79–96.

Pflueger, H. J., Braeunig, P., and Hustert, R. (1988). The organization of mechanosensory neuropils in locust thoracic ganglia. *Phil Trans R Soc Lond*, 321:1–26.

Phelps, C. B. and Brand, A. H. (1998). Ectopic gene expression in drosophila using gal4 system. *Methods*, 14(4):367–379.

Pisarev, A., Poustelnikova, E., Samsonova, M., and Reinitz, J. (2009). Flyex, the quantitative atlas on segmentation gene expression at cellular resolution. *Nucleic Acids Res*, 37(Database issue):D560–D566.

Poirier, C., Vellema, M., Verhoye, M., Meir, V. V., Wild, J. M., Balthazart, J., and Linden, A. V. D. (2008). A three-dimensional mri atlas of the zebra finch brain in stereotaxic coordinates. *Neuroimage*, 41(1):1–6.

Power, M. E. (1948). The thoracico-abdominal nervous system of an adult insect, drosophila melanogaster. *J Comp Neurol*, 88(3):347–409.

Ramon y Cajal, S. (1888). Sobre las fibras nerviosas de la capa molecular del cerebelo. *Rev. Trim. Histol. Normal Patol.*, 1:33–49.

Ramon y Cajal, S. (1898). Estructura del kiasma óptico y teoria general de los entrecruzamientos de las vias nervosias. *Rev. Trim. Micrograf́ica*, 3.

Rein, K., Zoeckler, M., Mader, M. T., Grbel, C., and Heisenberg, M. (2002). The drosophila standard brain. *Curr Biol*, 12(3):227–231.

Reye, D. N. and Pearson, K. G. (1987). Projections of the wing stretch receptors to central flight neurons in the locust. *J Neurosci*, 7(8):2476–2487.

Reye, D. N. and Pearson, K. G. (1988). Entrainment of the locust central flight oscillator by wing stretch receptor stimulation. *J Comp Phys A*, 162:77–89.

Rohlfing, T., Brandt, R., Menzel, R., and Maurer, C. R. (2004). Evaluation of atlas selection strategies for atlas-based image segmentation with application to confocal microscopy images of bee brains. *Neuroimage*, 21(4):1428–1442.

Sandstrom, D. J. and Weeks, J. C. (1991). Reidentification of larval interneurons in the pupal stage of the tobacco hornworm, manduca sexta. *J Comp Neurol*, 308(2):311–327.

Sanyal, S. (2009). Genomic mapping and expression patterns of c380, ok6 and d42 enhancer trap lines in the larval nervous system of drosophila. *Gene Expr Patterns*.

Sanyal, S., Narayanan, R., Consoulas, C., and Ramaswami, M. (2003). Evidence for cell autonomous ap1 function in regulation of drosophila motor-neuron plasticity. *BMC Neurosci*, 4:20.

Schmitt, S., Evers, J. F., Duch, C., Scholz, M., and Obermayer, K. (2004). New methods for the computer-assisted 3-d reconstruction of neurons from confocal image stacks. *Neuroimage*, 23(4):1283–1298.

Stokes, T. M., Leonard, C. M., and Nottebohm, F. (1974). The telencephalon, diencephalon, and mesencephalon of the canary, serinus canaria, in stereotaxic coordinates. *J Comp Neurol*, 156(3):337–374.

Sweeney, S. T., Broadie, K., Keane, J., Niemann, H., and O'Kane, C. J. (1995). Targeted expression of tetanus toxin light chain in drosophila specifically eliminates synaptic transmission and causes behavioral defects. *Neuron*, 14(2):341–351.

Talairach, J. & Tournoux, P. (1988). *Atlas of the Human Brain*. Thieme, New York.

Tripodi, M., Evers, J. F., Mauss, A., Bate, M., and Landgraf, M. (2008). Structural homeostasis: compensatory adjustments of dendritic arbor geometry in response to variations of synaptic input. *PLoS Biol*, 6(10):e260.

Truman, J. W., Schuppe, H., Shepherd, D., and Williams, D. W. (2004). Developmental architecture of adult-specific lineages in the ventral cns of drosophila. *Development*, 131(20):5167–5184.

Tyrer, N. M., Shepherd, D., and Williams, D. W. (2000). Methods for imaging labeled neurons together with neuropil features in drosophila. *J Histochem Cytochem*, 48(11):1575–1582.

Wagh, D. A., Rasse, T. M., Asan, E., Hofbauer, A., Schwenkert, I., Duerrbeck, H., Buchner, S., Dabauvalle, M.-C., Schmidt, M., Qin, G., Wichmann, C., Kittel, R., Sigrist, S. J., and Buchner, E. (2006). Bruchpilot, a protein with homology to elks/cast, is required for structural integrity and function of synaptic active zones in drosophila. *Neuron*, 49(6):833–844.

White, K., Grether, M. E., Abrams, J. M., Young, L., Farrell, K., and Steller, H. (1994). Genetic control of programmed cell death in drosophila. *Science*, 264(5159):677–683.

Wolf, R. and Heisenberg, M. (1991). Basic organization of operant behavior as revealed in drosophila flight orientation. *J Comp Physiol [A]*, 169(6):699–705.

Xiong, W. C., Okano, H., Patel, N. H., Blendy, J. A., and Montell, C. (1994). repo encodes a glial-specific homeo domain protein required in the drosophila nervous system. *Genes Dev*, 8(8):981–994.

Yeh, E., Gustafson, K., and Boulianne, G. L. (1995). Green fluorescent protein as a vital marker and reporter of gene expression in drosophila. *Proc Natl Acad Sci U S A*, 92(15):7036–7040.

Zhang, H., Wainwright, M., Byrne, J. H., and Cleary, L. J. (2003). Quantitation of contacts among sensory, motor, and serotonergic neurons in the pedal ganglion of aplysia. *Learn Mem*, 10(5):387–393.

Acknowledgements

An erster Stelle möchte ich mich bei meinem Betreuer Herrn Prof. Dr. Carsten Duch bedanken, der mir diese Dissertation ermöglicht hat. Unter seiner Betreuung konnte ich erste Einblicke in die unbegrenzten Möglichkeiten der Drosophilaforschung gewinnen und das Land der unbegrenzen Möglichkeiten kennenlernen. Mit seinem unendlichen Ideenreichtum und seiner Hilfestellung konnte ich zahlreiche Methoden erlernen und verbessern.
Herrn Prof. Dr. Hans-Joachim Pflüger möchte ich danken für die Unterstützung in Berlin und die Bereitstellung von Labor und Geräten. Danke auch für die vielen Empfehlungsschreiben und die Begutachtung meiner Arbeit.
Ganz besonders möchte ich mich bei meiner gesamten Arbeitsgruppe in Tempe bedanken. Durch die enge Zusammenarbeit und eine gute Laboratmosphäre war die Arbeit stets eine Freude. Vielen Dank an Fernando Vonhoff für die Bereitstellung von MN5-Rekonstruktionen und der Identifizierung von subtrees, auch noch in letzer Minute. Claudia Kühn möchte ich für die Hilfestellung bei der Färbung und Rekonstruktion des MN5s und darüber hinaus für die freundschaftlichen Begleitung in allen Lebenssituationen danken. Thanks to Erin McKiernan for the great time at work and coffee. Marco Herrera-Valdes, thanks for the help with MATLAB and the GUI. Vielen Dank auch an Sandra Berger und Stefanie Ryglewski.
Heike Wolfenberg, Bettina Stocker und Doreen Johannes möchte ich danken für die tolle Zeit im berliner Labor und die nette Unterstützung im Laboralltag. Danken möchte ich auch meinen LeidensgenossinnenMelanie Hähnel und Anja Fröse, geteiltes Leid ist halbes Leid. Und natürlich danke ich auch dem Rest der Neurobiologie in Berlin für die netten Stunden im Garten.
Bei meiner Familie möchte ich mich am meisten bedanken. Mit ihrer Unterstützung konnte ich immer meine Ziele verfolgen.